Quantification of interventricular dyssynchrony using a standard 12-lead ECG based solution to the inverse ECG problem

Frederik Samuelsen[a], Gry Bruun Grønborg[a], Maria Goncalves Møller[a]

[a]*Department of Health Science and Technology, Aalborg University, Fredrik Bajers Vej 7D, Aalborg, 9220, Aalborg Oest, Denmark*

Abstract

Background: Severe left bundle branch block (LBBB) is treated with cardiac resynchronisation therapy (CRT), however more than 30% treated with CRT are non-responders, likely due to absence of electrical dyssynchrony. In order to improve patient selection, interventricular dyssynchrony can potentially be quantified by solving the inverse electrocardiography (ECG) problem. Existing solutions are based on >100 body surface measurements and patient specific geometries, which limits the clinical applicability. This study aims to determine the electrical activation of the ventricles from standard 12-lead ECG recordings and a generic heart-torso model, and quantify the interventricular electrical dyssynchrony.

Method: Standard 12-lead ECG recordings from 100 normal subjects, 100 LBBB subjects, and 135 subjects admitted to CRT were included. The ventricular myocardial activation was determined in six dipoles. The accuracy and robustness of Gaussian regularisation and Tikhonov regularisation with regularisation parameter $\lambda=0$ and $\lambda=30$ was compared. Interventricular dyssynchrony was determined as the left-right ventricular uncoupling (LRVU) and compared to QRS duration, QRS area and Q-LV.

Results: Tikhonov $\lambda=0$ yielded the most accurate ECG reconstruction in both normal and LBBB subjects. LRVU was higher in LBBB subjects compared to normal subjects. The correlation of LRVU with QRS duration and QRS area was higher in LBBB($r^2=0.359$, 0.791) and CRT subjects($r^2=0.328$, 0.630) compared to normal subjects($r^2=0.178$, 0.093). Furthermore LRVU was correlated with Q-LV in CRT subjects ($r^2=0.441$).

Conclusion: Interventricular dyssynchrony can be quantified by solving the inverse ECG problem by standard 12-lead ECG and a generic heart-torso model.

1. Introduction

Cardiac resynchronisation therapy (CRT) is a treatment recommended to chronic heart failure (HF) patients with left bundle branch block (LBBB) [1]. The treatment is offered to patients, who do not experience sufficient improvement from medical treatment [2, 3]. More than 30% of patients with CRT do not respond to the treatment [4] and hence it remains a clinical challenge to predict which patients will benefit from CRT. One of the causes for the lack of response to resynchronisation is thought to be absence of delayed activation of the left ventricular (LV) free wall [5], generally termed interventricular dyssynchrony.

Current clinical practice when selecting patients for CRT is based on QRS duration and morphology on 12-lead electrocardiography (ECG) [1], which provide measures of the global electrical dyssynchrony of the ventricles. Prolonged QRS duration can be a result of several different pathophysiologies [6], hence it is not necessarily an indicator of interventricular dyssynchrony. Several studies have investigated alternative measures of electrical dyssynchrony in order to provide measures with prognostic value for CRT treatment. An alternative measure is the QRS area which is calculated from the single dipole of the vectorcardiogram [7]. Several studies have shown the potential of QRS area as a predictor for CRT response [8, 9], with a larger QRS area prior to treatment being associated with greater survival after CRT [8]. Another measure associated with CRT response is the Q-LV measure, which is obtained using an invasive LV electrode placed in an appropriate branch of the coronary sinus during CRT implantation. The Q-LV measure is a direct measure reflecting the degree of delay at the pacing site in the LV, measured from QRS onset on the 12-lead ECG to the last activation of the

LV determined from the LV electrogram.[10] However, the Q-LV measure is limited by the possible positions of the LV electrode in the coronary sinus, and can furthermore not be used for CRT patient selection since it is recorded invasively in patients already admitted to CRT implantation.

Thereby, the existing measures of dyssynchrony are limited by either reflecting only a global activation of both ventricles or by requiring invasive measurements making it unsuitable for patient selection. A few studies have investigated electrocardiographic imaging (ECGi) as a tool for dyssynchrony quantification [11, 12, 13]. ECGi is a noninvasive technique that maps the epicardial electric activation using body surface potential (BSP) measurements and patient specific geometric heart-torso models achieved from computed tomography scans [11, 13]. The BSPs are typically measured using an ECGi vest with more than 250 electrodes, hence the measurement is expensive and impractical. The ECGi provides a tool for assessing the localisation of epicardial activation delays, as opposed to the global QRS measures. Several dyssynchrony measures have been derived from ECGi [11, 12, 13, 14, 15], such as ventricular electrical uncoupling (VEU), which is determined as the difference between the mean activation times of the LV and the right ventricle (RV) [11, 12, 13]. The study by Ploux et al. [11] found that VEU outperforms both QRS duration and the presence of LBBB in prediction of CRT response.

The task of achieving the epicardial activation from the body surface measurements and heart-torso geometry is called the inverse ECG problem. The problem is ill-posed and hence no unique solution exists. Therefore, the solution is sensitive to geometric and measurement noise which can cause significant errors [16]. Several studies have investigated different approaches to achieve robust and accurate solutions to the inverse ECG problem by restricting the solution using regularisation and model assumptions. The most widely used approach is the Tikhonov regularisation, especially zero-order [17, 18, 19]. Most of the studies investigating the inverse ECG problem are based on simulated BSPs in about 150-770 leads [20, 21] and estimates the epicardial potentials in up to 2500 epicardial sites [17] achieving high localisation accuracy of the epicardial activation. However, the need for high localisation accuracy can be questioned in the task of dyssynchrony quantification. This is for instance indicated by the VEU as it is derived from the mean activation of the entire RV and LV respectively, disregarding the details of the individual epicardial sites.

Rather than providing high localisation accuracy, it is of relevance to determine the epicardial activation using an approach applicable in clinical practice. The requirement of a patient specific geometric model and a large amount of BSP measurements constitutes a practical limitation of the method in clinical settings. Hence it is of great interest to investigate the possibility of determining dyssynchrony from standard 12-lead ECG recordings and a generic geometric model. Determination of the localisation of cardiac sources from a 12-lead ECG have been studied by Nakano et al. [22] and Potyagaylo et al. [23], however none of these studies investigated the interventricular electrical dyssynchrony.

The aim of this study was therefore to 1) determine the electrical activation of the ventricles from standard 12-lead ECG recordings and a generic heart-torso model, and 2) quantify the interventricular electrical dyssynchrony.

2. Method

2.1. Data

The data in this study consisted of 12-lead ECG recordings from 100 normal subjects and 100 LBBB subjects from the MUSE® Cardiology Information System Database, which contains ECG recordings of patients who consulted their general practitioner between 2001 and 2015. Furthermore 12-lead ECG recordings with corresponding Q-LV measures from 135 subjects who were admitted to CRT implantation were used in the study, and provided by Sommer et al. 2016 [24]. A geometric heart-torso model with a corresponding measured 12-lead ECG along with locations of the electrodes were provided by the simulation program ECGSim [25] and used in the current study. The model was based on magnetic resonance imaging of a male with a normal ECG and the heart model was defined by 131 epicardial nodes.

The normal and LBBB subjects were categorised by the GE Healthcare Marquette 12SL analysis program version 23. The LBBB subjects fulfilled the LBBB criteria and had absence of other abnormalities in the ECG [26]. The normal subjects did not show any ECG abnormalities.

The subjects in the CRT group typically suffered from LBBB and HF (NYHA class II-IV).

All ECG recordings included in the study were median ECG signals sampled at 500 Hz, with a length of 200 ms and the QRS aligned in the middle.

2.2. Inverse ECG problem

The inverse ECG problem is the task of determining myocardial activation from BSP measurements. The myocardial activation can mathematically be calculated as dipoles, which are vectors with directions and time dependent amplitudes. Physiologically, dipoles represent the current originating from the myocardial depolarisation. The solution to the inverse problem can be extracted from the formula of the forward ECG problem, by isolation $x(t)$, see Equation 1.

$$ECG_{measured}(t) = A \cdot x(t) \tag{1}$$

where $ECG_{measured}(t)$ is the measured ECG to the time t, $x(t)$ is the dipole amplitudes to the time t and A is a transformation matrix. The transformation matrix was in this study solely geometrically determined, since the torso was assumed to be a homogeneous volume conductor, see Equation 2.

$$A_n = \sum_{m=1}^{M} \overrightarrow{z_{mn}^T} \overrightarrow{u_m} = \sum_{m=1}^{M} \frac{\overrightarrow{e_{mn}^T} \cdot \overrightarrow{u_m}}{r_{mn}^2} \tag{2}$$

where A_n defines the row vectors of the transformation matrix A. z_{mn} is the lead vectors determined from the unit vectors e_{mn} and distances r_{mn} from each dipole position m to each unipolar electrode n. m denotes the dipole number and n denotes the ECG lead. u_m is the unit vectors of the dipoles. The lead vectors of the bipolar limb leads were calculated as shown in Equation 3.

$$\overrightarrow{z_{m(I)}} = \frac{\overrightarrow{e_{m(LA)}}}{r_{m(LA)}^2} - \frac{\overrightarrow{e_{m(RA)}}}{r_{m(RA)}^2} \qquad \overrightarrow{z_{mII}} = \frac{\overrightarrow{e_{m(LL)}}}{r_{m(LL)}^2} - \frac{\overrightarrow{e_{m(RA)}}}{r_{m(RA)}^2} \tag{3}$$

The resulting 8x6 A-matrix has column vectors defining the contribution of one dipole to all eight ECG leads, and row vectors defining the contribution of all dipoles to one ECG lead. The unit of a dipole is ampere×meter $(A \cdot m)$, however in this study the conductance constant was omitted, due to the assumption of homogeneous torso conductance, and therefore the dipole unit is referred to as an arbitrary unit (a.u.).

2.3. Solutions to the inverse ECG problem

In order to determine the dipole amplitudes x(t), i.e. solve the inverse problem, regularisation is needed due to the ill-posedness of the problem. The regularisations implemented and tested in this study were: Gaussian regularisation and two variations of the zero-order Tikhonov regularisation. One with a regularisation parameter $\lambda = 0$ and one with $\lambda = 30$, which was determined from an L-curve analysis.

The dipoles were in this study placed on the epicardial surface, in six different areas of the ventricles, pointing outward from the heart centre to represent the endocardial to epicardial direction of the electrical cardiac activation. The six dipoles were orthogonal to each other.

The dipole activations were approximated by the Interior-point optimisation algorithm. The objective function used in the optimisation was the sum of squared error (SSE) between the measured ECG and the ECG reconstructed from the dipoles, see Equation 4.

$$SSE = \sum \left(ECG_{reconstructed}(t) - ECG_{measured}(t) \right)^2 \tag{4}$$

The reconstructed ECG, $ECG_{reconstructed}(t)$, was calculated by multiplying the A-matrix and the dipole activations, i.e. the forward problem in Equation 1. In the case of Tikhonov regularisation

the objective function additionally included the regularisation term, $\lambda^2||L \cdot x||_2^2$, making the objective function of Tikhonov regularisation: $SSE + \lambda^2||L \cdot x||_2^2$.

The Gaussian regularisation constrained the dipole activations to be Gaussian shaped as a function of time, whereas the Tikhonov regularisation did not cause temporal constraints to the dipole activations. Further constraints were applied to the variable parameters of the solutions to limit the optimisation search to physiologically meaningful solutions, see Table 1.

		Constraints	
Regularisation	Gaussian	Tikhonov $\lambda = 0$	Tikhonov $\lambda = 30$
Constraints	$0 < \mu < 200$ ms $0 < a < 100$ a.u. $0 < d < 200$ ms	$0 < a < 100$ a.u.	$0 < a < 100$ a.u.

Table 1: Constraints of the implemented solutions. a = dipole amplitude, μ = time of peak activation, d = duration of activation, a.u.= arbitrary unit.

The solutions of all three methods were constrained to only attain positive amplitudes. The upper bound of the amplitude was set to 100 a.u., which was more than 2000-fold the typical maximum amplitude of the dipoles and hence just a practical notation. The Gaussian solution was constrained to have a duration shorter than the signal length (200 ms) as well as a peak activation within the signal length.

2.4. Dipole positions

To solve the inverse ECG problem, the six dipoles had to be fixed in position and direction. To determine the optimal position of the dipoles the accuracy of the ECG reconstruction, determined by the SSE, was investigated with the dipoles placed in various positions. The dipoles were simultaneously rotated with 10 degrees intervals of x-,y- and z-rotation from 0 to 80 degrees, yielding 729 different positions of the dipoles on the epicardial surface. The orthogonal relation between the dipoles were preserved in all rotations. The SSE in each position was calculated for 100 normal subjects and 100 LBBB subjects, respectively. The dipoles were optimised using the Tikhonov λ=0 regularisation, as it is the most commonly used method to solve the inverse ECG problem. The optimal dipole position was selected as the position yielding the generally lowest SSE across both groups of subjects.

2.5. Robustness

The robustness of the Gaussian, Tikhonov $\lambda = 0$ and Tikhonov $\lambda = 30$ methods to geometric and measurement noise was tested by comparing noise affected dipoles with control dipoles. The robustness test was performed using the geometric model and the corresponding ECG from ECGSim. The control dipoles were calculated without added noise.

The geometric noise was added by simultaneously shifting the positions of all six dipoles to random neighbour-nodes (median displacement of each dipole = 14.3 mm) while preserving the dipole directions. Measurement noise was applied by adding white Gaussian noise to the measured ECG signal. A signal to noise ratio of 20 dB was chosen, similar to other studies [27, 28, 29]. A total of 100 iterations with random measurement and geometric noise was performed, respectively.

The noise affected dipoles were compared to the control dipoles using three metrics: the difference in SSE, correlation between dipole activations, and difference in activation time. The activation time was determined as the time point of 50% cumulative activation.

2.6. Accuracy of the reconstructed ECG signals

The accuracy of the ECG signals reconstructed from dipoles achieved by the Gaussian, Tikhonov $\lambda = 0$ and Tikhonov $\lambda = 30$ regularisation was evaluated as SSE in 100 normal and 100 LBBB subjects. The type of regularisation yielding the lowest SSE in both the normal and LBBB subjects was selected for further analysis.

2.7. Dipole characteristics

The characteristics of the dipole activations were quantified by the activation time, amplitude and duration within the QRS complex. The amplitude was determined as the maximal amplitude of the dipole activation, the duration was determined as the time difference between 25 % and 75 % cumulative activation, and the activation time was defined at 50% cumulative activation, see Figure 1.

2.8. Quantification of dyssynchrony

The electrical interventricular dyssynchrony between the RV and LV was determined as the uncoupling of the global right ventricular (GRV) and global left ventricular (GLV) activation. The dyssynchrony measure was called left-right ventricular uncoupling (LRVU). GRV and GLV activations were calculated as a summation of the dipoles positioned in the RV and LV, respectively. Dipoles positioned at the border between the RV and LV were excluded. To assess LRVU, the GRV was subtracted from the GLV yielding a time dependent difference signal. Delayed GLV activation yields a biphasic difference signal with a negative wave followed by a larger positive wave. The LRVU was determined as the area of the positive wave of the difference signal, see Figure 2.
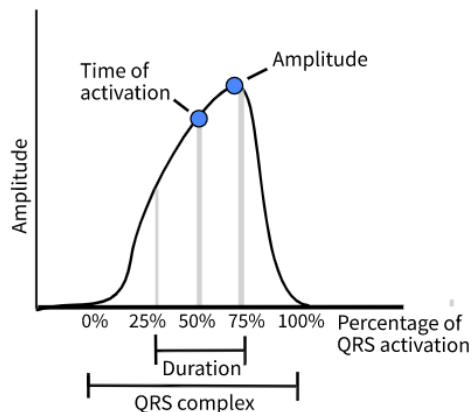

Figure 1: Conceptual illustration of a dipole activation with markings of activation time, amplitude, and duration.
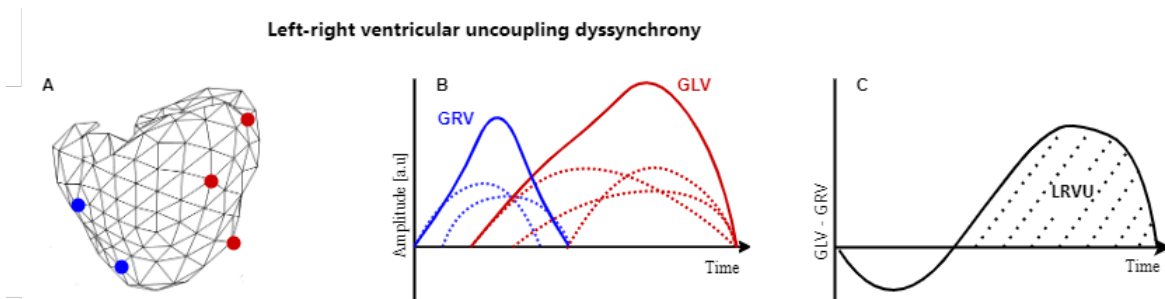

Figure 2: Conceptual illustration of the dyssynchrony measure left-right ventricular uncoupling (LRVU). Figure A illustrates dipole positions in the right (blue) and left (red) ventricle. Figure B represents the global right ventricular (GRV) activation and the global left ventricular (GLV) activation constituted by the sum of dipole activations (marked by dotted lines) in right and left ventricle, respectively. Figure C represents LRVU and the difference curve GLV-GRV from which LRVU is calculated as the marked area under the positive curve.

2.9. Statistical methods

All results were tested for normality using the Anderson-Darling test. Median, 25th percentile and 75th percentile were provided for non-normal distributed data. Outliers were defined as data points greater than $q_3 + 1.5(q_3 - q_1)$ or smaller than $q_1 - 1.5(q_3 - q_1)$, where q_1 and q_3 are the 25th and 75th percentile, respectively. Mean and standard deviation were provided for normal distributed data.

Comparisons of multiple dependent samples were performed using the Friedman's test followed by a post hoc analysis conducted with the Bonferroni test. Comparison of multiple independent samples were performed using a Kruskal-Wallis test followed by a Dunn post hoc test. The Mann-Whitney U test and two sample t-test were used for comparison of two groups with independent samples with non-normal and normal distribution, respectively. A Chi-square test was used to compare two independent binomial distributions.

The slope of linear regressions was tested using t-test, and the correlation was assessed by the squared Pearson correlation, denoted as r^2.

In all statistical tests, a significance level of 5% was used.

3. Results

3.1. Subject demographics

The demographics of the subjects from which the included data was recorded is presented in Table 2

Subject demographics			
	Normal	LBBB	CRT
Subjects, n	100	100	135
Female sex, n (%)	63 (63.0)	63 (63.0)	32 (23.7)*
Age [years]	20.0 [20, 20]	72 [63, 84]	71 [63, 77]
QRS duration [ms]	89.9 ±8.8	146.4 ±13.6	170.8 ±22.5*
QRS area [$\mu V \cdot s$]	9.8 [8.2, 11.3]	18.6 [15.9, 22.6]	14.9 [11.9, 18.6]*
Q-LV [ms]	-	-	134.9 ±28.6
Ischemic heart disease, n (%)	0 (0)	0 (0)	63 (46.6)*

Table 2: Demographics of included subjects. n abbreviates number. The age, QRS duration, QRS area and Q-LV are stated as mean ± standard deviation or in case of non-normality as median [p25, p75]. * denotes difference between LBBB and CRT groups.

3.2. Dipole positions

The dipole position yielding the generally lowest SSE across the normal and LBBB subjects was achieved with a rotation of x=60°, y=40°, z=0°. The optimal position and direction of the dipoles are shown in Figure 3.
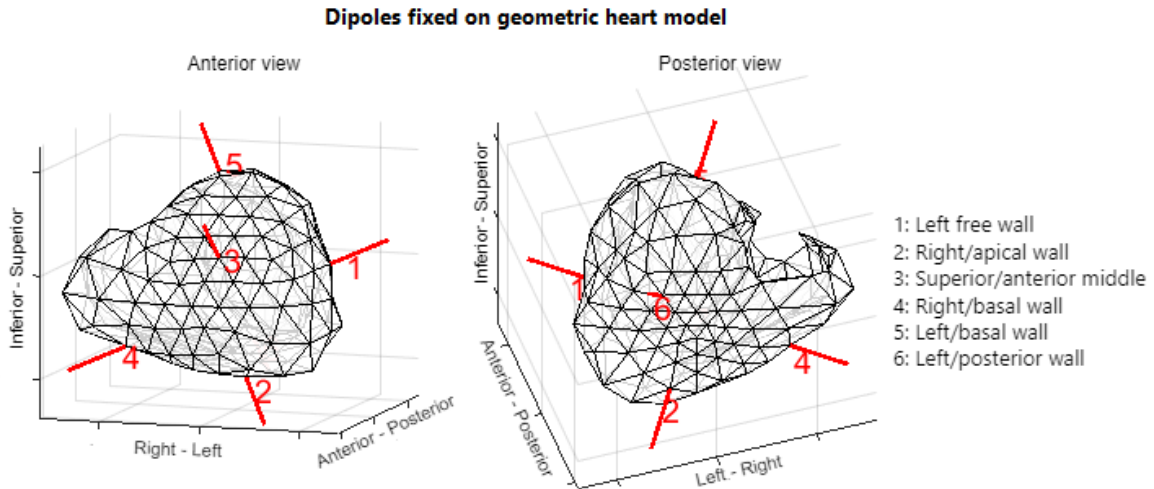

Figure 3: Optimal dipole position and direction with corresponding numeration.

These positions and directions of the dipoles were the foundation of all following results.

3.3. Robustness

The control dipoles of the Gaussian, Tikhonov $\lambda = 0$ and Tikhonov $\lambda = 30$ regularisation yielded different reconstructions of the ECG recording from ECGSim and hence different SSE values. The SSE of Gaussian control dipoles was $8.46mV^2$, whereas it for the Tikhonov $\lambda = 0$ was $7.66\ mV^2$ and for Tikhonov $\lambda = 30$ was $23.91\ mV^2$

All types of regularisation were more robust to measurement noise than to geometric noise, see Table 3.

Robustness to noise

Regularisation	Activation time difference from control [ms]	Correlation with control	SSE difference from control $[mV^2]$
	Geometric noise		
Gaussian	1 [0, 5]	0.86 [0.72, 0.94]	15.31 [4.94, 26.74]
Tikhonov $\lambda = 0$	2 [1, 6]	0.82 [0.68, 0.93]	14.74 [4.73, 25.30]
Tikhonov $\lambda = 30$	1 [0, 3]	0.96 [0.94, 0.98]	5.53 [1.67, 12.23]
	Measurement noise		
Gaussian	0 [0, 0]	1.00 [1.00, 1.00]	1.83 [1.57, 1.99]
Tikhonov $\lambda = 0$	0 [0, 1]	0.99 [0.99, 0.99]	0.66 [0.52, 0.88]
Tikhonov $\lambda = 30$	0 [0, 1]	0.99 [0.99, 0.99]	0.98 [0.63, 1.24]

Table 3: Median [p25,p75] of the Gaussian regularisation and Tikhonov using regularisation parameter λ=0 and λ=30 in 100 iterations of random noise. SSE = sum of squared error.

The Tikhonov λ=30 was more robust to geometric noise compared to the other types of regularisation. The Gaussian regularisation was extremely robust to measurement noise in terms of activation time difference and correlation of the noise affected dipoles to the control dipoles. The SSE difference however was highest in the Gaussian regularisation.

3.4. Accuracy of the reconstructed ECG signals

Significantly lower SSEs in both the normal and the LBBB subjects were achieved using Tikhonov λ=0 compared with Gaussian or Tikhonov λ=30 regularisation, see Table 4.

SSE in normal and LBBB subjects

	Normal	LBBB	P-value
Gaussian	7.36 [4.81,10.68]*	14.68 [10.01, 21.02]	<0.001
Tikhonov $\lambda = 0$	4.80 [3.03, 8.25]*	5.56 [3.03, 9.68]*	0.351
Tikhonov $\lambda = 30$	11.83 [7.14, 16.44]*	13.43 [9.39, 22.42]	0.003
P-value	<0.001	<0.001	

Table 4: Median [p25,p75] sum of squared error (SSE) of the Gaussian, Tikhonov $\lambda = 0$ and Tikhonov $\lambda = 30$ regularisation in 100 normal and 100 LBBB subjects. * indicates a difference from one type of regularisation to the two other types of regularisation within either normal or LBBB subjects. P-values in right column indicate a difference between normal and LBBB subjects. P-values in bottom row indicate difference among types of regularisations.

Tikhonov λ=0 yielded no significantly different SSE between the normal and LBBB subjects. Both the Gaussian and Tikhonov λ=30 achieved less accurate ECG reconstructions in the LBBB subjects compared to the normal subjects. The 75th percentiles of the SSE using the Gaussian and the Tikhonov λ=30 were 21.02 and 22.42 respectively, which were approximately twice as large as the Tikhonov $\lambda = 0$.

Examples of the reconstructed ECGs, the measured ECGs and the corresponding SSE is shown in Figure 4.
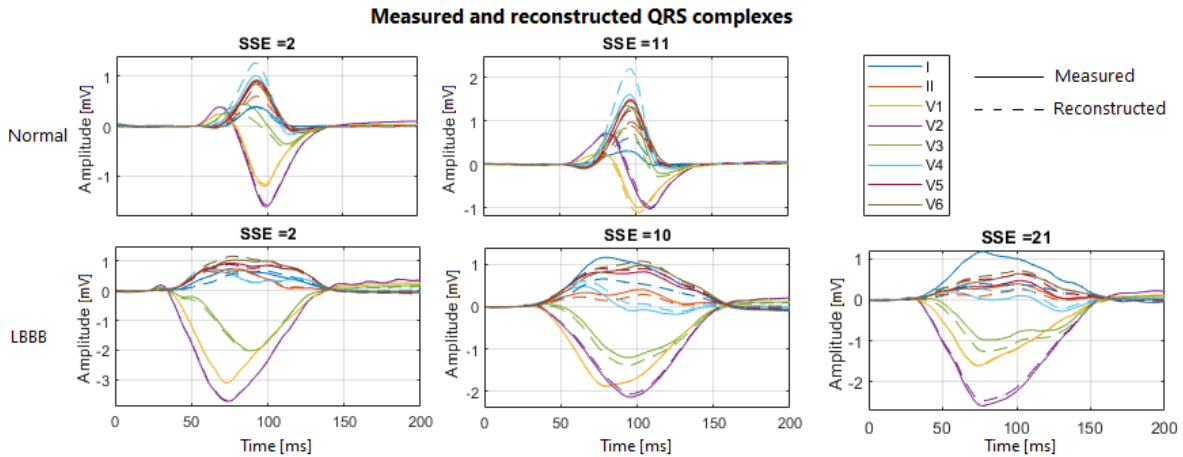
Figure 4: Reconstructed ECGs with different sum of squared error (SSE) values in normal and LBBB subjects. The ECGs were reconstructed from dipoles calculated with Tikhonov $\lambda=0$.

Since Tikhonov $\lambda=0$ was superior in ECG reconstruction in both normal and LBBB subjects, this regularisation was selected for the further assessment of the dipoles.

3.5. Dipole characteristics

The morphology of the dipoles was generally similar across the normal subjects. The activation pattern was Gaussian shaped, see Figure 5. Furthermore, there was a tendency in the normal subjects of simultaneous activation of dipole 1, 2, 3, 4 and 6 followed by a later activation of dipole 5.
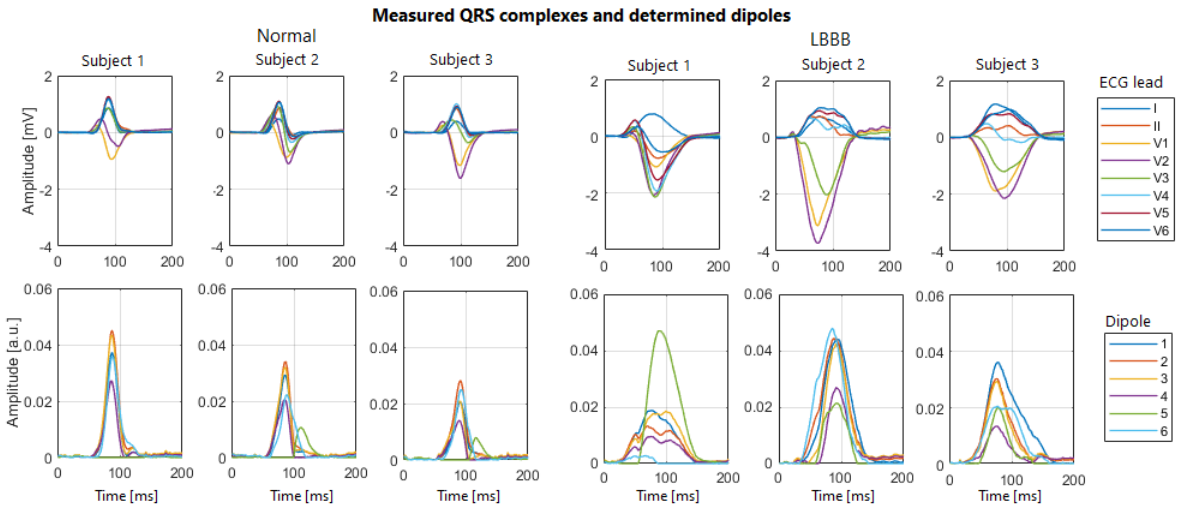
Figure 5: Example of dipoles determined using Tikhonov $\lambda=0$ along with measured ECG in three representative normal and three LBBB subjects. a.u. = arbitrary unit.

The dipoles of the LBBB subjects were more heterogeneous and not as Gaussian shaped as in the normal subjects. The QRS complexes of the LBBB subjects were also more different across subjects compared to the QRS complexes of normal subjects. The activation of the dipoles was less simultaneous in the LBBB subjects, and the dipole 5 was not as late activated as seen in the normal subjects.

The boxplot in Figure 6A supports the tendency of simultaneous activation in dipole 1, 2, 3, 4 and 6 and later activation of dipole 5 in the normal subjects.
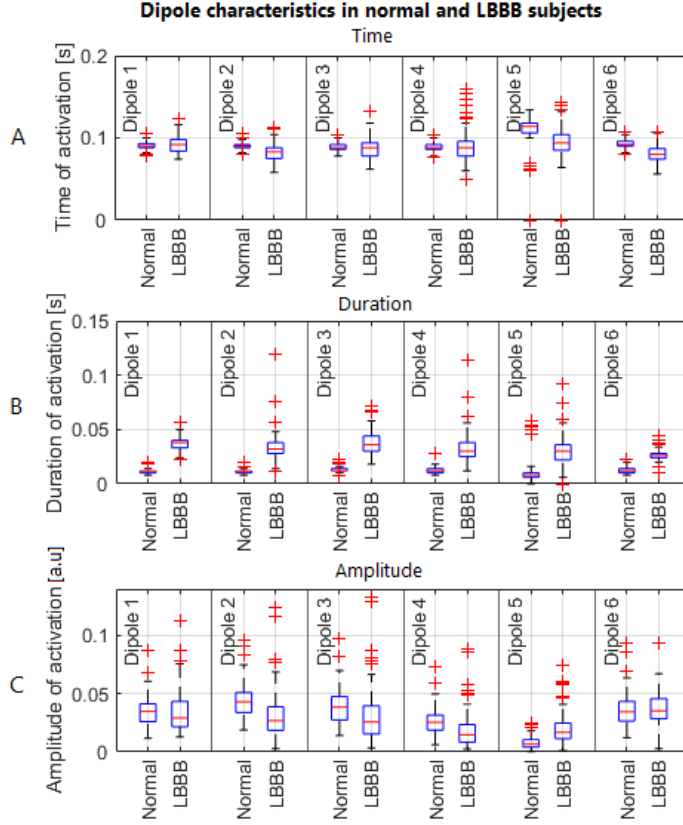
8

Figure 6: Time, duration and amplitude of the dipole activations across 100 normal and 100 LBBB subjects. The boxplots presents the median [p25, p75] along with whiskers and outliers. Whiskers extend to the most extreme data point that are not considered outliers. Outliers are data points greater than $q_3 + 1.5 \cdot (q_3 - q_1)$ and less than $q_1 - 1.5 \cdot (q_3 - q_1)$, where q_1 and q_3 are the 25th and 75th percentile, respectively. a.u. = arbitrary unit.

The interquartile range and whiskers of the LBBB subjects were wider in both time of activation (Figure 6A) and duration (Figure 6B), indicating more heterogeneous dipole activations compared to the normal subjects. The duration was longer in LBBB subjects compared to the normal subjects in all dipoles. The amplitudes of dipoles 2, 3 and 4 were remarkably lower in the LBBB subjects compared to the normal subjects, see Figure 6C. The dipoles with the lowest amplitudes in both normal and LBBB subjects were the basal dipoles; 4 and 5.

3.6. Quantification of dyssynchrony

The GRV activation was determined by dipole 2 and 4 and the GLV activation was determined by dipole 1, 5 and 6.

The LRVU of the LBBB subjects (2.4 [1.9, 3.1]) and the CRT subjects (2.0 [1.3, 2.7]) were higher than the normal subjects (0.3 [0.2, 0.4]). The LRVU was significantly different among all groups of subjects.

LRVU was positively correlated with QRS duration, QRS area and Q-LV in the normal, LBBB and CRT subjects. The LRVU had a higher correlation to the QRS area than to the QRS duration when assessed in the LBBB ($r^2 = 0.791, 0.359$) and CRT subjects ($r^2 = 0.630, 0.328$), see Figure 7A and 7B. The correlation between LRVU and both the QRS area ($r^2 = 0.178$) and the QRS duration ($r^2 = 0.093$) was lower in the normal subjects compared to the LBBB and CRT subjects.

The LRVU of the CRT subjects was also positively correlated with the Q-LV measure ($r^2 = 0.441$), see Figure 7C.
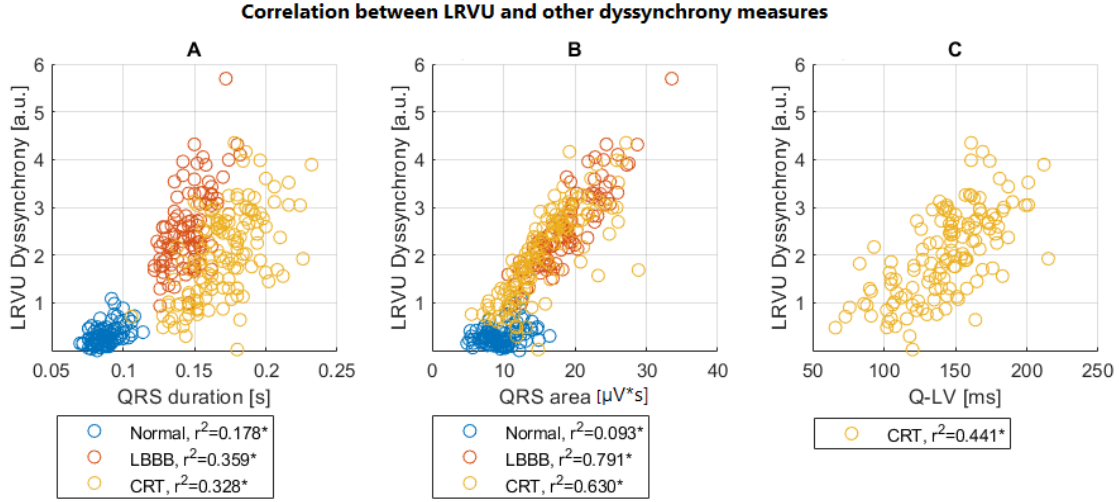
Figure 7: Correlation between left-right ventricular uncoupling (LRVU) and A: QRS duration and B: QRS area, in the normal, LBBB and CRT subjects. Figure C shows the correlation between LRVU and Q-LV in the CRT subjects. Significant linear slope within each group is denoted with '*'. a.u.=arbitrary unit.

Although all correlations were significant, the correlations of LRVU with QRS duration and QRS area were highest in the LBBB and CRT subjects compared to the normal subjects.

4. Discussion

Our study showed that it is possible to quantify interventricular dyssynchrony from epicardial dipoles determined by standard 12-lead ECG recordings and a generic heart-torso model. To our knowledge, this is the first study to solve the inverse ECG problem in only six epicardial dipoles by using standard 12-lead ECG recordings and a non-patient specific heart-torso geometry.

The interventricular electrical dyssynchrony, measured as LRVU, was positively correlated with QRS duration and QRS area in subjects with LBBB and in subjects admitted to CRT. The LRVU was furthermore positively correlated with Q-LV.

Regularisation of the dipole activations was performed due to the ill-posedness of the inverse ECG problem. Three types of regularisation were investigated of which zero-order Tikhonov regularisation with a regularisation parameter of $\lambda=0$ yielded the most accurate reconstructions of the ECG signals in both the normal and LBBB subjects. Tikhonov regularisation with a regularisation parameter of $\lambda = 30$ yielded the most robust solutions to geometric noise. However, the accuracy of the reconstructed ECGs was low, particularly in the LBBB subjects. The Gaussian regularisation yielded solutions that were extremely robust to measurement noise, but similar to the Tikhonov $\lambda = 30$ a low accuracy was seen in the reconstruction of the ECG signals from LBBB subjects. Hence both the Gaussian regularisation and Tikhonov $\lambda = 30$ regularisation yielded over-regularised solutions unsuitable for reflecting epicardial activation of LBBB subjects. The Tikhonov $\lambda=0$ did in fact not regularise the solutions, but solely optimised the dipole activations yielding minimum SSE complying with a requirement of positive amplitudes. A possible reason why the non-regularised solution was superior might be caused by the low number of dipoles and the constraint of positive amplitudes being a sufficient inherent regularisation yielding accurate and robust solutions.

The dipoles were assumed to reflect the surrounding myocardial depolarisation. A fundamental prerequisite for the dipole activations to actually reflect the myocardial activation is their ability to reconstruct the ECG accurately. This was, as before mentioned, achieved in both the LBBB and normal subjects when using Tikhonov $\lambda = 0$ regularisation. Furthermore, the morphology of the dipoles should comply with the expected physiological activation of the tissue surrounding each dipole. Therefore,

the characteristics of the dipoles were assessed in relation to the expected activations. The estimated dipoles showed that the time of activation was simultaneous in the normal subjects, except a later activation in the dipole representing the left/basal wall (dipole 5). This is in accordance with the physiology of the normal ventricular depolarisation [30]. The lowest dipole amplitudes were seen in the basal dipoles (dipole 4 and dipole 5) in both normal and LBBB subjects, which can be related to the lower amount of myocardial mass in that particular area. It was in the LBBB subjects expected that the dipoles representing the RV would have a similar activation as the normal subjects. However, the duration increased in both RV and LV dipoles, which indicates that the inverse solution might not be capable of separating the ECG into six independent dipoles. Despite the prolonged duration in all dipoles, an increased relative difference between the activation of the RV and LV dipoles was seen, which yielded a measure of the electrical dyssynchrony between the RV and LV, called LRVU.

The LRVU reflects the amount of global left ventricular, GLV, activation, that does not occur simultaneously with the global right ventricle, GRV. In case of a normal heart the RV and LV are expected to be activated simultaneously causing a small difference between GLV and GRV, hence a smaller LRVU. A dyssynchronously activated LBBB heart, however, is expected to have a delayed activation of the LV causing a larger difference between GLV and GRV, hence a larger LRVU.

LRVU was higher in the LBBB (2.4 [1.9, 3.1]) and CRT subjects (2.0 [1.3, 2.7]) compared to the normal subjects (0.3 [0.2, 0.4]). This is in accordance with the general assumption that a majority of LBBB and CRT subjects suffer from dyssynchronous activation of the ventricles whereas the normal subjects do not. The highest correlation of LRVU with QRS duration and QRS area was achieved in the LBBB subjects. A similar but lower correlation was seen in the CRT subjects. In contrary, the LRVU in the normal subjects had a low correlation with the QRS duration and QRS area. The ECG signals of the normal subjects were very homogeneous, and thus only small variations in QRS duration and QRS area existed. These small variations might not be related to dyssynchronous ventricular activation but to other individual physiological and anatomical differences.

A ground truth of the electrical dyssynchrony between RV and LV is not available and no feasible way of obtaining it exists. Hence other measures are required to evaluate the validity of the developed dyssynchrony measure. In the study by Haq et al. [31] QRS duration and QRS area were also used to evaluate VEU. The QRS duration and QRS area as well as Q-LV, as used in this study, are indirect measures of electrical dyssynchrony and are associated with CRT response to a varying degree [1, 8, 9, 10]. Thereby some degree of correlation between LRVU and QRS duration, QRS area and Q-LV is expected, if LRVU in fact is a measure of electrical dyssynchrony associated with CRT response. However, no significant correlation between the interventricular dyssynchrony measure VEU and QRS duration or QRS area was found in the study by [31], even though an association between VEU and CRT response was shown in the study by Ploux et al. [11]. The lack of correlation of VEU with QRS duration and QRS area could be caused by their heterogeneous study population with a low number of subjects (n=32) or due to a difference between interventricular dyssynchrony and global dyssynchrony. Thereby, it is uncertain to which degree LRVU should be correlated with QRS duration, QRS area and Q-LV in order to predict CRT response.

A way of creating a ground truth of the electrical dyssynchrony is by simulating the electrical activity. In simulations studies, the cardiac potentials are simulated which enables comparison between calculated and simulated action potentials [20, 32, 33]. However, it remains uncertain whether the inverse solution is capable of determining the myocardial activation in a real heart.

In future studies, the proposed inverse solution should be tested on larger and more heterogeneous populations. Since the proposed solution is based on standard 12-lead ECG recordings and a generic heart-torso model, it is possible to assess the LRVU in previously recorded data, and hence utilise existing databases with longitudinal ECG recordings and ECG recordings of various patient groups. Furthermore, the validity of the LRVU should be investigated by correlating it with the clinical outcome after CRT implantation, and thereby evaluate the potential of the measure to improve patient selection for CRT.

5. Limitations

The population of subjects with normal ECGs were all 20 years old and the LBBB subjects included only patients with LBBB and no other abnormalities in the ECG. The homogeneous groups of subjects limit the insight into how the LVRU performs in a more general population. Evaluation of LRVU in populations with other and more heterogeneous cardiac diseases is of great importance for LRVU to be clinically applicable.

The solutions were in this study achieved from a single heart-torso model. For further validation of using a generic heart-torso model, the LRVU should be determined and compared using several different heart-torso geometric models.

6. Conclusion

Interventricular dyssynchrony can be quantified as left-right ventricular uncoupling (LRVU) from six epicardial dipoles determined by standard 12-lead ECG recordings and a generic heart-torso model. A higher LRVU was found in subjects with LBBB and subjects admitted to CRT compared to normal subjects.

LRVU is correlated with QRS duration and QRS area, particularly in LBBB patients and is further correlated with Q-LV measured in subjects admitted to CRT implantation. Solving the inverse ECG problem, based on 12-lead ECG, to obtain interventricular electrical dyssynchrony has great clinical applicability and has the potential to assist patient selection for CRT treatment.

References

[1] M. Brignole, A. Auricchio, G. Baron-Esquivias, P. Bordachar, G. Boriani, O.-A. Breithardt, J. Cleland, J.-C. Deharo, V. Delgado, P. M. Elliott, B. Gorenek, C. W. Israel, C. Leclercq, C. Linde, L. Mont, L. Padeletti, R. Sutton, P. E. Vardas, 2013 ESC Guidelines on cardiac pacing and cardiac resynchronization therapy - The Task Force on cardiac pacing and resynchronization therapy of the European Society of Cardiology (ESC). Developed in collaboration with the European Heart Rhythm Association, Europace 15 (8) (2013) 1070–1118. doi:10.1093/europace/eut206.

[2] J. J. Mcmurray, S. Adamopoulos, S. D. Anker, A. Auricchio, M. Böhm, K. Dickstein, V. Falk, G. Filippatos, C. Fonseca, M. A. Gomez-Sanchez, T. Jaarsma, L. Kober, G. Y. Lip, A. P. Maggioni, A. Parkhomenko, B. M. Pieske, B. A. Popescu, P. K. Ronnevik, F. H. Rutten, J. Schwitter, P. Seferovic, J. Stepinska, P. T. Trindade, A. A. Voors, F. Zannad, Zeiher, ESC Guidelines for the diagnosis and treatment of acute and chronic heart failure 2012, European Journal of Heart Failure 14 (8) (2012) 803–869. doi:10.1093/eurjhf/hfs105.

[3] F. M. Kusumoto, M. H. Schoenfeld, C. Barrett, J. R. Edgerton, K. A. Ellenbogen, M. R. Gold, N. F. Goldschlager, R. M. Hamilton, J. A. Joglar, R. J. Kim, R. Lee, J. E. Marine, C. J. McLeod, K. R. Oken, K. K. Patton, C. N. Pellegrini, K. A. Selzman, A. Thompson, P. D. Varosy, 2018 ACC/AHA/HRS Guideline on the Evaluation and Management of Patients With Bradycardia and Cardiac Conduction Delay: A Report of the American College of Cardiology/American Heart Association Task Force on Clinical Practice Guidelines and the Heart Rhyth, Circulation 140 (2019) e382–e482. doi:10.1161/CIR.0000000000000628.

[4] B. J. Sieniewicz, J. Gould, B. Porter, B. S. Sidhu, T. Teall, J. Webb, G. Carr-White, C. A. Rinaldi, Understanding non-response to cardiac resynchronisation therapy: common problems and potential solutions, Heart Failure Reviews 24 (1) (2019) 41–54. doi:10.1007/s10741-018-9734-8.

[5] A. Noheria, S. Sodhi, G. J. Orme, The evolving role of electrocardiography in cardiac resynchronization therapy, Current Treatment Options in Cardiovascular Medicine 21 (2019) 1–14. doi:10.1007/s11936-019-0784-6.

[6] A. L. Goldberger, Z. D. Goldberger, A. Shvilkin, Ventricular Conduction Disturbances: Bundle Branch Blocks and Related Abnormalities, Elsevier, 2017.

[7] C. J. van Deursen, K. Vernooy, E. Dudink, L. Bergfeldt, H. J. Crijns, F. W. Prinzen, L. Wecke, Vectorcardiographic qrs area as a novel predictor of response to cardiac resynchronization therapy, Journal of Electrocardiology 48 (2015) 45–52. doi:10.1016/j.jelectrocard.2014.10.003.

[8] N. Tokavanich, N. Prasitlumkum, W. Mongkonsritragoon, A. Trongtorsak, W. Cheungpasitporn, R. Chokesuwattanaskul, Qrs area as a predictor of cardiac resynchronization therapy response: A systematic review and meta-analysis, Pacing and Clinical Electrophysiology 45 (2022) 393–400. doi:10.1111/pace.14441.

[9] K. Emerek, D. J. Friedman, P. L. Sørensen, S. M. Hansen, J. M. Larsen, N. Risum, A. M. Thøgersen, C. Graff, J. Kisslo, P. Søgaard, B. D. Atwater, Vectorcardiographic qrs area is associated with long-term outcome following cardiac resynchronization therapy, Heart Rythm 16 (2019) 213–219. `doi:10.1016/j.hrthm.2018.08.028`.

[10] M. R. Gold, U. Birgersdotter-Green, J. P. Singh, K. A. Ellenbogen, Y. Yu, T. E. Meyer, M. Seth, , P. J. Tchou, The relationship between ventricular electrical delay and left ventricular remodelling with cardiac resynchronization therapy, European Heart Journal 32 (2011) 2516–2524. `doi:10.1093/eurheartj/ehr329`.

[11] S. Ploux, J. Lumens, Z. Whinnett, A. Zemmoura, A. Denis, M. D. Guillebon, A. Shah, M. Hocini, P. Jaïs, P. Ritter, M. Haïssaguerre, B. L. Wilkoff, P. Bordachar, Noninvasive electrocardiographic mapping to improve patient selection for cardiac resynchronization therapy, Journal of the American College of Cardiology 61 (2013) –. `doi:10.1016/j.jacc.2013.01.093`.

[12] L. R. Bear, P. R. Huntjens, R. D. Walton, O. Bernus, R. Coronel, R. Dubois, Cardiac electrical dyssynchrony is accurately detected by noninvasive electrocardiographic imaging, Heart Rhythm 15 (2018) 1058–1069. `doi:10.1016/j.hrthm.2018.02.024`.

[13] N. Varma, P. Jia, Y. Rudy, Electrocardiographic imaging of patients with heart failure with left bundle branch block and response to cardiac resynchronization therapy, Journal of Electrocardiology 40 (2007) 174–178. `doi:10.1016/j.jelectrocard.2007.06.017`.

[14] L. G. Tereshchenko, E. Ghafoori, M. M. Kabir, M. Kowalsky, Electrical dyssynchrony on noninvasive electrocardiographic mapping correlates with sai qrst on surface ecg, Computing in Cardiology 2015 (2015) 69–72. `doi:10.1109/CIC.2015.7408588`.

[15] S. Ghosh, J. N. Silva, R. M. Canham, T. M. Bowman, E. K. Zhang, Junjie andnRhee, P. K. Woodard, Y. Rudy, Electrophysiologic substrate and intraventricular left ventricular dyssynchrony in nonischemic heart failure patients undergoing cardiac resynchronization therapy, Heart Rhythm 8 (2011) 692–699. `doi:10.1016/j.hrthm.2011.01.017`.

[16] A. J. Pullan, L. K. Cheng, M. P. Nash, A. Ghodrati, R. MacLeod, D. H. Brooks, The Inverse Problem of Electrocardiography, Springer, London, 2010, chapter 9.

[17] V. Kara, H. Ni, E. A. P. Alday, H. Zhang, Corrigendum: Ecg imaging to detect the site of ventricular ischemia using torso electrodes: A computational study, Frontiers in physiology 10 (2019) 692. `doi:10.3389/fphys.2019.00692`.

[18] P. R. Johnston, Accuracy of electrocardiographic imaging using the method of fundamental solutions, Computers in Biology and Medicine 102 (2018) 433–448. `doi:10.1016/j.compbiomed.2018.09.016`.

[19] M. Jiang, L. Xia, G. Shou, Q. Wei, F. Liu, S. Crozier, Effect of cardiac motion on solution of the electrocardiography inverse problem, IEEE transactions of biomedical engineering 56 (2009) 923–931. `doi:10.1109/TBME.2008.2005967`.

[20] J. P. Barnes, P. R. Johnston, Application of robust generalised cross-validation to the inverse problem, Computers in Biology and Medicine 69 (2016) 213–225. `doi:10.1016/j.compbiomed.2015.12.011`.

[21] Y. Serinagaoglu, D. H. B. R. S. MacLeod, Improved performance of bayesian solutions for inverse electrocardiography using multiple information sources, IEEE transactions of biomedical engineering 52 (2006) 2024–2034. `doi:10.1109/TBME.2006.881776`.

[22] Y. Nakano, E. Rashed, T. Nakane, A. Laakso, I. andSensors Hirata, Ecg localization method based on volume conductor model and kalman filtering, Sensors 21 (2021) 4275. `doi:10.3390/s21134275`.

[23] D. Potyagaylo, O. Dossel, P. van Dam, Influence of modeling errors on the initial estimate for nonlinear myocardial activation times imaging calculated with fastest route algorithm, IEEE Transactions on Biomedical Engineering 63 (2016) 2576–2584. `doi:10.1109/TBME.2016.2561973`.

[24] A. Sommer, M. B. Kronborg, B. L. Nørgaard, S. H. Poulsen, K. Bouchelouche, M. Böttcher, H. K. Jensen, J. M. Jensen, J. Kristensen, C. Gerdes, P. T. Mortensen, J. C. Nielsen, Multimodality imaging-guided left ventricularlead placement in cardiac resynchronizationtherapy: a randomized controlled trial, European Journal of Heart Failure 18 (2016) 1365–1374. `doi:10.1002/ejhf.530`.

[25] A. van Oosterom, T. Oostendorp, P. van Dam, Ecgsim, latest seen - 25.05.2022 (2022).
URL `https://www.ecgsim.org/`

[26] GE Healthcare, Marquette 12SL - ECG Analysis Program - Physician's Guide (2019).

[27] G. Shou, L. Xia, F. Liu, M. Jiang, S. Crozier, On epicardial potential reconstruction using regularization schemes with the l1-norm data term, Physics in Medicine and Biology 56 (2011) 57–72. `doi:10.1088/0031-9155/56/1/004`.

[28] J. van der Waal, V. Meijborg, S. Schuler, R. Coronel, T. Oostendorp, In silico validation of electrocardiographic imaging to reconstruct the endocardial and epicardial repolarization pattern using the equivalent dipole layer source model, Medical and Biological Engineering and Computing 58 (2020) 1739–1749. `doi:10.1007/s11517-020-02203-y`.

[29] S. Schuler, M. Schaufelberger, L. R. Bear, J. Bergquist, M. Cluitmans, J. Coll-Font, O. N. Onak, B. Zenger, A. Loewe, R. Macleod, D. H. Brooks, O. Doessel, Reducing line-of-block artifacts in cardiac activation maps estimated using ecg imaging: A comparison of source models and estimation methods, IEEE Transactions on Biomedical Engineering 2021 (2021) Dec 14. `doi:10.1109/TBME.2021.3135154`.

[30] J. Malmivuo, R. Plonsey, Principles and Applications of Bioelectric and Biomagnetic Fields, Oxford University Press, New York, 1995.

[31] K. T. Haq, N. M. Rogovoy, J. A. Thomas, C. Hamilton, K. J. Lutz, A. Wirth, A. B. Bender, D. M. German, R. Przybylowicz, P. van Dam, T. A. Dewland, K. Dalouk, E. Stecker, B. Nazer, P. M. Jessel, K. S. MacMurdy, I. G. E. Zarraga, B. Beitinjaneh, C. A. Henrikson, M. Raitt, C. Fuss, M. Ferencik, L. G. Tereshchenko, Adaptive cardiac resynchronization therapy effect on electrical dyssynchrony (acrt-elsync): A randomized controlled trial, Heart Rhythm O2 2 (2021) 374–381. `doi:10.1016/j.hroo.2021.06.006`.

[32] T. Konttila, V. Mäntynen, M. Stenroos, Comparison of minimum-norm estimation and beamforming in electrocardiography with acute ischemia, Physiological Measurement 35 (4) (2014). `doi:10.1088/0967-3334/35/4/623`.

[33] P. M. van Dam, T. F. Oostendorp, A. C. Linnenbank, A. van Oosterom, Non-invasive imaging of cardiac activation and recovery, Annals of Biomedical Engineering 37 (2009) 1739–1756. `doi:10.1007/s10439-009-9747-5`.

Worksheets: Quantification of interventricular dyssynchrony using a standard 12-lead ECG based solution to the inverse ECG problem
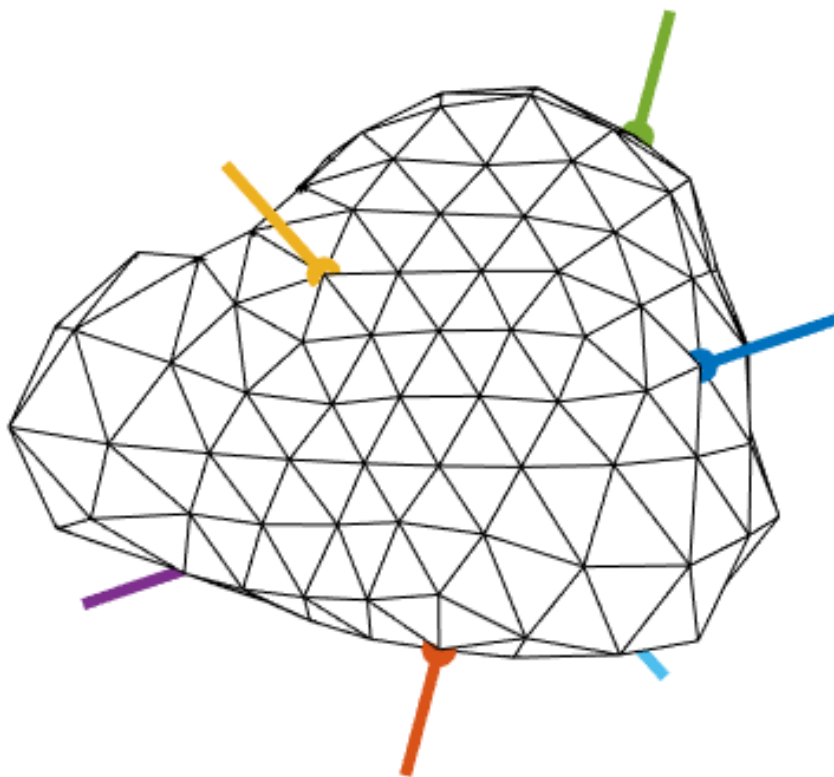
P10 Project - Group 14
Frederik Samuelsen, Gry Bruun Grønborg and
Maria Goncalves Møller
Biomedical Engineering and Informatics
Aalborg University
The 1st of June 2022

AALBORG UNIVERSITET

STUDENTERRAPPORT

Titel:

Kvantificering af interventrikulær dyssynkroni ved brug af en standard 12-aflednings EKG baseret løsning af det inverse EKG problem

Projekt:

Kandidatspeciale i sundhedsteknologi

Projektperiode:

Februar 2022 - Juni 2021

ECTS:

30

Projektgruppe:

Gruppe 14

Deltagere:

Frederik Samuelsen
Gry Bruun Grønborg
Maria Goncalves Møller

Vejleder:

Claus Graff

Bivejledere:

Jacob Melgaard
Johannes Jan Struijk

Artikel: 12 sider
Arbejdsblade: 62 sider
Bilag: 12 sider
Afsluttet: 01-06-2022

Resumé

Baggrund: Alvorlige tilfælde af venstresidig grenblok (LBBB) behandles med cardiac resynchronisation therapy (CRT), dog responderer mere end 30% af patienterne ikke på behandlingen, hvilket potentielt skyldes manglende elektrisk dyssynkroni. For at forbedre udvælgelsen af patienter til CRT implantation, kan ventrikel dyssynkroni potentielt kvantificeres ved at løse det inverse EKG-problem. Eksisterende løsninger baserer sig på >100 overflademålinger samt patientspecifikke modeller, hvilket begrænser anvendeligheden i klinisk praksis. Dette studie forsøger at bestemme den elektriske aktivering af ventriklerne ud fra 12-aflednings EKG målinger og en generisk hjerte-torso model, samt at kvantificere den interventrikulære elektriske dyssynkroni.

Metode: Standard 12-aflednings EKG målinger fra 100 normale, 100 LBBB subjekter og 135 subjekter inden implantation af CRT, var inkluderet. Ved at løse det inverse EKG problem kunne ventrikel-aktiveringen bestemmes i seks dipoler. Præcision og robusthed ved Gaussisk og Tikhonov regularisering med regulariseringsparameter $\lambda=0$ og $\lambda=30$ blev sammenlignet. Interventrikulær dyssynkroni blev målt som venstre-højre venkrikulær dyssynkroni (LRVU), og blev sammenlignet med QRS varighed, QRS areal og Q-LV.

Resultater: Tikhonov $\lambda=0$ havde den mest akkurate EKG rekonstruktion i både normale og LBBB subjekter. LRVU var højere i LBBB subjekter sammenlignet med normale subjekter. Korrelationen af LRVU med QRS varighed og QRS areal var højere for LBBB($r^2=0.359$, 0.791) og CRT subjekter($r^2=0.328$, 0.630) sammenlignet med normale subjekter($r^2=0.178$, 0.093). Yderligere var LRVU korreleret med Q-LV i CRT subjekter($r^2=0.441$).

Konklusion: Interventrikulær dyssynkroni kan kvantificeres ved at løse det inverse EKG problem ved standard 12-aflednings EKG og en generisk hjerte-torso model.

AALBORG UNIVERSITY
STUDENT REPORT

Title:

Quantification of interventricular dyssynchrony using a standard 12-lead ECG based solution to the inverse ECG problem

Theme:

Master's Thesis in biomedical engineering and informatics

Project period:

February 2022 - June 2022

ECTS:

30

Project group:

Group 14

Participants:

Frederik Samuelsen

Gry Bruun Grønborg

Maria Goncalves Møller

Supervisor:

Claus Graff

Co-supervisors:

Jacob Melgaard

Johannes Jan Struijk

Article: 12 pages
Worksheets: 62 pages
Appendix: 12 pages
Completed: 01-06-2022

Abstract

Background: Severe left bundle branch block (LBBB) is treated with cardiac resynchronisation therapy (CRT), however more than 30% treated with CRT are non-responders, likely due to absence of electrical dyssynchrony. In order to improve patient selection, interventricular dyssynchrony can potentially be quantified by solving the inverse electrocardiography (ECG) problem. Existing solutions are based on >100 body surface measurements and patient specific geometries, which limits the clinical applicability. This study aims to determine the electrical activation of the ventricles from standard 12-lead ECG recordings and a generic heart-torso model, and quantify the interventricular electrical dyssynchrony.

Method: Standard 12-lead ECG recordings from 100 normal subjects, 100 LBBB subjects, and 135 subjects admitted to CRT were included. The ventricular myocardial activation was determined in six dipoles. The accuracy and robustness of Gaussian regularisation and Tikhonov regularisation with regularisation parameter $\lambda=0$ and $\lambda=30$ was compared. Interventricular dyssynchrony was determined as the left-right ventricular uncoupling (LRVU) and compared to QRS duration, QRS area and Q-LV.

Results: Tikhonov $\lambda=0$ yielded the most accurate ECG reconstruction in both normal and LBBB subjects. LRVU was higher in LBBB subjects compared to normal subjects. The correlation of LRVU with QRS duration and QRS area was higher in LBBB(r^2=0.359, 0.791) and CRT subjects(r^2=0.328, 0.630) compared to normal subjects(r^2=0.178, 0.093). Furthermore LRVU was correlated with Q-LV in CRT subjects (r^2=0.441).

Conclusion: Interventricular dyssynchrony can be quantified by solving the inverse ECG problem by standard 12-lead ECG and a generic heart-torso model.
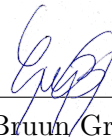
Preface

This project is a Master's Thesis in Biomedical Engineering and Informatics carried out during the spring of 2022. The project was conveyed as an article with supplementary worksheets, containing elaboration of the problem domain, methods and results. Furthermore a collaboration portfolio is presented in Appendix A.

We would like to thank our supervisor Claus Graff for competent and committed supervision throughout the semester. We are also thankful to Jacob Melgaard and Johannes Jan Struijk for their readiness in co-supervision of the project.

All methods, statistical tests and graphs are executed and visualised using MATLAB. All illustrations are made by the group members or are licensed for use.

Frederik Samuelsen	Gry Bruun Grønborg

Maria Goncalves Møller

Contents

1 | Problem analysis

The problem analysis includes two major sections, with the first being an elaboration of left bundle branch block (LBBB) and its clinical challenges and the second being an overview of novel approaches to quantify ventricular electrical dyssynchrony along with state of the art solutions to the inverse ECG problem.

1.1 Left bundle branch block

In the following sections, the patophysiology, diagnose criteria, prevalence, prognosis and treatment of LBBB are elaborated.

1.1.1 Pathophysiology

The pathophysiology of LBBB originates from the conduction pathways of the ventricles, shown in Figure 1.1. The bundle of His connects the atrioventricular node to the bundle branches. The bundle branch extends to both left bundle branch (LBB) and right bundle branch (RBB). The LBB is divided further into the left anterior fascicle and left posterior fascicle, from where Purkinje fibers spread to the subendocardium and facilitates the activation of myocardium. [Tan et al., 2020]

Lesions in the bundle of His, bundle branches or fascicles hinders the normal electrical conduction through the ventricles. LBBB is the condition when a lesion occurs proximally in the specialised conduction system in the left ventricle (LV), causing interventricular dyssynchrony, since the left ventricle activates later than the right ventricle (RV). The red stars in Figure 1.1 represent locations where the lesions can occur. Star No. 2 illustrates LBBB, whereas star No. 1, No.3 and No.4 illustrates locations of lesions causing other conduction disorders.
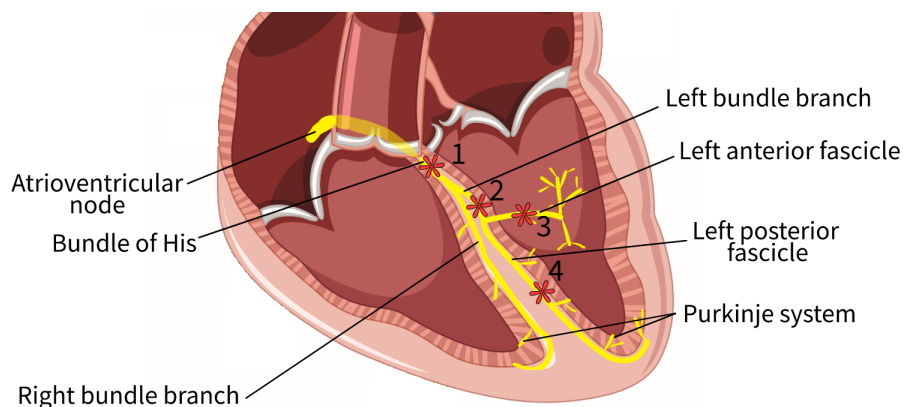

Figure 1.1. *Cross section of the heart, with the conduction path from the atrioventricular node to the Purkinje system. Numerated left stars defines lesions that results in 1: Infranodal atrioventricular block, 2: Left bundle branch block, 3: Left anterior fascicular block, and 4: Left posterior fascicular block. The figure was inspired by Tan et al. [2020].*

Lesion located in star no. 1 results in infranodal atrioventricular block and lesions in no. 3 or 4 results in left anterior fascicular block or left posterior fascicular block, respectively.

1.1.1.1 Electrophysiological ventricular dyssynchrony

The electrical activation of the ventricles is abnormal in LBBB subjects, since the activation through the left bundle branch is blocked. In a healthy heart, the depolarisation of the RV and LV is synchronously activated through the bundle branches and Purkinje fibres, starting with activation of the septum followed by a depolarisation of the apex and eventually the parts of the ventricles near the base are depolarised [Malmivuo and Plonsey, 1995; Hall and Guyton, 2011]. In LBBB subjects, the sequence of electric activation of the ventricles starts in the right septum through the intact right bundle branch. The rest of the RV myocardium is activated through the right bundle branch and Purkinje system. The activation of the LV is however not facilitated through the bundle branch and Purkinje system, but propagates from the RV through septum to the lateral and posterior wall through gap junctions from cell to cell. This electrical activation through the myocardium is slower than through the normal conduction system, which causes prolonged QRS duration on the electrocardiogram (ECG) in LBBB subjects [Tan et al., 2020]. The prolonged QRS complex caused by a block has been demonstrated in canine hearts by inducing LBBB using radiofrequency ablation which caused the QRS duration to increase from 66 ± 8.4 ms before inducing LBBB to 113 ± 12.8 ms after inducing LBBB [Verbeek et al., 2003].

The altered conduction paths in LBBB subjects thereby causes electric interventricular dyssynchrony, which can further result in mechanical dyssynchrony [Sieniewicz et al., 2019].

1.1.1.2 Mechanical ventricular dyssynchrony

The abnormal electrical activation of the heart in LBBB subjects yields altered mechanical movements of the heart. In LBBB subjects, the RV is initially contracted followed by a contraction of septum, which stretches the relaxed left posterior and lateral walls. Subsequently these walls are activated, but because of the dyssynchrony the septum is now relaxed and therefore passively stretched out. The dyssynchrony between the septum and lateral/posterior walls results in a decreased contraction efficiency, which is reflected as a reduction in the left ventricular ejection fraction (LVEF). [Tan et al., 2020; Baldasseroni et al., 2002]

1.1.2 Diagnose criteria

LBBB is defined by the American Heart Association, American College of Cardiology Foundation and Heart Rhythm Society as a QRS complex duration of ≥ 120 ms along with several other morphological descriptions of individual leads, presented on the list below [Kusumoto et al., 2019] and shown on Figure 1.2. [Kusumoto et al., 2019]

1. *QRS duration ≥ 120 ms in adults*

2. *Broad notched or slurred R wave in leads I, aVL, V5, and V6 and an occasional RS pattern in V5 and V6 attributed to displaced transition of QRS complex*

3. *Absent Q waves in leads I, V5, and V6, but in the lead aVL, a narrow Q wave may be present in the absence of myocardial pathology*

4. *R peak time > 60 ms in leads V5 and V6 but normal in leads V1 , V2, and V3 , when small initial R waves can be discerned in the precordial leads*

5. *ST and T waves usually opposite in direction to QRS*

(Quoted from [Kusumoto et al., 2019])
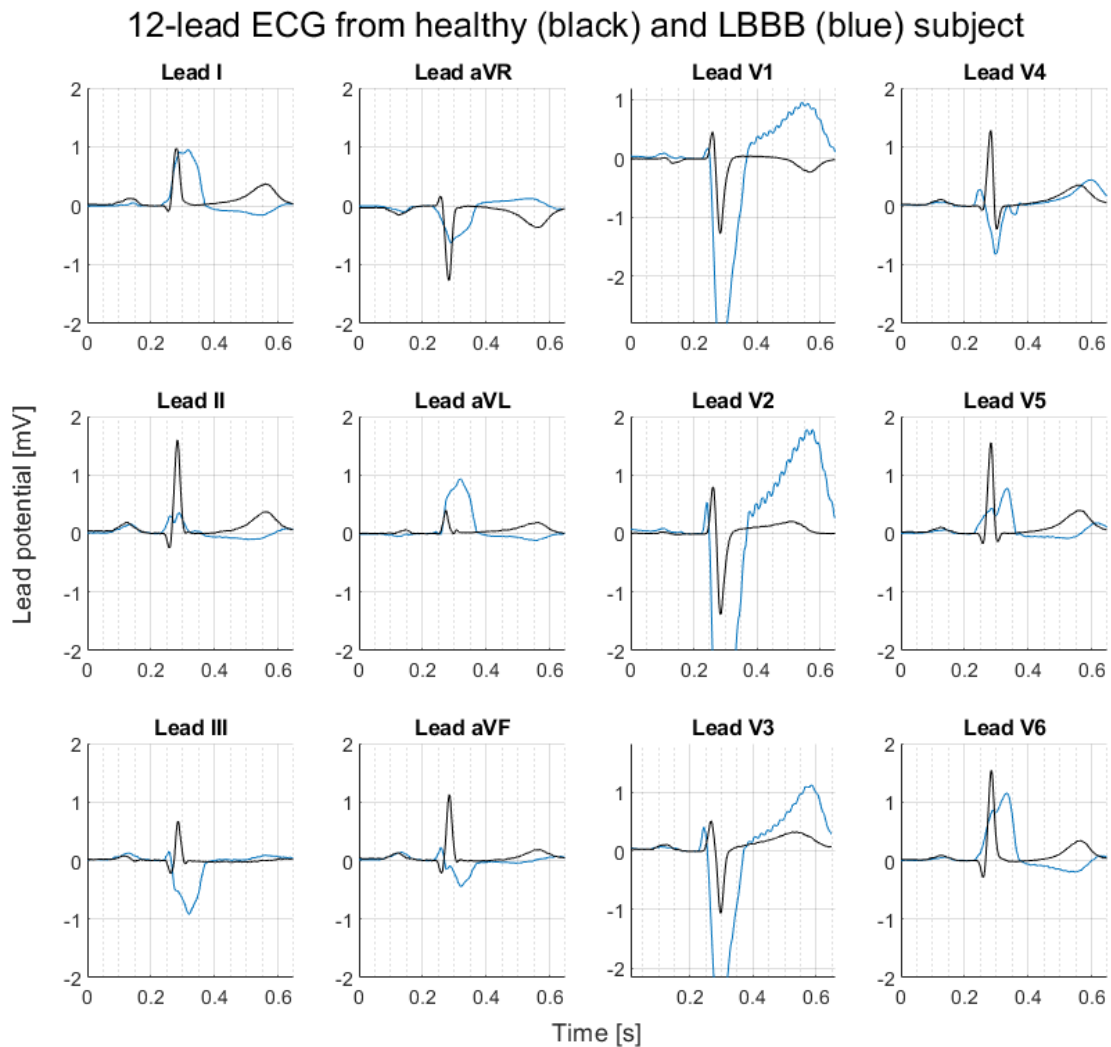
Figure 1.2. *12-lead ECG of a healthy (black) and LBBB (blue) subject.*

Figure 1.2 presents ECGs from a healthy and LBBB subject. The criteria for LBBB is

fulfilled, since (1): QRS is $\geq$ to 120 ms, defined by the first sample of QRS wave in any lead to the last sample of the QRS in any lead. (2): multiple leads, and especially V5 presents a broad notched R wave. (3): Absent Q wave in lead V5 (and lead I and V6). (4): R peak time is > 60 ms in lead V5 and V6, and is defined as the first sample of the Q wave to the sample of the R-peak. V1, V2 and V3 have normal R-peak time (5): All leads present a QRS with opposite operational sign compared to the T wave.

1.1.3 Prevalence and development

Generally, LBBB is more prevalent in elderly and in women. The prevalence of LBBB is 0.4 % for men and 0.6 % for women based on an older population with median age of 71 and 76 years, respectively [Rasmussen et al., 2019]. Several studies report a positive association between the prevalence of LBBB and age [Rasmussen et al., 2019; Eriksson et al., 1998; Imanishi et al., 2006]. In both men and women it is shown that the incidence increases dramatically with age from 1.9 and 2.2 per 100,000 person-years before age 50 years to 157.3 and 113.5 after age 80 years, respectively. [Imanishi et al., 2006] The average age for LBBB diagnosis is 69.6 ± 10 years in men and 68.3 ± 10.9 years in women [Imanishi et al., 2006].

The development of LBBB can occur due to multiple factors, such as fibrosis in the cardiac conduction system and remodelling of the LV [Sieniewicz et al., 2019]. In 54% of LBBB subjects no abnormalities are present in the ECG before the LBBB onset [Rabkin et al., 1980], however in cases of abnormalities the most prevalent are ventricular hypertrophy and ST-T abnormalities, which were significantly more prevalent, compared with subject without development of LBBB [Rabkin et al., 1980; Imanishi et al., 2006]. At the time of LBBB diagnosis there is an increased prevalence of LV hypertrophy [Hardarson et al., 1987] hypertension, ischaemic heart disease and ST-T abnormalities [Imanishi et al., 2006].

1.1.4 Prognosis

The prognosis of LBBB has been investigated in several studies, concluding that LBBB is an independent predictor for cardiac mortality [Schneider et al., 1979; Rabkin et al., 1980; Zhang et al., 2012] and that LBBB leads to cardiac remodelling potentially resulting in heart failure (HF) [Eriksson et al., 1998; Zannad et al., 2007].

LBBB is an independent predictor for cardiac mortality, which is shown in the cohort study of Rasmussen et al. [2019] based on a large LBBB population (N=1037), which showed a modest association between LBBB and cardiovascular death in men with hazard ratio of 1.80 (95 % CI: 1.38 to 2.35), which in addition, significantly incremented with increased QRS duration. The association between LBBB and cardiovascular death was agreed upon in the Framingham study by Schneider et al. [1979] which showed that 50 % of subjects with LBBB died from cardiovascular diseases within 10 years after diagnosis. Furthermore in terms a five-year incidence of sudden cardiac death the presence of LBBB was associated with a 10 fold increase [Rabkin et al., 1980].

Studies suggest that LBBB might be a marker for a progressively degenerating disease that affects both the conduction system, but also the myocardium, resulting in ventricular remodelling and potentially HF [Eriksson et al., 1998; Zannad et al., 2007]. In 5517 HF patients the prevalence of LBBB was 25 % (N=1391) [Baldasseroni et al., 2002]. Furthermore LBBB was associated with an increased hazard ratio of HF in both men (HR 3.96, 95% CI: 3.30 - 4.76) and women (HR 2.51, 95% CI: 2.15 - 2.94), which in addition was shown to further increase with increasing QRS duration [Rasmussen et al., 2019]. In the study of Eriksson et al. [1998] it was shown that during follow-up, after initial diagnosis of LBBB, the total heart volume and the incidence of HF increased. Also, the Framingham study by Schneider et al. [1979] showed that 48 % of LBBB subjects developed either clinical coronary disease or HF after onset of LBBB. Mortality from HF [Imanishi et al., 2006], myocardial infarction [Imanishi et al., 2006] and cardiomyopathy [Hardarson et al., 1987] was also higher for subjects suffering from LBBB.

The review by Zannad et al. [2007] suggest that LBBB might lead to development of HF because of a sequence of consequences of LBBB. LBBB causes intraventricular dyssynchrony, which reduces the efficiency of the ventricles. The reduced haemodynamic function initiates compensatory neurohumoral mechanisms that may be harmful in the long term by contributing to hypertrophy in the left lateral wall. The hypertrophy might cause dilation and thereby remodelling of the heart, which reduces the function and potentially leads to HF.

1.1.5 Treatment

Management of LBBB depends on the severity of findings in the ECG, symptoms related to HF and objective findings from echocardiogram and potentially other imaging modalities [Brignole et al., 2013]. First, medical treatment is initiated using diuretics, ACE inhibitor and/or beta-blockers [Mcmurray et al., 2012]. If the medical treatment is not successful, determined by New York Heart Association (NYHA) class still being $\geq$ II or LVEF still $\leq$ 35 %, the treatment by cardiac resynchronisation therapy (CRT) is considered, with the aim of reducing risk of HF hospitalisation and premature death [Mcmurray et al., 2012]. CRT counteracts the dyssynchrony since it restores the AV, inter- and intra-ventricular synchrony, and thereby restores a mechanical efficient contraction of the LV. This improves LV function and reverses the LV remodelling [Brignole et al., 2013; Sieniewicz et al., 2019].

Criteria for initialisation of CRT are not completely agreed upon among Danish [Schrøder et al., 2021], European [Mcmurray et al., 2012; Brignole et al., 2013] and American [Kusumoto et al., 2019] guidelines. According to the European guidelines of Brignole et al. [2013] (European Society of cardiology (ESC) and European Heart Rhythm Association (EHRA)) CRT is recommended in chronic HF patients (NYHA class II, III and IV) with diagnosed LBBB (QRS duration $\geq$ 120 ms) and LVEF $\leq$ 35 %. However there is a higher level of evidence for implementation of CRT when QRS duration $\geq$ 150 ms. [Brignole et al., 2013]

Optimal initiation of CRT is not addressed in current European [Mcmurray et al., 2012; Brignole et al., 2013] and American [Kusumoto et al., 2019] guidelines for management of HF, however it is recommended to initialise medical treatment for at least three months before considering CRT. In relation to initiation of CRT, the study by Wang et al. [2018] concluded that because of progressively cardiac remodelling due to LBBB, the timing of initiation is an important factor for its success. The study showed that early initiation of CRT is preferred, since LVEF was improved when CRT was performed in the first 9 months after diagnosis compared to after 9 months after diagnosis. [Wang et al., 2018]

1.1.5.1 Response to CRT

The response to CRT is affected by multiple factors, and the percentage of non-responders is estimated to be around 30-50 % [Sieniewicz et al., 2019]. The definition of CRT responders is in the literature determined through different measures such as event-based, functional based, remodelling based and clinical composite measures [Sieniewicz et al., 2019]. The study by Ypenburg et al. [2009] showed that, even though the criteria for CRT was fulfilled, 22 % of the patients responded negatively to CRT determined from an increased LV end systolic volume (LVESV). On the other hand 22 % of patients were classified as "super-responders", determined by a decreased LVESV ($\geq$ 30 %) and during follow-up, had better survival rate, lower HF related hospitalisation, higher quality of life, improved LVEF, and reduction of left ventricular end diastolic volume compared with negative responders. Also, negative responders had higher rate of death and HF related hospitalisation compared to non-responders, which shows that even though the criteria for CRT are fulfilled, the CRT can have a negative effect on the outcome. These findings suggest that long term effects from CRT varies remarkably among patients.

The lack of response to CRT can be caused by multiple factors, as listed below:

- Absence of sufficient LV electrical dyssynchrony - Even though criteria for initiation of CRT are fulfilled [Noheria et al., 2019; Ypenburg et al., 2009]
- Suboptimal placing of left ventricular pacing electrode - The placement of the left ventricular electrode is limited by feasible coronary veins [Sieniewicz et al., 2019; Noheria et al., 2019].
- Myocardial fibrosis and cardiomyopathy - Blocking or slowing the electrical activation through the LV myocardium [Sieniewicz et al., 2019; Noheria et al., 2019; Ypenburg et al., 2009].
- Suboptimal timing of LV pacing - Inadequately early pacing of the LV relative to the RV [Noheria et al., 2019]
- Cardiac arrhythmia - The efficiency of CRT is limited due to competing arrhythmias in the heart [Sieniewicz et al., 2019; Noheria et al., 2019].

In order to lower the rate of non-responders to CRT it is of great relevance to quantify the electrical dyssynchrony, since this is the pathophysiology that CRT corrects.

1.2 Quantification of electrical dyssynchrony

It is of clinical relevance to quantify the electrical dyssynchrony to ultimately predict, if a patient is likely to respond to CRT treatment. In the following sections the existing dyssynchrony measures and their limitations are represented followed by an elaboration of the state of the art solutions to the inverse ECG problem.

1.2.1 Electrical dyssynchrony measures

The prolonged QRS duration, which is part of the diagnostic criteria for LBBB, yields an indirect and global measure of the ventricular dyssynchrony. However, due to the large proportion of non-responders to CRT, the QRS duration seems to be an insufficient dyssynchrony measure in some patients.

Several studies have investigated the possibility to obtain alternative electrical dyssynchrony measures with prognostic value for CRT treatment. An alternative measure that has been widely studied for prediction of CRT prognosis is the QRS area [van Deursen et al., 2015], which is a parameter associated with increased risk of incident HF diagnosis [Andersen et al., 2021]. The QRS area is calculated from the vectorcardiogram (VCG), which is a representation of the global activation of the heart in a 3D Cartesian coordinate system. The global activation is represented as a single dipole pointing in the direction of the mean activation at every instance of time during the cardiac cycle. When plotting the dipole coordinates to every instance of time it forms the vector loop, as shown in Figure 1.3. From the vector loop, the QRS area is calculated as $QRS_{area} = \sqrt{QRSx^2 + QRSy^2 + QRSz^2}$ where QRSx, QRSy and QRSz are the integrals of the QRS in the x, y and z lead respectively [van Deursen et al., 2015].
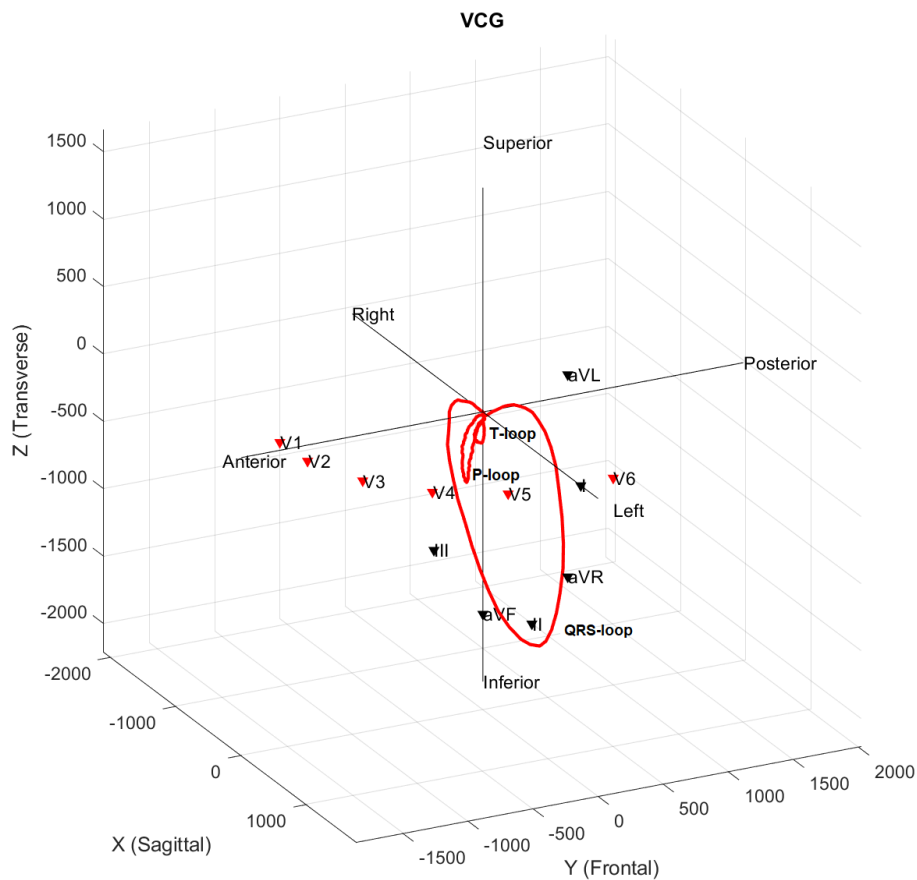
Figure 1.3. *Plot of a vector loop calculated from a 12-lead ECG from a healthy subject using inverse Dower transformation. The vector loop consists of a P-, QRS- and T-loop. The limb and precordial electrodes are marked with black and red triangles. Lead I, II, III, aVR, aVL and aVF are positioned in the frontal plane whereas lead V1-V6 are in the transverse plane.*

Studies have shown that the QRS area is a predictor for CRT response [Tokavanich et al., 2022; Andersen et al., 2021; Emerek et al., 2019]. The review study by Tokavanich et al. [2022], which included five studies with a total of 4931 patients, found that a larger QRS area prior to CRT was strongly associated with better survival. In addition, better survival was achieved in patients with larger QRS area reduction after implantation. Since the VCG is based on one single dipole at each time instance, it is not possible to assess the area of myocardial activation and thus can not evaluate the interventricular dyssynchrony of the RV and LV.

Several other alternative measures have been derived from the ECG, which as summarised in the review by Noheria et al. [2019] for instance includes; R-wave peak time divided by QRS-duration in defined leads, median-frequency based parameters and duration from R-wave to nadir of S-wave in lead V1. However, all of these measures are also limited by the fundamental fact that the ECG is a superimposed signal representing the global activation of both ventricles, see Figure 1.4.
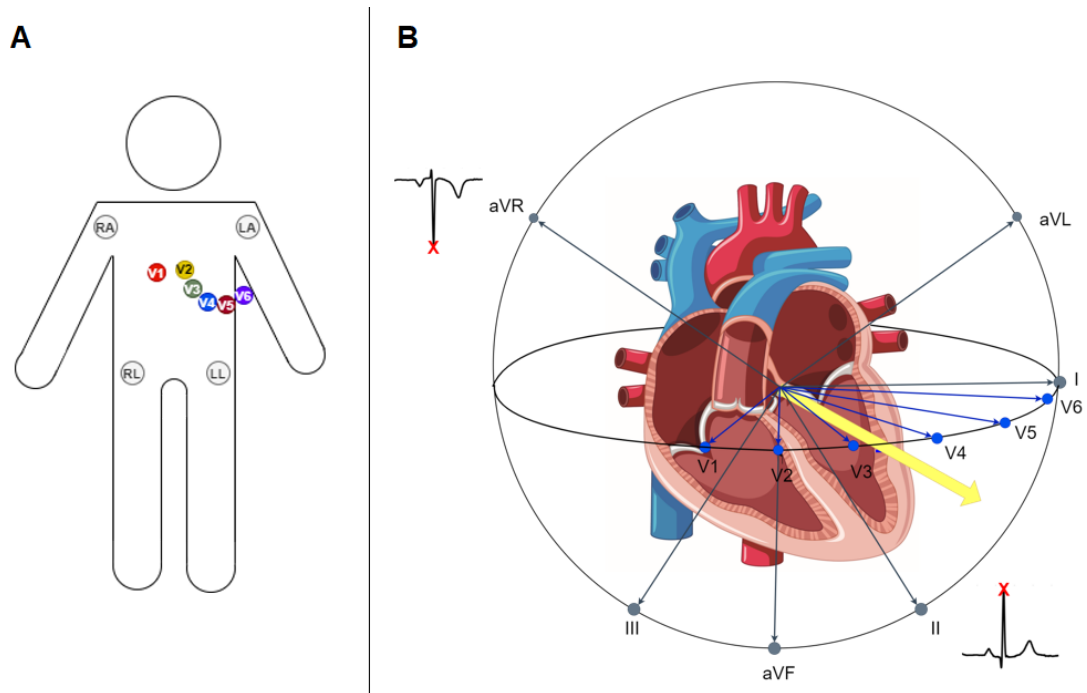
Figure 1.4. *A: ECG electrode placement. B: The global activation of the myocardium (yellow arrow) is projected onto the ECG leads, with the projection being dependent on the similarity between the direction of the myocardial activation and the direction of the lead. The measured signals of lead aVR and II are shown to exemplify the importance of the lead direction in relation to the direction of the myocardial activation. The red crosses on the ECG leads mark the instance of time corresponding to the global activation*

Another measure assessed in relation to CRT therapy is the Q-LV, which is the duration from QRS onset to the first large peak in the LV electrogram, obtained from an invasive LV electrode placed in the branch of the coronary sinus during CRT implantation. The Q-LV is hence a direct measure of LV dyssynchrony, which reflects the degree of delay at the pacing site in the LV. The Q-LV measure can be used to determine pacing sites resulting in better response to CRT, by pacing in areas with late activation. [Gold et al., 2011] However, the Q-LV measure is unsuited for CRT patient selection since it is obtained invasively.

Thereby, the existing measures of dyssynchrony are limited by either reflecting only a global activation of both ventricles or by requiring invasive measurements making it unsuitable for patient selection.

A few studies have investigated electrocardiographic imaging (ECGi) as a tool for dyssynchrony quantification [Ploux et al., 2013; Bear et al., 2018b; Varma et al., 2007]. ECGi is a noninvasive technique that maps the epicardial electric activation using body surface potentials (BSP) measurements and a geometric heart-torso model [Ploux et al., 2013; Varma et al., 2007]. The ECGi technique is based on the inverse ECG problem, that is

further elaborated in Section 1.2.2.

Several dyssynchrony measures have been derived from ECGi, such as ventricular electrical uncoupling (VEU), which is determined as the difference between the mean activation times of the LV and the RV during the QRS complex [Ploux et al., 2013; Bear et al., 2018b; Varma et al., 2007]. An illustration of VEU is presented on Figure 1.5.
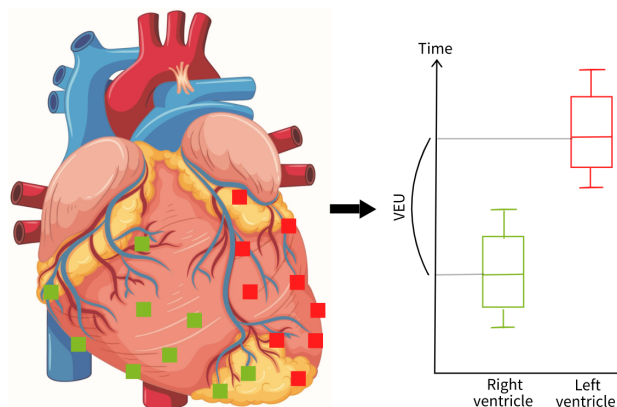

Figure 1.5. *Left side shows placements of dipoles representing right ventricle (green squares) and left ventricle (red squares). Myocardial activation times estimated from each dipole are presented in the boxplot to the right. The VEU measure is the time difference between the mean activation times of right and left ventricle. VEU is the ventricular electrical uncoupling.*

The study by Ploux et al. [2013] found that VEU outperforms both QRS duration and the presence of LBBB in the prediction of CRT response.

Although ECGi has the potential of effectively selecting patients responding CRT, the mentioned studies used a high number of body surface electrodes, which in practice is expensive and time consuming. Furthermore the studies used patient specific heart/torso models, which were acquired using imaging modalities as CT and MRI.

The ECGi is achieved by solving the inverse ECG problem. Numerous studies have investigated various solutions to the inverse ECG problem with the aim of obtaining accurate and robust solutions.

1.2.2 The inverse ECG problem

The aim of the inverse ECG problem is to determine the myocardial activation from BSP measurements. The estimation is the opposite of the forward problem where the activations of the heart are known and the BSP are calculated, see Figure 1.6.
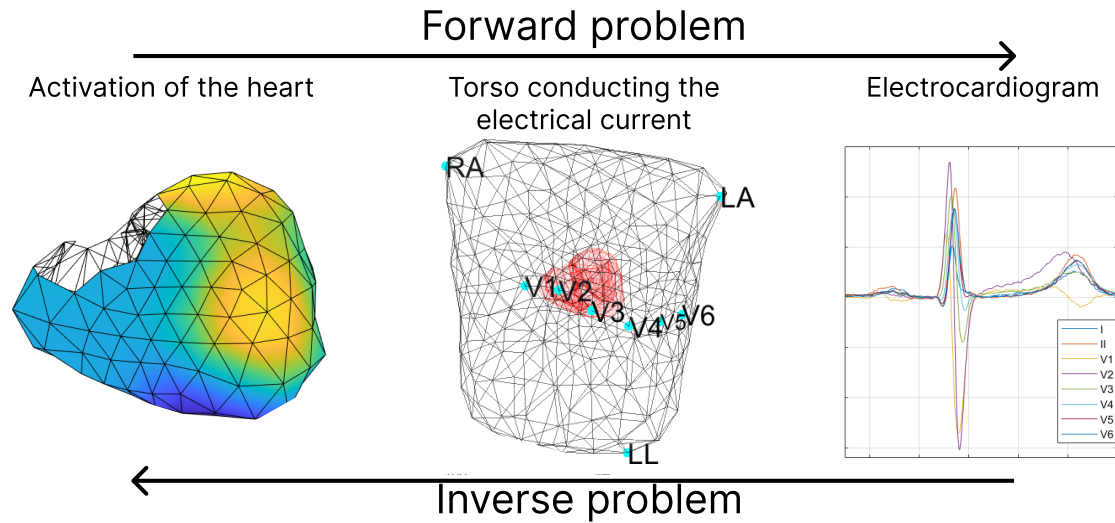
Figure 1.6. *The forward problem is used to calculate the body surface potentials (BSP) based on the activation of the heart. The inverse problem is used to calculate the activation of the heart based on the BSP.*

The electrical sources can be estimated as dipoles, which are vectors describing the electrical moment of a direction with a positive and negative pole. The dipoles exist due the excitation of the heart muscle which occurs in a sequence, rather than all at once. Hence at some time during the heart cycle some parts of the heart are depolarised while other parts are not. This produces what can be explained as electrical dipoles, as shown in Figure 1.7.
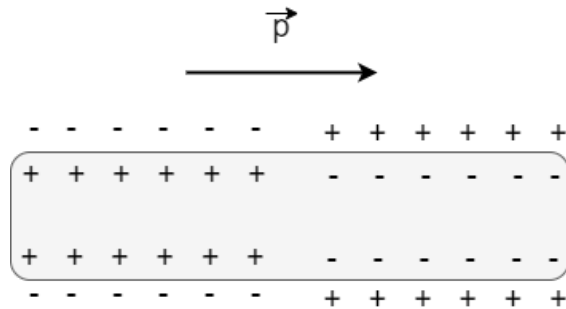
Figure 1.7. *Equivalent dipole of the heart, which occur when the heart is partially activated. The right side illustrates the polarised heart at rest with a negative inside. The left side illustrates the depolarised side which is positive inside the muscle. $\vec{p}$ illustrates the dipole.*

The electrical dipoles are defined as $\vec{p} = q_+\vec{d}$ with $\vec{d}$ being a vector pointing from charge q_- to q_+. q_+ is the charge magnitude separated with the distance d, and thereby the unit of the dipoles is ampere×meter $(A \cdot m)$. A complete derivation of the dipole unit is presented in Appendix B. The dipoles are surrounded by electrical potentials which constitutes the potentials on the body surface. Since the activation generally occurs in an

endocardial to epicardial direction, the dipoles generally point outwards from the heart.

By defining a set of dipoles and considering the distance and conduction of the torso, the contribution of each dipole to the measurable potentials at the body surface can be described as in Equation 1.1.

$$BSP = \sum_{i=1}^{I} dipoles_i * A \qquad (1.1)$$

where BSP is the measured surface potentials, $dipoles_i$ is a dipole, with i being the numeration of the dipole, and A being the transfer matrix with the rows being the number of surface electrodes and the columns the number of dipoles on the heart wall. This equation would have a unique solution in the case with an equal number of surface electrodes and dipoles.

In practice the solution to the inverse ECG problem is ill-posed, hence no unique solution exists. This is due to the smoothing and dispersing effect of the torso, leading to different degrees of attenuation in the forward solution. High frequencies are typically attenuated more than lower frequencies, and by inverting the forward solution directly this attenuation will be amplified. This is explained by the solution not being well-posed in the sense of Hadamard [Hadamard, 1923], meaning that the solution is not unique and not continuously dependent on the data. Therefore small geometric and measurement noises will dominate the solution and cause significant errors. [Pullan et al., 2010]

In order to ensure a unique and meaningful solution, constraints should be applied. This can be done by deterministic frameworks called regularisation, which constraints the solution to become less influenced by noise. However by constraining the solution, it will be influenced by a model, and hence make the solution less data-driven. Therefore there is a tradeoff between making the the solution stable in relation to noise but influenced by assumptions versus making a solution in accordance to the input data but less stable in relation to noise. [Pullan et al., 2010] The choice of regularisation is therefore crucial and depends on the application. When quantifying the dyssynchrony between ventricles the same regularisation should be used independently of the diagnosis of the subject, i.e. refrain from using regularisation that assumes properties of a normal heart in normal subject and vice versa in subjects with LBBB. Also the regularisation should not limit the solution from the physiological correct solution. Different regularisation frameworks for solving the inverse problem exist and is elaborated in the following section.

1.2.2.1 State of the art

In the literature, several authors have experimented with different regularisation techniques and transfer matrices in order to obtain the most accurate and robust activation of the myocardium, see Table 1.1. The articles of the table were found by the literature search described in Section 3.1 on page 37.

Forward	Inverse	Constraints/ regularisation	Data	Study
-	Linear solution	Non-negative	Measured data 11 EP 126 BSP	[Lynn et al., 1967]
BEM		Tikhonov zero-, first- and second-order	In-silico 2499 EP 32-1024 leads	[Kara et al., 2019]
	Kalman filter	Smoothing effect of the filter	In-silico 490 EP	[Aydin and Dogrusoz, 2011]
			In-silico 490/502 EP 192/163 electrodes	[Erenler and Dogrusoz, 2019]
	BEM	Tikhonov zero-order	In-silico 114 EP 168 electrodes	[Barnes and Johnston, 2016]
			In-silico 1012 EP 128 electrodes	[Bear et al., 2018a]
			In-silico 490 EP 192/64/32 leads	[Gharbalchi et al., 2020]
			In-silico 122 EP 192 leads	[Jiang et al., 2006]
		Tikhonov second-order	In-silico 578 EP 200 electrodes	[Schuler et al., 2021]
		Least squares QR(LSQR) factorisation.	In-silico 279 EP 412 leads	[Jiang et al., 2007]
		Combination of L1, L2 norm and variance	In-silico 98 EP 352 leads	[Shou et al., 2011]
		Temporal and spatial regularisation	In-silico 257 EP 367 electrodes	[Yao and Yang, 2016]
	Beamformer method	L2-norm	In-silico 1500 EP 123 leads	[Konttila et al., 2014]
	Multivariate adaptive regression splines	Twomey regularisation	In-silico 490/502 EP 192 leads/ 163 electrodes	[Onak et al., 2019]
	Heart surface source method	LSQR+Tikhonov	In-silico 187 EP 220 leads	[Jiang et al., 2008]
		LSQR		[Jiang et al., 2009a]

		Tikhonov zero-order	In-silico 339 EP 412 leads	[Jiang et al., 2009b]
	Bayesian maximum	Statistical assumption of noise	In-silico 490 EP 771 leads	[Serinagaoglu and MacLeod, 2006]
	Gradient projection for sparse reconstruction	L1-norm	In-silico 180 EP 220 leads	[Wang et al., 2011]
Measured/BEM	BEM		In-silico/in-vivo 242/490/1 EP 384/160-192 electrodes	[Ghosh and Rudy, 2009]
Static bidomain problem/Measured	Method of Fundamental Solution (MFS)	Tikhonov + Discrete picard condition	In-silico/Experimental 184 electrodes	[Chamorro-Servent et al., 2019]
BEM		Tikhonov zero-order	In-silico 610 EP 610 leads	[Johnston, 2018]
BEM+EDL	Support vector regression	-	In-silico 478 EP 412 leads	[Jiang et al., 2011]
				[Jiang et al., 2012]
-				[Jiang et al., 2013]
BEM+Green's	Generalised SVD	Tikhonov zero-, first- and second-order	In-silico	[Alday et al., 2019]
FEM	BEM			[Kalinin et al., 2019]
Scalar-potential finite-difference	Orthogonal matching pursuit + Kalman filter	Assumed conduction velocity	In-silico 909 EP 9 electrodes	[Nakano et al., 2021]
H-adaptive BEM	Truncated total least squares	Regularisataion parameter	In-silico 165 EP 248 electrodes	[Shou et al., 2008]
-	Hybrid metaheuristic algorithm	Tikhonov	In-silico 2000 EP 180 electrodes	[Potyagaylo et al., 2014]
Measured	Equivalent dipole layer	Tikhonov second-order	Ex-vivo 50 EP 61 electrodes	[van der Waal et al., 2021]
FEM		Regularisation term	In-silico 1500 EP 120 electrodes	[van der Waal et al., 2020]
-	Simple and double layers of electrical sources	Tikhonov	In-silico 1500 EP 40-50 electrodes	[Zhikhareva et al., 2020]
Measured	Artificial neural network	A priori and physician validation. Finding initial pacing site	Experimental 512 EP (32)192 leads	[Szilágyi et al., 2005]

BEM		A priori. Finding initial pacing site	In-silico 265(1) EP 200 leads	[Li and He, 2001]

Table 1.1. *Current research on the inverse ECG problem, found by a structured literature search described in Section 3.1 on page 37. Forward describes the method of obtaining body surface electrodes, and inverse the method of obtaining myocardial potentials. BEM = boundary element model, FEM = finite element model, EP= epicardial potentials, EDL = Equivalent dipole layer, SVD = singular value decomposition*

The idea of regularising is to incorporate knowledge about the cardiac sources, to make the range of possible solutions smaller, while keeping the solution as data driven as possible [Pullan et al., 2010].

One of the simplest regularisations is presented by Lynn et al. [1967], where the dipoles on the epicardium is assumed to be non-negative. This is reasoned by the dipoles representing the depolarisation of the myocardium going from endocardium to epicardium, and that a depolarisation would not happen in the opposite direction (with the exception of external pacing). This however still yields unreliable results, suggesting that more regularisation is needed.

1.2.2.2 Tikhonov regularisation

The most commonly used regularisation is Tikhonov regularisation(15/32 articles of the table), which is a best-fit solution based on constraining the magnitude of the solution (or derivatives of the magnitude), see Equation 1.2. The amount of regularisation is controlled by a regularisation parameter λ, which adjusts the tradeoff between the amount of regularisation and the fitness of data.

$$dipoles = argmin[||A * dipoles - ECG||_2^2 + \lambda^2 ||R * dipoles||_2^2] \qquad (1.2)$$

Where *dipoles* are the heart potentials, *A* is the transfer matrix and *ECG* is the BSPs [Pullan et al., 2010]. This first term aims to fit the solution to the measured ECG, by finding the smallest difference between the dipoles multiplied with the transfer matrix and the BSPs. The difference is calculated as the Euclidean distance, and is also called the L2-norm as used in [Konttila et al., 2014]. Another distance term is the L1-norm, also known as the Manhattan distance as used in [Wang et al., 2011; Ghosh and Rudy, 2009].

The second term is the regularisation that constraints the solution. This is a penalty term that is applied by a matrix *R* for constraining the dipole potentials, and λ for regularising it. Tikhonov employs different orders of regularisation. The orders are zero-order, first-order and second-order Tikhonov regularisation. Zero-order regularises the total magnitude of the dipole amplitudes by *R* being an identity matrix. First-order Tikhonov regularises the steepness of the solution by *R* being a discrete approximation of the surface gradients. Second-order Tikhonov regularises the change of steepness by *R* being an

approximation of the surface Laplacian operator[Pullan et al., 2010]. By Tikhonov regularisation, no physiological information is used for selecting or constraining the solution. Additionally choosing the regularisation parameter is of essence. Too small regularisation parameters cause dipoles to be noise sensitive, called under-regularised solutions, and too large regularisation parameters tend to overly smooth the dipole amplitude, called over-regularised [Gulrajani, 1998].

1.2.2.3   Twomey regularisation

Tikhonov searches for a solution by minimising the dipole amplitudes at every instant in time [Pullan et al., 2010]. The information of the potential at the time before and after the instant is therefore not used, although a correlation must exist [Gulrajani, 1998]. Regularisation methods using the temporal information includes TwomeyOnak et al. [2019]. This method is based on Tikhonov, where the regularisation term is replaced with a temporal penalty term: $||\phi_H(t) - \phi_H(t-1)||_2^2$. This constrains the dipole to being similar to the epicardial potential (EP) at the previous time instant. The Twomey regularisation does not use other temporal information than that of the previous time instant, nor any other constraints of the potential, with the cost of losing the regularisation of the magnitude as Tikhonov provides. Additionally the Twomey regularisation suffers from depending on a guess of the initial amplitudes of the first time instant [Pullan et al., 2010].

1.2.2.4   Alternative types of regularisation

Other ways of solving the inverse problem includes Kalman filtering [Aydin and Dogrusoz, 2011; Erenler and Dogrusoz, 2019] and Bayesian maximum estimation[Serinagaoglu and MacLeod, 2006]. Kalman filtering estimates the temporal evolution of the potentials by considering previous samples and an error term. The noise, both geometric and measurement noise is assumed Gaussian. The EP at every time instant is estimated by the directly calculated potential and regulated by a state transition matrix along with the estimated noise. This gives a smoothing of the solution, but does not constrain the solution to be physiological meaningful. The Bayesian estimation uses prior information about EP distributions. Some of the information used in the article by Serinagaoglu and MacLeod [2006] are the measured intravenous potentials measured simultaneously with the torso recording. This counteracts the non-invasive advantage of the solution. Additionally the EP are estimated at every time instance without considering the temporal correlation of the epicardium.

As shown above, only a few of the regularisation methods uses the temporal knowledge of the epicardial activation. An attempt to incorporate temporal information to the regularisation was in the study by Yao and Yang [2016]. Here both a temporal and spatial regularisation term was used, achieving a relative error 2.5 times lower than Tikhonov zero-order, with a greater robustness to noise. This shows a potential of using both spatial and temporal regularisation in achieving a greater solution to the inverse problem of ECG.

1.2.2.5 Determination of the transfer matrix

The inverse solution is typically solved as described in Equation 1.1 on page 12, with the transfer matrix computed by methods such as boundary element method (BEM) and finite element method(FEM). The BEM includes the boundaries between tissues of the torso, but assumes a constant conduction in each type of tissue. FEM on the other hand are calculated based on the entire volume, which demands a higher number of calculations. [Gulrajani, 1998]

Both inhomogeneity of the torso as well as the geometry, if not accounted for, can cause errors in the reconstruction of the ECG. Some of the methods in Table 1.1 rely on extensive human conduction models, thus limit the solution to only fit patients of normal anatomy. Another way of overcoming the geometric error of the methods is to have individualised heart-torso models achieved by an imaging techniques such as magnetic resonance imaging (MRI) or computed tomography (CT), which is expensive and in the case of CT harmful to the patient [Nakano et al., 2021].

Alternatively homogeneous torso models can be used. The challenge is that the homogeneous model depends solely on the torso geometry, disregarding the conduction differences of the body e.g. high conduction of the blood and low conduction in the lungs. This might introduce errors into the estimation. In the study by Ramanathan and Rudy [2001] the significance of a patient specific volume conductor was investigated. The accuracy of the homogeneous torso model was not significantly different from the accuracy of the patient specific model.

1.2.2.6 Limitation of a high number of dipoles and body surface electrodes

The activation of the heart is sought depicted in many dipoles, which corresponds to EP, in Table 1.1. This is to achieve a high spatial resolution of the activation. But with an increasing amount of EPs to calculate, the solution becomes increasingly ill-posed [Gulrajani, 1998]. Therefore the solutions rely on a multitude of body surface electrodes, with studies using up to 1024 body surface electrodes [Kara et al., 2019]. In general, attachment of large arrays of electrodes are time-consuming, therefore an electrode vest has been invented to make application easier. However the electrode vest is limited to fit only patients of normal weight and anatomy [Pereira et al., 2020]. It is of higher clinical relevance to limit the number of electrodes, since it will allow for a simpler setup of electrodes. Additionally, the high number of myocardial dipoles are only necessary if the goal is to depict the activation with high localisation accuracy, which might not be necessary for depicting interventricular dyssynchrony.

In the article by Nakano et al. [2021], 9 electrodes with the standard 12-lead configuration was used. The purpose was to estimate the current source localisation (the initial point of activation). With Kalman filtering the activation sequence at each time point were decided and by assumption of the conduction velocity of 1.9 m/s the activation sequence

of 909 dipoles were calculated. In the article by Potyagaylo et al. [2016], the purpose was to estimate activation times of the heart by deciding the node of initial activation. Again, both the conduction velocity and the activation shape of each dipole were assumed. Lastly the article by van Dam et al. [2013] uses 12-lead ECG combined with MRI to obtain a patient specific model, to decide the specific localisation of points of premature ventricular contraction.

Thereby the solutions provided in the articles using 12-lead ECG, rely on model assumptions about the shape of activation as well as conduction velocity and patient-specific geometries, and are thus not completely data driven. By assumption of conduction velocity, there is a risk of limited performance on subjects with altered conduction paths, since areas of branch blocks might have slower conduction.

1.3   Aim

An alternative method for solving the inverse problem of ECG for quantification of inter-ventricular dyssynchrony is therefore of interest. It it of relevance both to use a standard body surface electrode setup as well as a heart-torso model that are embracing several heart-torso conductance and geometries. Lastly the solution should provide a data driven a solution. The aim of this study was therefore to 1) determine the electrical activation of the ventricles from standard 12-lead ECG recordings and a generic heart-torso model, and 2) quantify the interventricular electrical dyssynchrony.

2 | Method

This project aimed to determine the interventricular dyssynchrony using the solution to the inverse problem based on the 12-lead ECG rather. In this project six dipoles were used to determine the activation pattern of the ventricles. Three types of regularisation to the inverse ECG problem were implemented and tested for robustness, in order to achieve a data driven and robust method.

The concept of the dipoles representing the myocardial activation of areas of the ventricles during depolarisation are depicted in Figure 2.1.
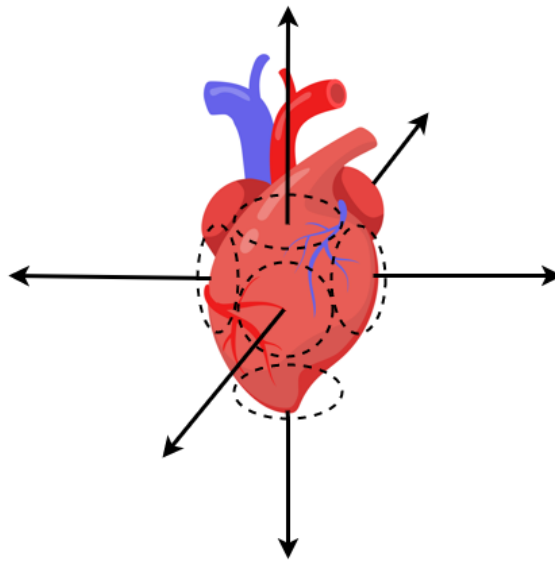
Figure 2.1. *Six dipoles (arrows) representing the activation of six areas of the ventricles.*

The method has three main sections describing the data used in the project, solutions to the inverse ECG problem and lastly a comparison of the solutions to the inverse problem. The content of these sections are depicted in Figure 2.2.
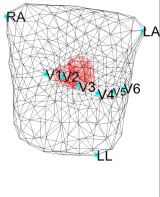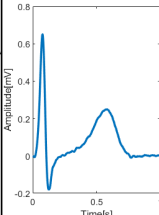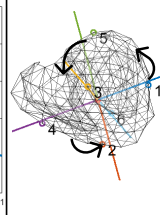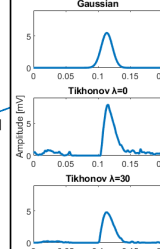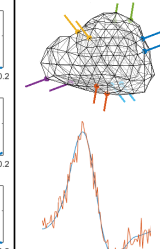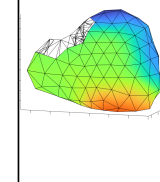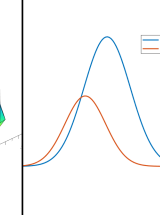
Figure 2.2. *An overview of the content of the method chapter with both sections and subsections.*

First the data is described as it constituted the basis for the methods later developed.

Next the method for finding the optimal position and direction for the dipoles is described. Then, the theory of the solutions of the inverse ECG problem is outlined. In order to evaluate the inverse solutions, several tests were performed. First is the method for testing the robustness of the solutions, next is the method for investigation of the dipole activations and lastly the method for investigation and quantification dyssynchronous ventricular activation is described.

2.1 Data

In the current project a geometric heart model was used along with ECG-recordings from subjects with LBBB, subjects admitted to CRT and subjects with no cardiac diseases, referred to as normal subjects in this project. The heart model was necessary for the calculation of dipoles whereas the ECG recordings were used to investigate the interventricular dyssynchrony of each population.

2.1.1 Geometric heart model

A geometric heart model of a "normal male" was provided by the cardiac simulation program ECGSim [van Oosterom et al., 2022], see Figure 2.3. The software provides a model of the heart and torso of a normal male, which is constructed from magnetic resonance images (MRI) [van Dam et al., 2011]. The ventricles were represented by 131 epicardial nodes.
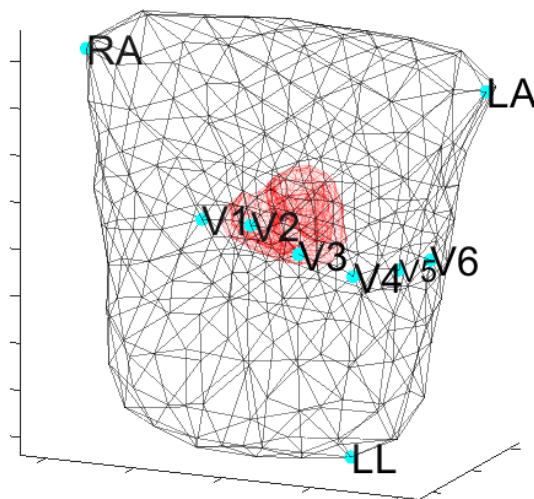
Figure 2.3. *Torso and heart model from a "normal male" from ECGSim. Electrode positions are plotted on the surface of the torso.*

A 12-lead ECG recorded from the same person as the geometric heart model was provided as well. The positions of the surface electrodes were known in relation to the torso and heart geometry. The ECG was sampled at 1000 Hz.

2.1.2 12-lead ECG recordings from normal, LBBB, and CRT subjects

A total of 100 ECG recordings from normal subjects, 100 ECG recordings from LBBB subjects and 135 ECG recordings with corresponding Q-LV measures from subjects, who were admitted to CRT implantation, were included in this project. The groups of subjects are referred to as normal, LBBB and CRT subjects.

The LBBB subjects fulfilled the criteria for LBBB defined by GE Healthcare [2019], and was categorised by the Marquette 12-SL ECG analysis program. The normal subjects did not show any ECG abnormality according to the program.

The normal and LBBB ECG's were provided from the MUSE® Cardiology Information System database from Copenhagen General Practitioners' Laboratory. The database contains ECG recordings of patients who consulted their general practitioner between 2001 and 2015. The ECG recordings of the CRT subjects were provided from the study by Sommer et al. [2016].

The recordings used in this study were the median ECG of a 10 second recording sampled with 500 Hz. Since this project focuses on the ventricular depolarisation only the QRS-segments of the recordings were included in the analysis. To ensure equal length of the ECG recordings the included signals were defined to have a length of 200 ms with the QRS aligned in the middle of the signals.

2.2 Solutions to the inverse ECG problem

The three implemented solutions to the inverse ECG problem were:

- Unconstrained inverse solution

- Gaussian regularisation

- Tikhonov regularisation

The unconstrained inverse solution was implemented to demonstrate that an entirely data-driven inverse solution is ill-posed and too sensitive to noise. The Gaussian regularisation is a novel type of regularisation developed in this project and provides a temporal regulated solution. The Tikhonov regularisation is widely used in the literature where hundreds of dipoles and measurement leads are used. Tikhonov was in this project implemented to investigate its efficiency in a solution with few leads and dipoles.

The inverse solution were based on the same epicardial dipole positions elaborated in the following section.

2.2.1   Determination of dipole positions and directions

Dipoles are vectors with a direction and a position on the epicardial surface of a geometric heart model. The dipoles are positioned in the epicardial nodes. The positions are referred to as "seed nodes" in this project. The direction of the dipoles are pointing outwards from the heart centre, since the activation of the myocardium typically occurs from endocardium to epicardium.

The determination of the dipole direction and placement of seed nodes was achieved by defining six orthogonal lines which intersect the centre of the heart, see Figure 2.4.
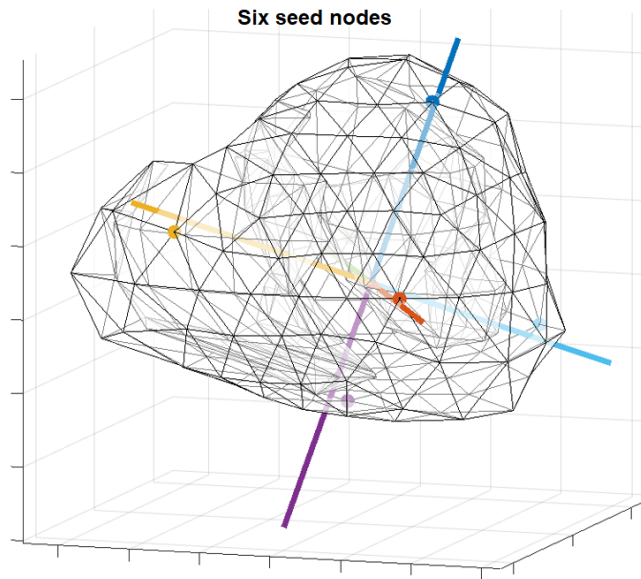
Figure 2.4. *Determination of six seed nodes using lines intersecting the centre of the heart. The seed nodes are marked with dots in colours corresponding to the lines used to determine the seed nodes.*

The centre was calculated as the mean of all epicardial nodes of the geometric heart model. Subsequently, the seed nodes were selected as the nodes closest to each of the lines, see Equation 2.1.

$$dist(P, l) = \frac{||\overrightarrow{C_0 P} \times \overrightarrow{r}||}{||\overrightarrow{r}||} \tag{2.1}$$

Where P is the position of the node, l is the line, C_0 is the heart centre which is intersected by the line, and $\overrightarrow{r}$ is the direction of the line. The node with the shortest distance to each line was thereby defined as a seed node.

As earlier described, the dipoles are also defined by a direction. The dipole directions were the same as the direction of the lines used to select the seed nodes. This approach of selecting the direction allowed controlled change of the dipole directions by simply rotating the lines in the x-, y- and z-direction. Hence the dipole directions were kept orthogonal regardless of the rotation.

2.2.1.1 Optimal dipole position

To find an optimal position and direction of the dipoles, different variations were tested using an iterative search on both 100 normal and 100 LBBB subjects.

All combinations with 10 degrees intervals of x-,y- and z-rotation from 0 to 80 degrees, leading to 729 combinations, were tested on 100 normal subjects and 100 LBBB subjects respectively. The notation of rotation was in the form [x-rotation, y-rotation, z-rotation]. In each combination the dipoles of all subjects were optimised using the Tikhonov $\lambda=0$ regularisation. The Tikhonov $\lambda=0$ regularisation was used as it is often used in the literature to solve the inverse ECG problem. The accuracy of the ECG reconstruction achieved for each subject at each combination was quantified as the difference between the reconstructed and measured ECG, calculated as the sum of squared error (SSE), see Equation 2.2.

$$SSE = \sum \left(ECG_{rec}(t) - ECG_{meas}(t) \right)^2 \tag{2.2}$$

The median and quartiles of the SSE across the subjects at each of the 729 directions were calculated. Subsequently the optimal dipole positions were selected as the positions yielding the lowest median SSE across all subjects. The median SSE was calculated from normal and LBBB subjects separately, and the best rotation was chosen as the one yielding the generally lowest SSE across both groups of subjects

Furthermore investigation of optimal dipole positions were repeated with respect to another heart from a healthy male. These results were presented in Appendix D.

2.2.2 Calculation of dipole activations

In the current project the body surface measurements were conventional 12-lead ECG and the myocardial activation was represented by the six orthogonal dipoles.

The relation between body surface measurements and dipole amplitudes can be described with the linear matrix equation in Equation 2.3.

$$ECG_{meas}(t) = A \cdot x(t) \tag{2.3}$$

Where ECG_{meas} is the measured ECG to the time t, x is the dipole amplitudes to the time t and A is a constant transformation matrix. The transformation matrix is constructed from the dipole position and direction and the electrode positions. An overview of the involved points and vectors in the calculation of the A-matrix is presented in Figure 2.5.
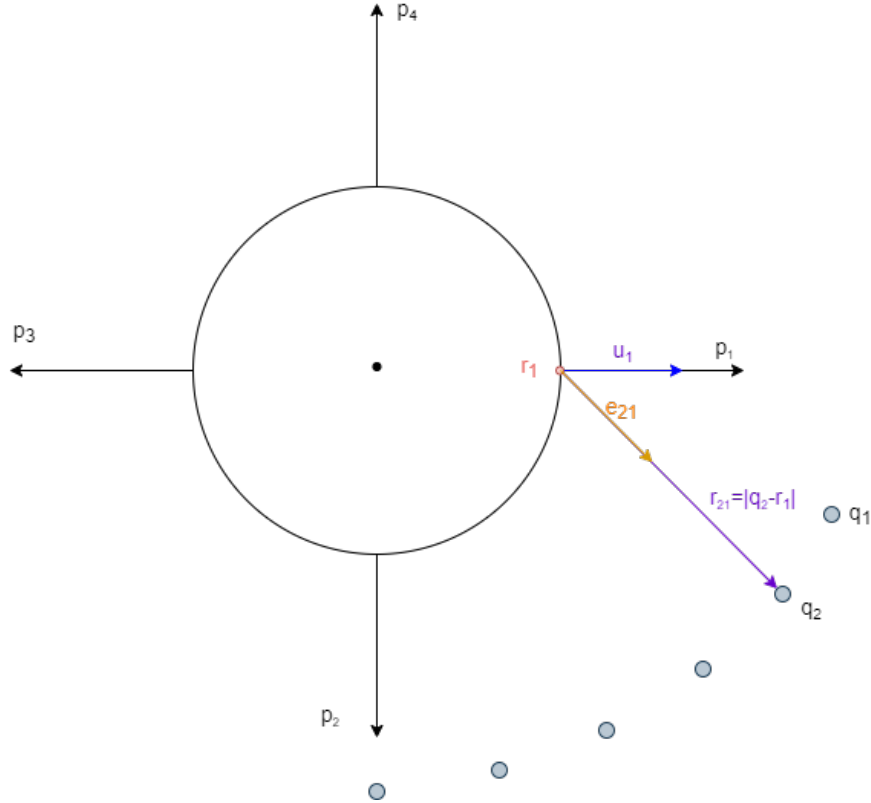
Figure 2.5. *Representation of the vectors and points that are used in the solution of the inverse ECG problem. The circle represents the heart. 'm' represent the number of the dipole and 'n' represent number of electrode. p_m are the dipoles, u_m are the unit vectors. r_m is the dipole position whereas q_m is the electrode positions. e_{mn} is the unit vector from the dipole position pointing at each electrode. r_{mn} is the distance between dipole position and electrode position.*

The 12-lead ECG contains eight independent ECG-leads (I,II,V1-V6) from nine measurement electrodes and one reference electrode. The electrical activity measured in a lead v_n can be written as a summation of all contributing dipoles, and is calculated as the product of the lead vector $\overrightarrow{z_{mn}}$ and the dipole p_m, see Equation 2.4.

$$v_n(t) = \sum_{m=1}^{M} < \overrightarrow{z_{mn}} \overrightarrow{p_m}(t) > \tag{2.4}$$

The lead vector $\overrightarrow{z_{mn}}$ is calculated using the unit vector pointing from the dipole position, r_m, to the electrode, q_n, divided by the squared distance between the dipole position and the electrode position. The lead vector is also influenced by the conductance of the tissue, described as a constant $\frac{1}{4\pi\sigma}$, see Equation 2.5.

$$\overrightarrow{z_{mn}} = \frac{1}{4\pi\sigma} \frac{\overrightarrow{e_{mn}}}{r_{mn}^2} \tag{2.5}$$

where $\overrightarrow{e_{mn}}$ is the unit vector pointing from the dipole position to the electrode, and r_{mn} is the distance between the dipole and the electrode. In the current project the conduction

of the torso is assumed to be homogeneous, and therefore the equation is simplified by eliminating the constant conductance term, see Equation 2.6.

$$\overrightarrow{z_{mn}} = \frac{\overrightarrow{e_{mn}}}{r_{mn}^2} \tag{2.6}$$

Due to the elimination of the conductance term, the unit of the dipoles will in this project be referred to as [a.u], since the unit is no longer A*m but a constant multiplied with A*m.

It should be noted that the precordial leads are unipolar, and therefore the lead vectors related to the precordial leads can be explained by the position of only one electrode and the dipole position. However, the limb leads I and II are bipolar and therefore the lead vectors related to the limb leads are defined using the position of two limb electrodes and the dipole position. The limb leads $\overrightarrow{z_{mI}}$ and $\overrightarrow{z_{mII}}$ are defined as in Equation 2.7.

$$\overrightarrow{z_{m(I)}} = \frac{\overrightarrow{e_{m(LA)}}}{r_{m(LA)}^2} - \frac{\overrightarrow{e_{m(RA)}}}{r_{m(RA)}^2} \qquad \overrightarrow{z_{mII}} = \frac{\overrightarrow{e_{m(LL)}}}{r_{m(LL)}^2} - \frac{\overrightarrow{e_{m(RA)}}}{r_{m(RA)}^2} \tag{2.7}$$

Where LA, RA, and LL are the electrodes on the left arm, right arm and left leg, respectively.

The dipoles are formulated as shown in Equation 2.8.

$$\overrightarrow{p_m}(t) = x_m(t)\overrightarrow{u_m} \tag{2.8}$$

where x_m is the time dependent amplitude of the dipole m and $\overrightarrow{u_m}$ is a unit vector describing the direction of dipole m.

By inserting the expression of p_m in Equation 2.4, matrix A is introduced as a gathered expression of z_{mn}^T and u_m, see Equation 2.9.

$$v(t) = \sum_{m=1}^{M} \overrightarrow{z_m^T}\overrightarrow{u_m}x_m(t) = Ax(t) \tag{2.9}$$

Matrix A is hence a transformation matrix describing the contribution of every dipole to each lead. A is a multiplication of matrix $\overrightarrow{z_{mn}}$ and vector u_m yielding a column vector A_m for each dipole m, see Equation 2.10.

$$A_m = \begin{bmatrix} z_{m1,x} & z_{m1,y} & z_{m1,z} \\ z_{m2,x} & z_{m2,y} & z_{m2,z} \\ ... & ... & ... \\ z_{mn,x} & z_{mn,y} & z_{mn,z} \end{bmatrix} * \begin{bmatrix} u_{m,x} \\ u_{m,y} \\ u_{m,z} \end{bmatrix} = \begin{bmatrix} z_{m1,x}u_{m,x} + z_{m1,y}u_{m,y} + z_{m1,z}u_{mz} \\ z_{m2,x}u_{m,x} + z_{m2,y}u_{m,y} + z_{m2,z}u_{mz} \\ ... \\ z_{mn,x}u_{m,x} + z_{mn,y}u_{m,y} + z_{mn,z}u_{mz} \end{bmatrix} \tag{2.10}$$

where the rows of z_{mn} correspond to the leads n. A_m can be calculated for every dipole m as column vectors, giving the full A matrix with columns corresponding to dipoles and

rows corresponding to leads. The dimension of A is the number of independent leads times the number of dipoles, hence A is a 8x6 matrix.

With the A-matrix defined, it is possible to approximate the dipole activations, x(t), and hence solve the inverse ECG problem. In the following sections the unconstrained, Gaussian regularisation and Tikhonov regularisation approach for calculating the dipole activations are elaborated.

2.2.2.1 Unconstrained inverse solution

The simplest solution to the inverse ECG problem is to solve the linear matrix equation by isolating x and thereby derive the dipole amplitudes of all six dipoles, see Equation 2.11.

$$x(t) = inv(A) \cdot ECG_{meas}(t) \tag{2.11}$$

However, to be able to solve this equation A must be invertible, hence it must be a square matrix. The 8x6 matrix obtained from 8 independent ECG leads and six dipoles is not invertible and can therefore not be used to solve the unconstrained inverse equation. The number of ECG leads was therefore reduced to six leads consisting of lead I, II, V1, V2, V4 and V6. These leads were selected to preserve as much information as possible from leads pointing in as different directions as possible. Thereby the A-matrix was an invertible 6x6 matrix in the unconstrained inverse solution.

2.2.2.2 Gaussian regularisation

The purpose of the Gaussian regularisation method was to develop a more robust and time dependent method with physiologically explainable constraints. The solution was constrained by forcing the dipoles to have a Gaussian shape of activation as a function of time. Hence the myocardial area that each dipole represent can only be depolarised once, but can vary in timing, amplitude and duration. The solution was furthermore constrained to only assume positive values.

The dipole amplitude as a function of time for dipole m is determined by the Gaussian function, as shown in Equation 2.12

$$x_m(t) = a_m \cdot e^{-(t-\mu_m)^2/2\sigma_m^2} \tag{2.12}$$

For each dipole m, the activation x_m is described by an amplitude, a, time of peak activation, μ, and duration of activation, σ. Hence the amount of variables to optimise is three times the amount of dipoles, i.e. 18 variables. The Gaussian activation of dipoles is illustrated on Figure 2.6.
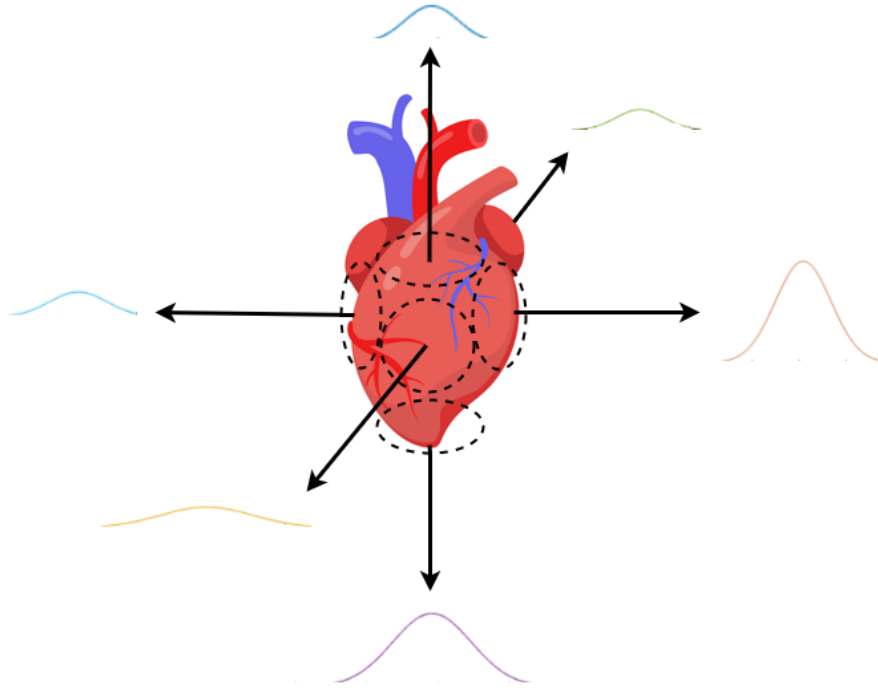
Figure 2.6. *Gaussian activation of dipoles representing areas of myocardial tissue depolarisation.*

The Gaussian activation of the dipoles were optimised by minimising an objective function defined as the SSE between the measured ECG and the ECG reconstructed from the dipoles. The reconstructed ECG was achieved by multiplication of the dipoles and the A-matrix, see Equation 2.13.

$$ECG_{rec}(t) = A \cdot x(t) \tag{2.13}$$

where ECG_{rec} is the reconstructed ECG, x is the dipole activations, and A is the transformation matrix described in Equation 2.10 on page 25.

The objective function to minimise was the difference between the measured ECG and the reconstructed ECG, measured as the SSE, see Equation 2.14.

$$min \sum_{t=0}^{t_{QRS}} (ECG_{rec}(t) - ECG_{meas}(t))^2 \tag{2.14}$$

where ECG_{meas} is the measured ECG (I, II, V1-V6).

The variables of the Gaussian dipole activations were determined using the interior-point optimisation algorithm, which is able to find the minimum of constrained non-linear multivariable functions and is the default optimisation method in MATLAB [MathWorks, 2022]. The dipoles were constrained to have positive amplitudes, have peak activation within the signal length (between 0 and 200 ms) and have a duration of activation between 0 and 200 ms.

2.2.2.3 Tikhonov regularisation

Tikhonov regularisation and especially the zero-order Tikhonov, is often used in the inverse ECG problem [Barnes and Johnston, 2016; Bear et al., 2018a; Gharbalchi et al., 2020; Jiang et al., 2006], as it minimises the amplitudes of the dipoles and therefore constrains the solution. The formula for Tikhonov regularisation is described in Equation 2.15.

$$x_\lambda = argmin_x\Big(||A \cdot x - ECG_{meas}||_2^2 + \lambda^2||L \cdot x||_2^2\Big) \qquad (2.15)$$

Where x_λ is the optimised dipoles regulated in accordance to the regularisation parameter, λ. L is defined as the identity matrix in the zero-order Tikhonov and $|| \ ||_2$ defines the Euclidean distance [Hansen, 2000]. The regularisation parameter defines the tradeoff between the residuals and the amplitude of the dipoles. If λ is equal to zero, no regularisation is performed, and x is optimised in order to minimise the residuals. If λ is a high value, x is optimised in order to minimise the amplitudes of the dipoles.

The regularisation parameter, λ, can be determined using L-curve [Pullan et al., 2010]. In this study the L-curve was used to calculate the optimal regularisation parameter, as it is often used in the literature and it is an intuitive tool to understand the tradeoff between the residuals and the dipole amplitudes. The L-curve is a function of the regularisation parameter, λ, and displays the residual against the dipole amplitudes [Hansen, 2000], see Equation 2.16.

$$L_{curve}(\lambda) = \Big(||A \cdot x_\lambda - ECG_{meas}||_2, ||L \cdot x_\lambda||_2\Big) \qquad (2.16)$$

The regularisation parameter was defined from the L-curve based on QRS complexes from 100 normal ECGs and 100 LBBB ECGs. The results of the L-curves are presented in Appendix C, and suggests using both the regularisation parameter $\lambda = 0$ and $\lambda = 30$.

The dipole activations using Tikhonov regularisation were optimised using the interior-point optimisation algorithm [MathWorks, 2022], which was the same optimisation algorithm as used for the Gaussian regularisation. The optimisation was performed at each sample individually since the Tikhonov regularisation includes no temporal regularisation. The dipoles were constrained to only have positive amplitudes.

2.2.2.4 Overview of the implemented solutions

An overview of the implemented solution, their constraints and the algorithm used to calculate the dipole activations is shown in Table 2.1.

Solution	Constraints	Optimisation algorithm
Unconstrained inverse solution	No constraints	Inverted A-matrix
Gaussian	Gaussian shape with: $0 < \mu < 200$ ms $0 < a < 100$ $0 < \sigma < 200$ ms	Minimisation of SSE using Interior-point algorithm
Tikhonov $\lambda = 0$	$0 < a < 100$	Minimisation of sum of SSE and regularisation term using Interior-point algorithm
Tikhonov $\lambda = 30$	$0 < a < 100$	Minimisation of sum of SSE and regularisation term using Interior-point algorithm

Table 2.1. *The implemented solutions to solve the inverse ECG problem along with their constraints and optimisation algorithm used to determine the dipole activations. Abbreviations: a = dipole amplitude, μ = time of peak activation, σ = duration of activation, SSE = sum of squared error*

2.3 Comparison of solutions to the inverse ECG problem

The three implemented solutions to the inverse ECG problem was investigated and compared. First, they were assessed for robustness. Next, their ability to reconstruct the ECGs in normal and LBBB subjects were investigated along with the dipole characteristics in activation time, duration and amplitude for normal and LBBB subject. Lastly, the ventricular dyssynchrony was quantified from selected representative dipoles.

2.3.1 Test of robustness

The implemented solutions were tested for robustness in order to investigate which was the most reliable. This investigation was relevant since the inverse ECG problem is ill-posed, which means that even small variations of the A-matrix or the ECG signal might cause large variations in the determined myocardial activation.

Both geometric noise as well as measurement noise were applied to test the robustness of the methods. The geometric model described in Section 2.1.1 along with the measured ECG of the normal male was used in evaluating the robustness. Hence the robustness test was performed using one single recording and a geometric model that was certain to match the recorded subject. The robustness was evaluated with respect to control dipoles, calculated with the Gaussian, Tikhonov $\lambda = 0$, Tikhonov $\lambda = 30$ and unconstrained solution based on the ECGSim ECG-recording with no measurement or geometric noise added. Robustness metrics are further elaborated in Section 2.3.1.3

2.3.1.1 Geometric noise

The different types of regularisation were tested for geometric robustness by addition of geometric noise. The geometric noise was achieved by shifting the position of all dipoles to random neighbour-nodes while preserving the dipoles directions, see Figure 2.7. The median and quartile displacement of each dipole position were 14.3 [12.4, 16.2] mm.
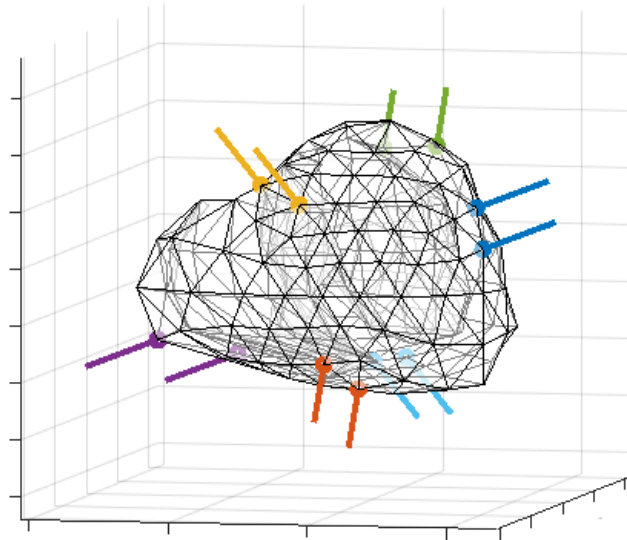

Figure 2.7. *Application of geometric noise by moving the dipole position to a neighbour node. Dipoles of the matching colour shows the original and shifted dipoles.*

The shift in position, and preservation of the direction, yielded a change in the A-matrix, corresponding to geometric noise, since the distances and directions between dipole positions and measurement electrodes were changed.

A total of 100 iterations of random geometric noise were performed.

2.3.1.2 Measurement noise

Measurement noise was applied by addition of white Gaussian noise to the measured 12-lead ECG, see Figure 2.8. A signal to noise ratio (SNR) of 20 dB was chosen to control the amount of added noise, as it is often used to simulate noise present in clinical practice [Shou et al., 2011; van der Waal et al., 2020; Schuler et al., 2021].
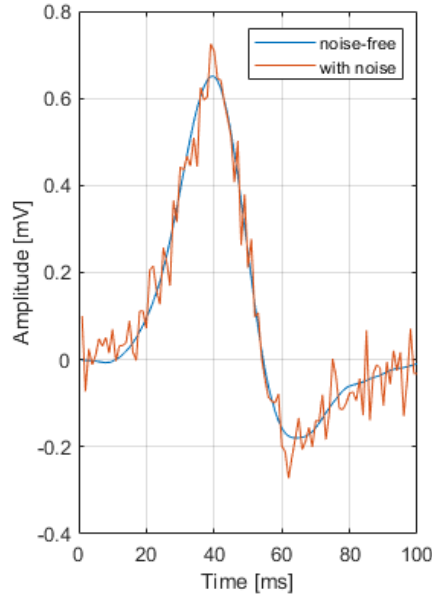
Figure 2.8. *White gaussian noise with SNR of 20 dB added to an ECG lead (orange) and the corresponding noise free signal (blue).*

A total of 100 iterations of random different noise addition was performed.

2.3.1.3 Robustness metrics

In a robust system, the dipoles affected by geometric or measurement noise would be expected to be equal to the control dipoles. Different metrics were used to assess the similarity between the control dipoles and dipoles generated from noise affected ECGs. The metrics included:

- SSE difference from control - The SSE reflects the dipoles ability to reconstruct the measured ECG. SSE difference indicates the difference in SSE between dipoles with noise and control dipoles.

- Correlation with control - Correlation between dipoles calculated from noise affected ECG's and control dipoles

- Activation time difference from control - The difference between the time of activation of the dipoles with noise and control dipoles.

The correlation with control is a measure of how similar the noise affected dipoles are to the control dipoles. The dipoles are organised in a 6x100 matrix (6 dipoles and 100 samples), hence the correlation was determined from two 6x100 matrices, one control and one noise affected, which in Equation 2.17 is denoted A and B.

$$corr_d = \frac{cov(A, B)}{\sigma_A \sigma_B} \tag{2.17}$$

where *cov* denotes the covariance of A and B, and σ the standard deviation of A and B.

The activation time, μ, is defined as the time for 50 % of the cumulative sum of dipole activation. For the Gaussian dipoles this is the peak, but for the Tikhonov regularised and the unconstrained dipoles this point might vary. The activation time difference from control is calculated as defined in Equation 2.18 and was used as a similarity metric since the timing is of great relevance in assessment of ventricular dyssynchrony.

$$\Delta\mu = |\mu_{control} - \mu_{noise}| \tag{2.18}$$

where $\mu_{control}$ is a 6x1 vector with activation times of the control dipoles and μ_{noise} a 6x1 vector containing the time of activation in the six noise affected dipoles. In a robust system, the absolute difference between the noise affected dipoles and the control dipoles is expected to be low.

The median and the 25th and 75th percentile were calculated for all the described measures. The median and percentiles of the activation times difference were stated as a average for all six dipoles, and displayed in boxplots for each dipole.

2.3.2 Characteristics of dipole activations

The dipoles of the different inverse solutions were assessed in terms of their ability to reconstruct the ECG along with the morphology of the dipoles quantified by three measures. The characteristics of the dipoles were quantified as:

- Activation time - The time point of 50% cumulative dipole activation within the duration of the QRS complex.
- Amplitude - The maximal amplitude of the dipole activation within the duration of the QRS complex
- Duration - The duration from 25 % to 75 % of the cumulative dipole activation within the QRS complex.

The measures are visualised on Figure 2.9.
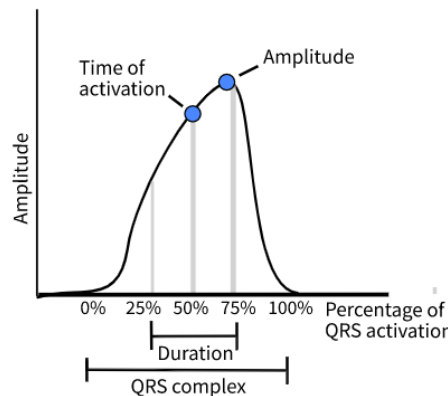
Figure 2.9. *Example of a dipole activation and visualisations of the measures: time of activation, amplitude and duration.*

2.3.3 Investigation of dyssynchrony

The primary goal of determining the activation of the myocardium in the current project was to be able to quantify the dyssynchronous activation of the ventricles in LBBB patients. In order to do this three dyssynchrony measures were invented. The dyssynchrony measures were quantified using the dipoles of the most accurate and robust type of regularisation.

2.3.3.1 Selection of representative dipoles from left and right ventricle

To determine the dyssynchrony between the LV and RV activation, two dipoles were selected, of which one reflected the activation of the LV and one reflected the activation of the RV. As multiple dipoles represented LV and RV, all combinations of left and right dipoles were tested. The pair of dipoles yielding best separation between normal and LBBB were chosen, under the assumption that normal subjects typically would not have dyssynchrony and a majority of the LBBB subjects are expected to have dyssynchrony.

2.3.3.2 Dyssynchrony quantification

The three dyssynchrony measures are referred to as dyssynchrony 1, dyssynchrony 2 and dyssynchrony 3 and are explained in the following.

Dyssynchrony 1 was defined as the time of activation difference between a dipole representing the RV and a dipole representing the LV, see Figure 2.10. Time of activation was defined as the time point were 50 % of the cumulative dipole activation has occurred within the duration of the QRS interval.
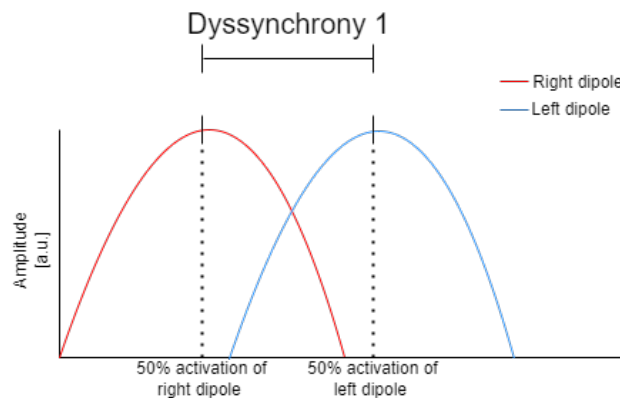
Figure 2.10. *Dyssynchrony 1. Two dipoles representing the activation of right and left ventricle, respectively, with markings of 50 % activation.*

Dyssynchrony 2 was determined as the positive area of the difference between the left dipole activation and the right dipole activation at each sample. Like Dyssynchrony 1, only two dipoles were used. One representing the RV and one representing the LV. On

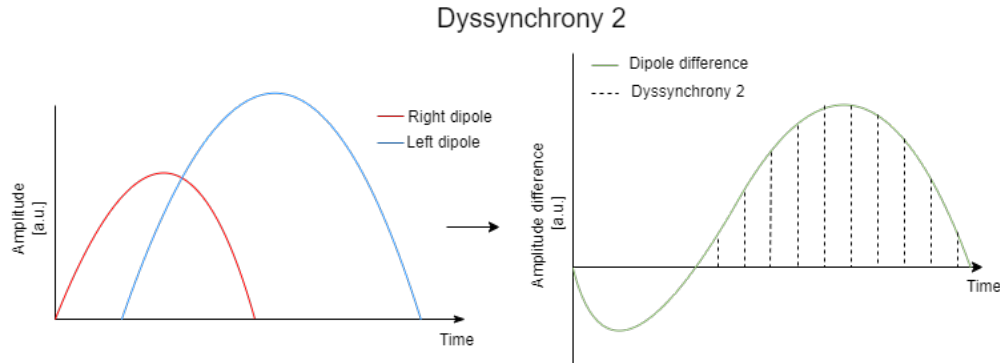Figure 2.11 left side presents the two dipoles, and right side presents the difference of the two dipoles.

Figure 2.11. *Dyssynchrony 2. Left graph present one right dipole and one left dipole. Right graph presents the difference between right and left dipole. The positive part of the curve reflects a more activated left dipole compared to right dipole.*

Dyssynchrony 3, also called left-right ventricular uncoupling (LRVU), was in contrast to dyssynchrony 1 and 2, based on global RV and LV activations rather than local activations. The global right and left activation was determined as a sum of all dipoles representing the RV and LV respectively. Dipoles positioned in boundary areas were excluded. The calculation of the ventricular activation difference between the global right and global left activation is described in Equation 2.19.

$$\text{Ventricular activation difference} = \Big(d_a(t) + d_b(t) + d_c(t)\Big) - \Big(d_d(t) + d_e(t) + d_f(t)\Big) \quad (2.19)$$

Where d_a, d_b, and d_c are dipole activations of the LV and d_d, d_e and d_f are dipole activations of the RV at each sample t. The dyssynchrony measure was determined as the positive area of ventricular activation difference. Thereby the dyssynchrony 3 represents the general uncoupling of the LV in relation to the RV, see Figure 2.12.
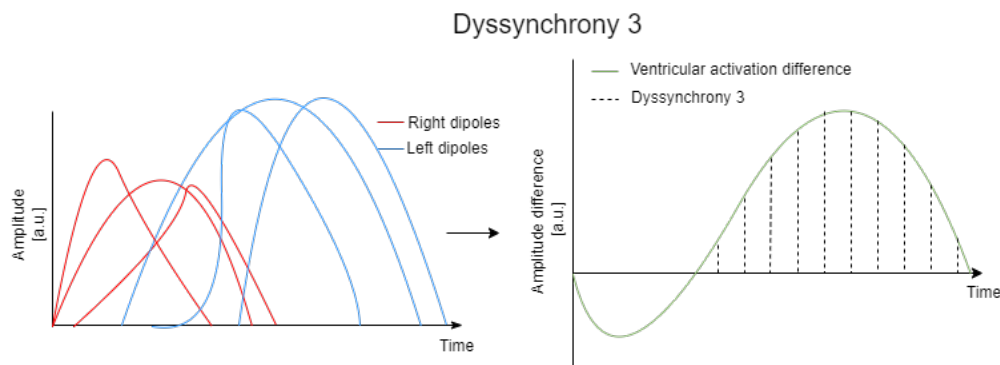
Figure 2.12. *Dyssynchrony 3. Left graph presents all dipoles representing right and left dipoles. Right graph present the difference between all the left dipoles and all the right dipoles. A positive curve reflects a more activated left ventricle compared to right ventricle.*

2.4   Statistics

All results were tested for normality using the Anderson-Darling test prior to statistical comparisons. Median and 25th and 75th percentile were stated for data with non-normal distribution in the form: median [25th percentile, 75th percentile]. Mean and standard deviation were stated for data with normal distribution in the form: mean $\pm$ standard deviation.

The results were visualised by boxplots containing markings of the median, 25th, 75th percentile, whiskers and outliers of the distribution. Whiskers extended to the most extreme data point that were not considered outliers. Outliers were data point greater that $q_3 + 1.5 \cdot (q_3 - q_1)$ and less than $q_1 - 1.5 \cdot (q_3 - q_1)$, where q_1 and q_3 were the 25th and 75th percentile, respectively. Significant difference between two groups were indicated with a horizontal black line between groups and with a star on the centre of the line.

Comparisons of multiple dependent samples were performed using the Friedman's test followed by a post hoc analysis conducted with the Bonferroni test. The Mann-Whitney-U test and two sample t-test were used for comparison of two groups with independent samples for non-normal and normal distribution, respectively. A Chi squared test was used to compare two binomial independent distributions.

The slope of linear regressions were tested using t-test, and the squared Pearson correlation was denoted as r^2.

In all statistical tests, a significance level of 5% was used.

3 | Literature search

3.1 Literature search

In order to find the existing published methods aiming to solve the inverse problem of ECG, a systematic literature search was conducted. The protocol of the conducted search is described in Table 3.1.

Aim	To find articles describing methods for solving the inverse ECG problem
Database	PubMed
Search strategy	• Search terms are found and categorised into a block diagram for a block search • The systematic block search is conducted using a search phrase
Search phrase	`("inverse problem" [Title/Abstract] OR "inverse ECG problem" [Title/Abstract] OR "inverse electrocardiography problem" [Title/Abstract]) AND (ECG [Title/Abstract] OR electrocardiogram [Title/Abstract] OR electrocardiology [Title/Abstract])`
Screening strategy	• Articles are assessed for eligibility based on title and abstract • Articles are assessed for eligibility based on full text
Exclusion criteria	1. Concerns the forward calculation of ECG without considering inverse calculation 2. Concerns the placement of electrodes 3. Comparisons of existing regularisation methods

Table 3.1. *Protocol of the literature search.*

To limit the search results to the most relevant articles, a title/abstract filter was applied. This filter constricted the results to only contain studies which mentioned the search terms in either the title and/or the abstract. The search terms were selected based on a quick search as well as by making a quick review of the found articles by the search terms. Using Boolean operators, the block search were set up as in Table 3.2.

	AND	
	Problem	**Domain**
OR	Inverse electrocardiography problem	ECG
	Inverse problem	Electrocardiogram
	Inverse ECG problem	Electrocardiology

Table 3.2. *Search terms used in the block search.*

This search provided 74 articles, of which 44 were eligible for full text reading, and finally 35 were included in the overview of existing state-of-art method in Table 1.1. The screening and exclusion process are described in the flowchart, see Figure 3.1.
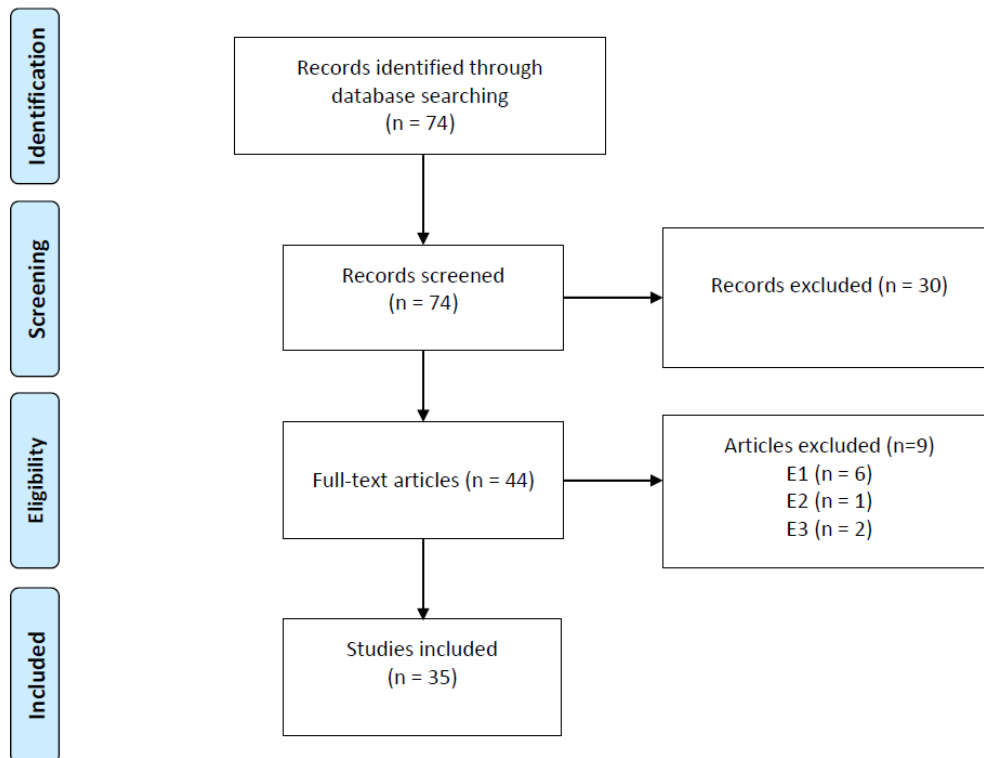
Figure 3.1. *The flowchart of screening the articles, inspired by Moher et al. [2009].*

4 | Results

4.1 Data

Standard 12-lead ECG recordings from 100 normal subjects, 100 subjects with LBBB and 135 CRT subjects were used in the current project. Q-LV was only provided for the CRT group. Demographics of the populations are presented in Table 4.1.

	Normal	LBBB	CRT
Subjects, n	100	100	135
Female sex, n (%)	63 (63.0)	63 (63.0)	32 (23.7)*
Age [years]	20.0 [20, 20]	72 [63, 84]	71 [63, 77]
QRS duration [ms]	89.9 ±8.8	146.4 ±13.6	170.8 ±22.5*
QRS area [µv*s]	9.8 [8.2, 11.3]	18.6 [15.9, 22.6]	14.9 [11.9, 18.6]*
Q-LV [ms]	-	-	134.9 ±28.6
Ischemic heart disease, n (%)	0 (0)	0 (0)	63 (46.6)*

Table 4.1. *Demographics of the normal, LBBB and CRT subjects. n abbreviates a number. The age, QRS duration, QRS area and Q-LV are stated as mean ± standard deviation or in case of non-normality as median [25th percentile, 75th percentile]. Notation with * denotes difference between mean or median value of LBBB and CRT groups.*

4.2 Optimal dipole position

A total 729 different combinations (rotations) of dipoles were investigated using a geometric heart-torso model from a normal male and the ECGs from 100 normal subjects and 100 LBBB subjects.

The median SSE across the normal and LBBB subjects at each rotation is shown in Figure 4.1. Yellow areas indicate low median SSE and hence a good rotation yielding dipoles with a relatively accurate reconstruction of the ECG. Conversely, the blue areas indicate high median SSE, as a result of a poor rotation yielding dipoles with a relatively inaccurate reconstruction of the ECG.
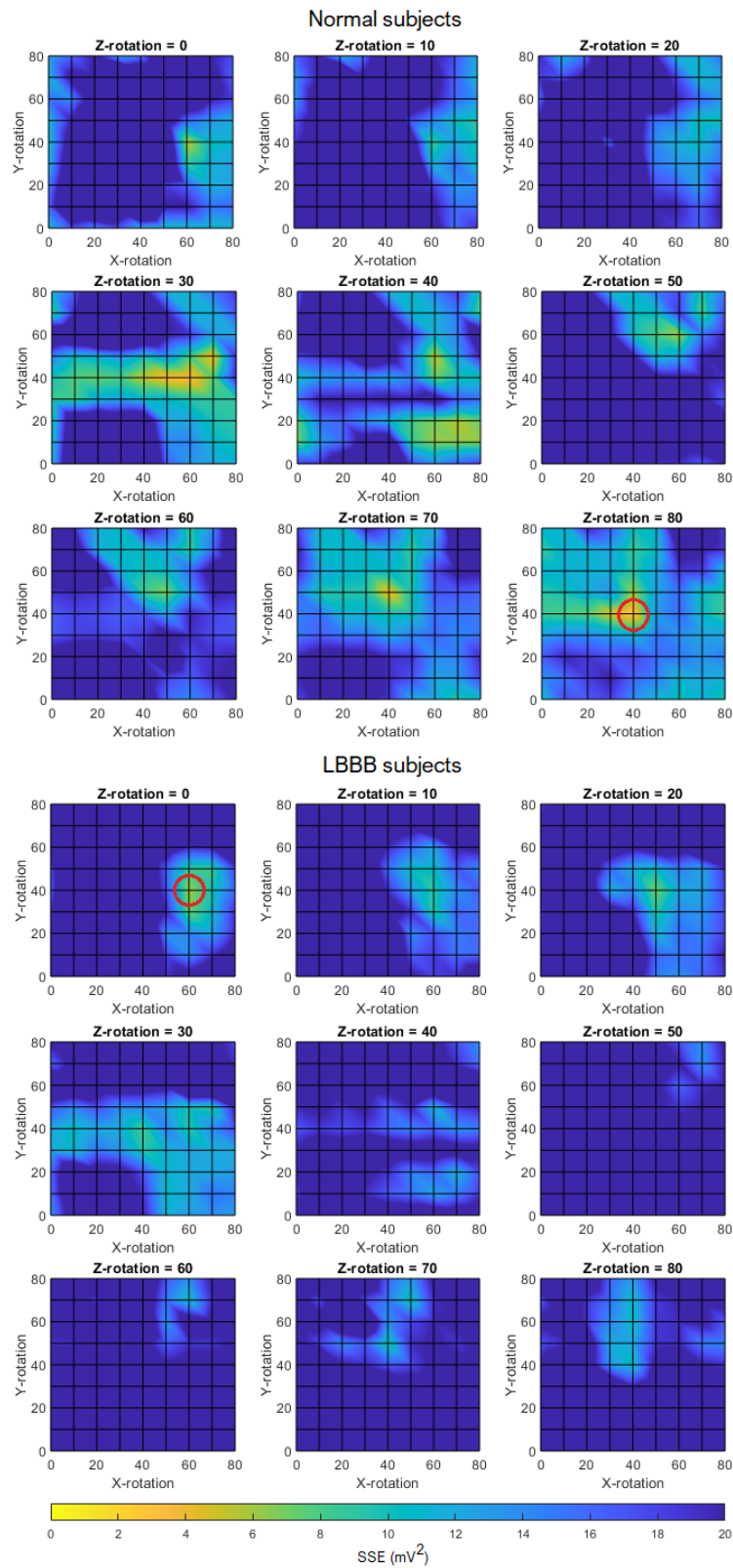
Figure 4.1. *Median SSE of the 100 normal subjects and 100 LBBB subjects in all evaluated rotation degrees. Rotations on x-, y-, and z-axes defines the rotation in degrees. The red circles mark the rotation yielding lowest SSE.*

The best dipole configuration for normal subjects was achieved in a rotation of [40 40 80] degrees (i.e. [rotation x = 40, rotation y = 40, rotation z = 80]) resulting in a median SSE of 1.88 mV^2 [1.19, 3.01]. The best dipole configuration for LBBB patients was achieved in a rotation of [60,40,0] degrees yielding a median SSE of 5.78 mV^2 [3.33, 9.04]. Generally the median SSE of the LBBB subjects were higher compared to the normal subjects, see the boxplot in Figure 4.2.
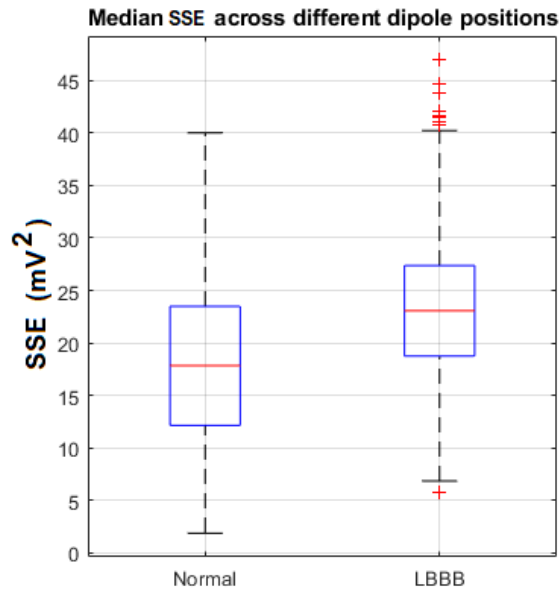
Figure 4.2. *Boxplot of the median SSE from 100 normal and 100 LBBB subjects at the 729 different rotations. Hence each boxplot contains 729 points. Each point is the median SSE of one rotation.*

Generally the normal subjects had lower SSE compared to LBBB subjects (median: 17.85 [12.15, 23.48]mV^2 and 23.06 [18.75, 27.37]mV^2, respectively).

Further insight into the SSE of different rotations in different subjects is provided in the boxplot in Figure 4.3. The boxplot shows the SSE of the 729 rotations for each of the 100 subjects in the normal and the LBBB population.
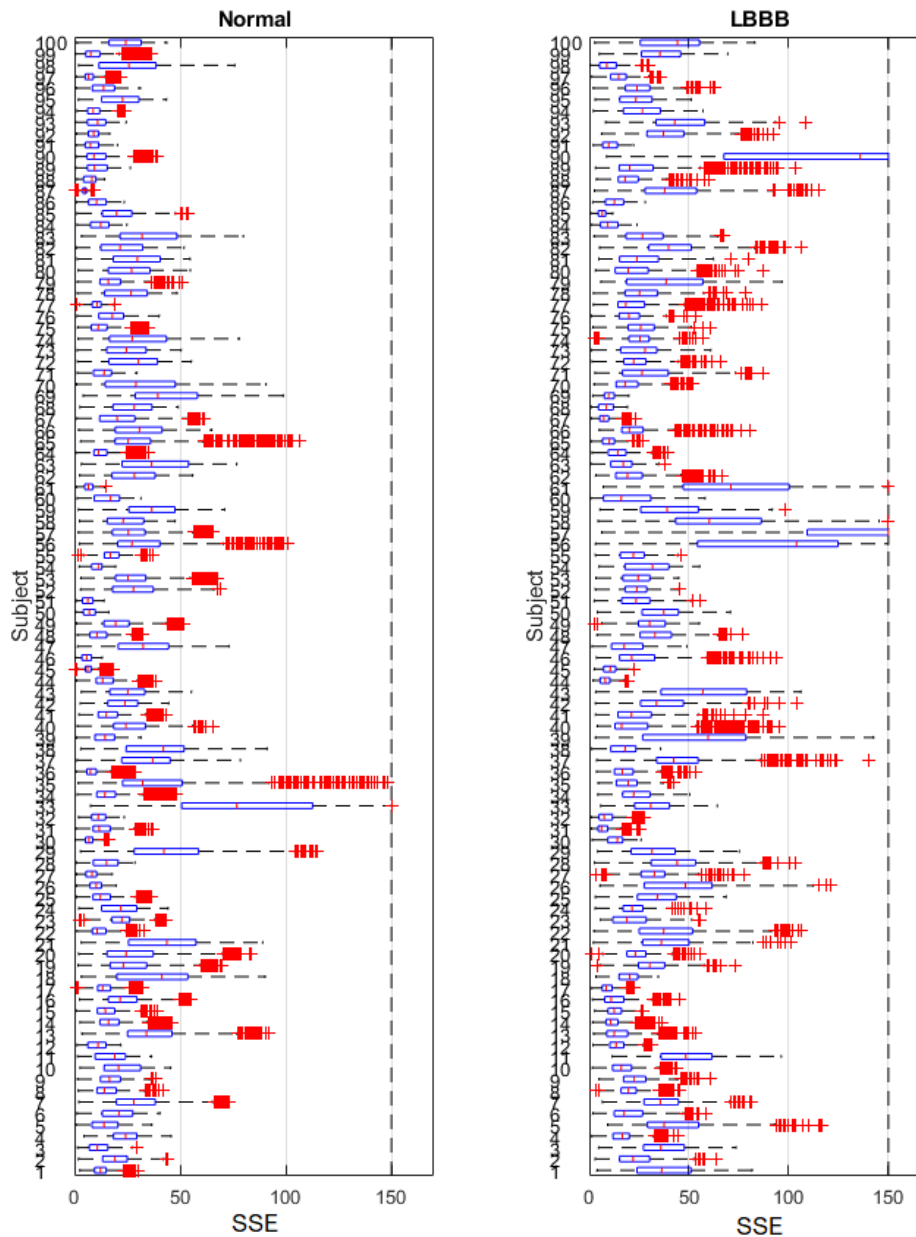
Figure 4.3. *The SSE at 729 different rotations in each person in the normal and the LBBB population. The SSE limit was set to 150 in the plot. Hence SSE>150 are plotted at the line of SSE=150.*

A larger amount of outliers was present in the LBBB population, meaning that the dipole rotation was more critical in LBBB patients since a poor dipole configuration led to very poor ECG reconstruction (SSE up to >350). More homogeneous SSE was achieved in the normal population, indicating that many dipole rotations were capable of reconstructing the normal ECG.

To get a visual overview of the best dipole positions, the median SSE of 100 normal and 100 LBBB subjects were plotted on the geometric heart model. When iterating through

729 rotations of six dipoles, multiple dipoles might be placed in the same node. In this case only the minimum, i.e. the best, median SSE of each node were plotted. The median SSE of the normal subjects is shown in Figure 4.4 and the LBBB subjects in Figure 4.5.
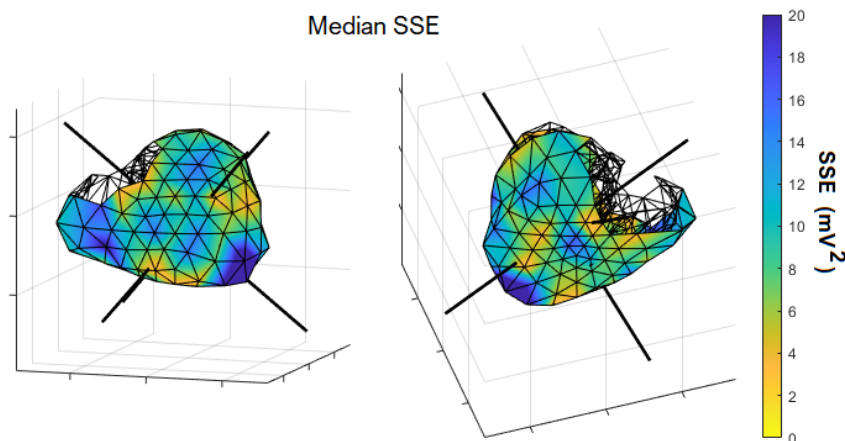
Figure 4.4. *Best median SSE across 100 normal subjects. Blue indicates high SSE and yellow indicates low SSE. The black lines visualise the optimal dipole positions. Left= frontal/superior view, right=posterior/inferior view*
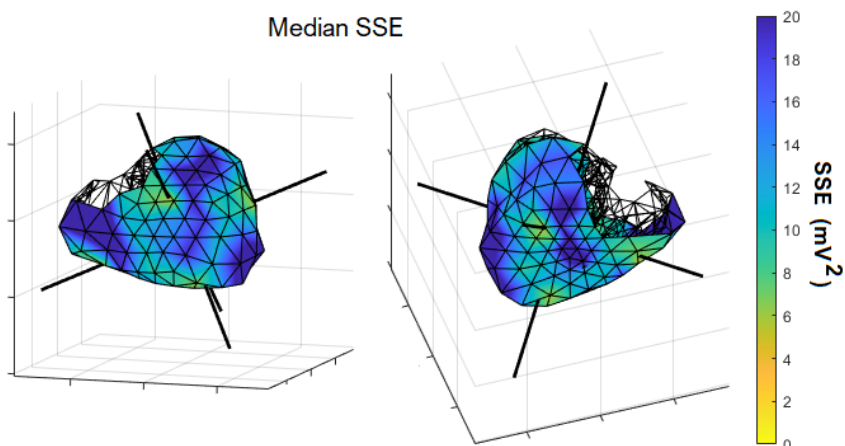
Figure 4.5. *Best median SSE across 100 LBBB patients. Blue indicates high SSE and yellow indicates low SSE. The black lines visualise the optimal dipole position. Left= frontal/superior view, right=posterior/inferior view*

As seen in both the colormaps of median SSE versus rotation in Figure 4.1 and in the visualisations on the heart model in Figure 4.4 and 4.5 the tendencies are similar in the normal and the LBBB population. In other words, the areas of poor and good dipole positions are similar despite the LBBB median SSE being generally higher than in the normal population. The optimal dipole position however differed with [40 40 80] versus [60 40 0]. It was decided to select only one dipole configuration achieving the lowest overall SSE for both normal and LBBB subjects. In Table 4.2 the median SSE [p25, p75] of the two best rotations used on the opposite population are presented.

Rotation	Normal [SSE (mV^2)]	LBBB [SSE (mV^2)]
[40 40 80]	1.88 [1.19, 3.01]	10.36 [4.96, 21.82]
[60 40 0]	4.80 [3.03, 8.25]	5.56 [3.03, 9.68]

Table 4.2. *Median SSE [p25,p75] of the rotation [40 40 80] and [60 40 0] on the normal and LBBB population*

Since the median SSE of the LBBB population using the rotation [40 40 80] was poor ($> 10\ mV^2$) and the SSE of the normal and LBBB was fairly low ($\sim 5\ mV^2$) in the [60 40 0] rotation, the selected rotation for further analysis was [60 40 0].

In Figure 4.6 it is shown that the dipoles of rotation [60 40 0] are also positioned in areas of low SSE for the normal population since the red dipoles (representing the optimal dipole position for the LBBB population i.e. [60 40 0]) are placed in areas where the heart is coloured in brighter colours.
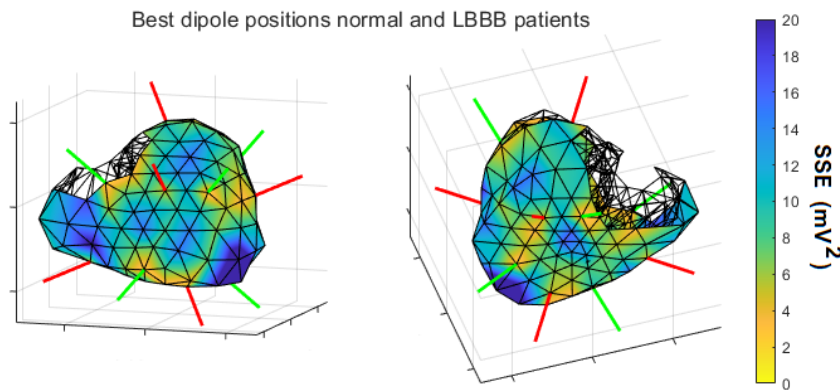
Figure 4.6. *Geometric heart model coloured with median SSE of different dipole positions for normal patients along with the optimal dipole position determined from an LBBB population (red dipoles) and normal population (green dipoles).*

The selected dipoles and the numeration which will be referred to in the following sections is shown in Figure 4.7.
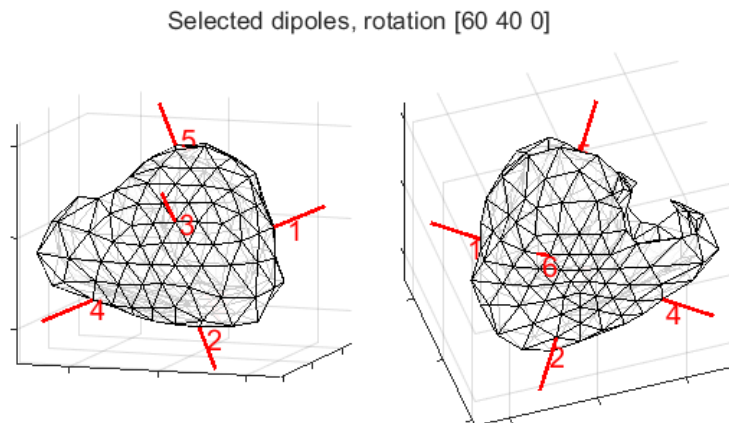
Figure 4.7. *Selected dipoles and their numeration.*

4.3   Comparison of solutions to the inverse problem

In the current section the four implemented solutions to the inverse problem are evaluated and compared. The compared solutions are:

- Gaussian
- Tikhonov $\lambda = 0$
- Tikhonov $\lambda = 30$
- Unconstrained

The dipole position and direction were fixed to [60 40 0] as described in the previous section. First, the robustness of the solutions to geometric and measurement noise are reported. Subsequently the dipole characteristics of the normal and LBBB subjects are presented. Lastly, the ventricular dyssynchrony quantification using the inverse solutions are shown and compared to the other dyssynchrony measures; QRS duration, QRS area and Q-LV.

4.3.1   Test of robustness

The robustness of the inverse solutions was tested using the 12-lead ECG from ECGSim. Hence the ECG originated from the same person as the geometric heart model.

4.3.1.1   Control dipoles

The control dipoles in the robustness test were calculated from an ECG-recording and heart model which had not been affected by noise. The SSE of the control dipoles of the four solutions: Gaussian, Tikhonov $\lambda = 0$, Tikhonov $\lambda = 30$ and unconstrained are presented in Table 4.3.

	Gaussian	Tikhonov λ=0	Tikhonov λ=30	Unconstrained
SSE (mV^2)	8.46	7.66	23.91	0

Table 4.3. *The SSE of the Gaussian, Tikhonov $\lambda = 0$ and $\lambda = 30$ and the unconstrained solution.*

The Gaussian and Tikhonov $\lambda = 0$ solutions yielded similar accuracy of the reconstructed ECG. The unconstrained solution had an SSE of 0, since the dipoles are directly calculated from the matrix equation. The solution of Tikhonov $\lambda = 30$ yielded the highest SSE and hence the least accurate ECG reconstruction.

The control dipoles calculated with each type of regularisation are depicted in Figure 4.8.
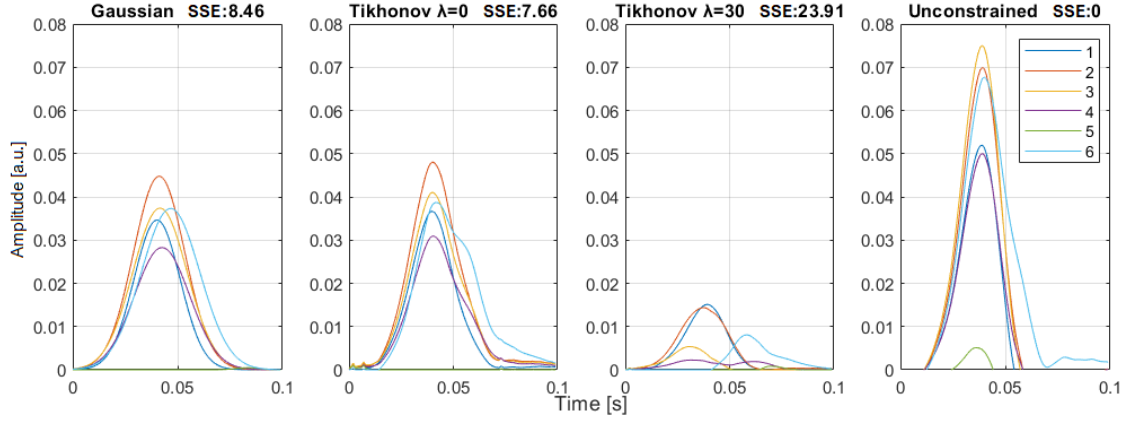
Figure 4.8. *The control dipoles calculated with each of the inverse solutions, along with the SSEs.*

The shape of the dipoles are generally more similar in the Gaussian and Tikhonov $\lambda = 0$. The Tikhonov $\lambda = 30$ has lower amplitudes and the unconstrained solution has higher amplitudes.

4.3.1.2   Geometric noise

The robustness to geometric noise was assessed in terms of difference in SSE, difference in activation time and correlation between each instance of dipoles with added noise and the control. The results are reported in Table 4.4.

	Activation time difference from control [ms]	Correlation with control	SSE difference from control
Gaussian	1 [0, 5]	0.86 [0.72, 0.94]	15.31 [4.94, 26.74]
Tikhonov $\lambda = 0$	2 [1, 6]	0.82 [0.68, 0.93]	14.74 [4.73, 25.30]
Tikhonov $\lambda = 30$	**1 [0, 3]**	**0.96 [0.94, 0.98]**	5.53 [1.67, 12.23]
Unconstrained	2 [1, 4]	0.90 [0.81, 0.94]	**0**

Table 4.4. *Median [p25, p75] of evaluation measures regarding the Gaussian, Tikhonov using regularisation parameter $\lambda=0$ and $\lambda=30$ and the unconstrained solution.*

The unconstrained solution yields an SSE of 0 in all cases due to the direct inverse linear solution, but has a larger difference in activation time. It should be noted that the unconstrained solution has several outliers with negative correlation, which is shown on the Figure 4.10. The Tikhonov $\lambda = 30$ yielded the lowest difference in the dipoles both in terms of activation time and general correlation, and a low SSE difference.

The differences in activation time in the six dipoles across the solutions are presented in Figure 4.9.
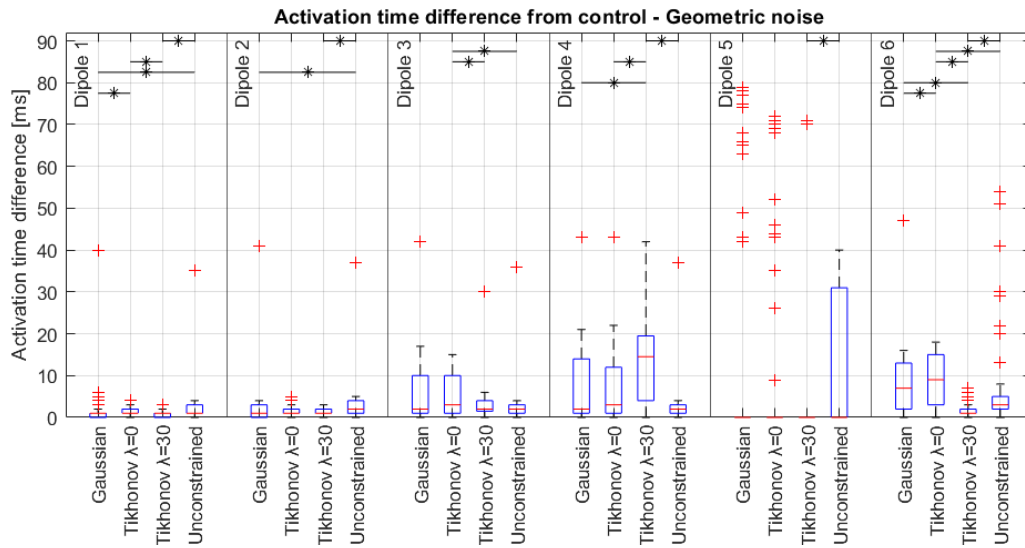
Figure 4.9. *The absolute activation time difference between the dipoles with geometric noise and the control dipoles using each regularisation. A horizontal line with an asterisk denotes a significant difference.*

Generally, all solutions had a more robust performance in terms of activation time in dipole 1 and 2. For dipole 5 the dipole activation time had a very small difference but with greater outliers, with the exception of the unconstrained solution where the activation time difference has a 75th percentile of 31 ms. By comparing the Gaussian regularisation and Tikhonov $\lambda=0$, a significant difference was seen in dipole 1 and 6, but otherwise they had a similar performance.

The correlation between the dipoles with geometric noise and control dipoles are depicted in Figure 4.10.
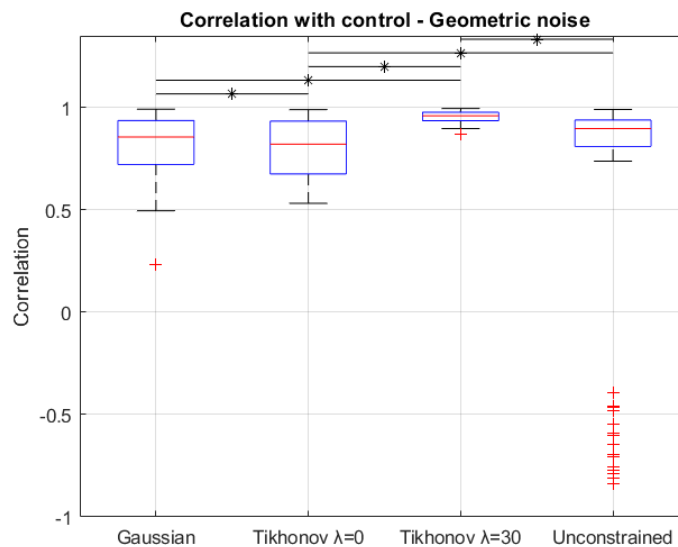
Figure 4.10. *The correlation between dipoles with geometric noise calculated with the Gaussian, Tikhonov $\lambda=0$ and $\lambda=30$ and unconstrained solution, and the control dipoles. A horizontal line with an asterisk denotes a significant difference.*

Tikhonov $\lambda = 30$ achieved significantly higher correlation compared to all other regularisations. The unconstrained solution yielded outliers with negative correlation, which were not seen in the other solutions. The smallest interquartile range (IQR) was achieved using Tikhonov $\lambda = 30$ regularisation, whereas the Gaussian optimisation and Tikhonov $\lambda = 0$ achieved similar median and IQR of the correlation.

The difference in SSE between the control dipoles and the dipoles with geometric noise is shown in Figure 4.11.
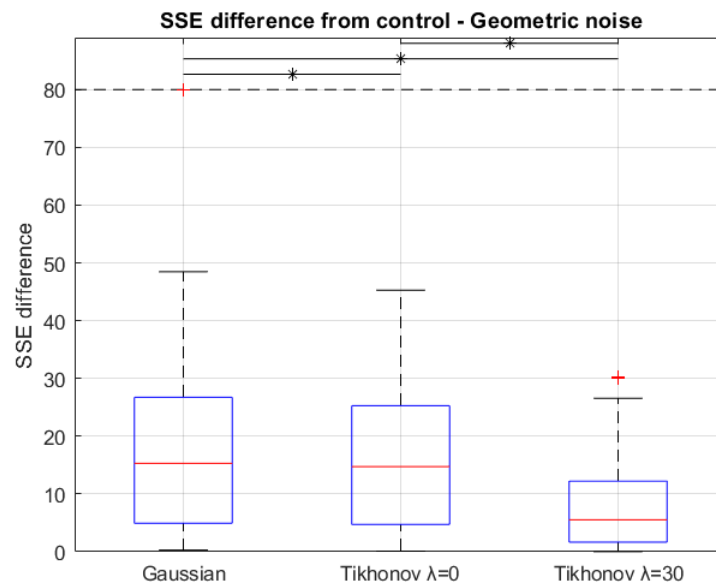
Figure 4.11. *The difference in SSE between the Gaussian and Tikhonov regularisation using regularisation parameter $\lambda=0$ and $\lambda=30$ with geometric noise and the control dipoles. A horizontal line with an asterisk denotes a significant difference.*

Tikhonov $\lambda = 30$ had the lowest SSE difference of 5.53[1.67, 12.23], with a more narrow IQR compared with the two other regularisations. However, the SSE of Tikhonov $\lambda = 30$ was higher than the two other regularisations, meaning that the solution might be robust but less accurate in reconstructing the ECG. The SSE of the unconstrained solution is 0 in all cases and is therefore not presented in the boxplot.

4.3.1.3 Measurement noise

The results of the solutions with white Gaussian noise affected ECG recordings are reported in Table 4.5.

	Activation time difference from control [ms]	Correlation with control	SSE difference from control
Gaussian	**0 [0, 0]**	**1.00 [1.00, 1.00]**	1.83 [1.57, 1.99]
Tikhonov $\lambda = 0$	0 [0, 1]	0.99 [0.99, 0.99]	0.66 [0.52, 0.88]
Tikhonov $\lambda = 30$	0 [0, 1]	0.99 [0.99, 0.99]	0.98 [0.63, 1.24]
Unconstrained	0 [0, 1]	0.96 [0.96, 0.96]	**0**

Table 4.5. *Median [p25, p75] of evaluation measures regarding the Gaussian, Tikhonov using regularisation parameter λ=0 and λ=30, and the unconstrained solution.*

The activation time differences in the individual dipoles of each solution are presented in Figure 4.12.
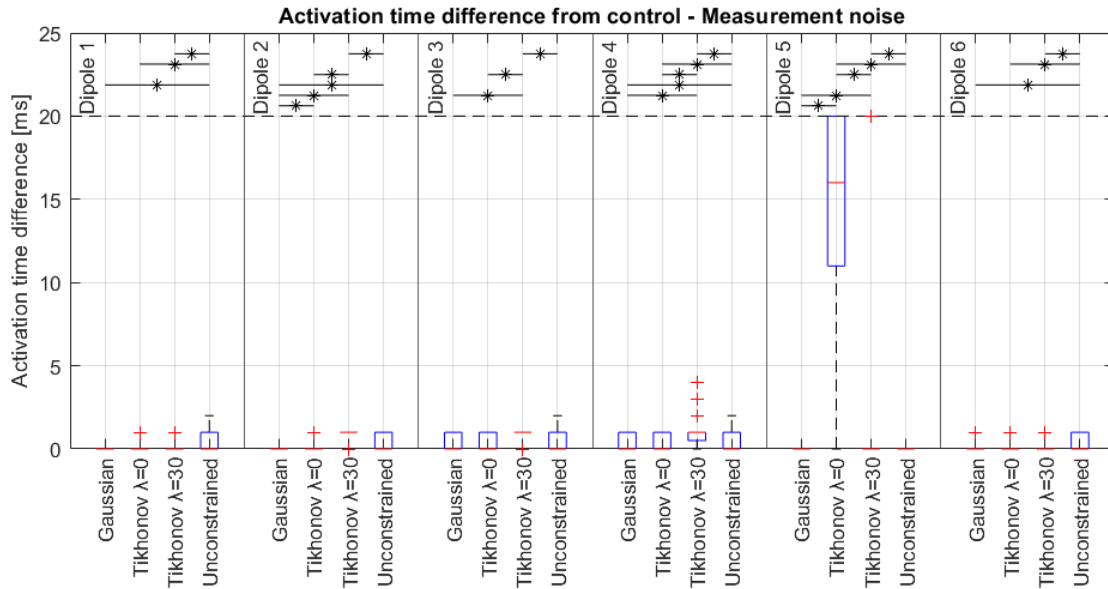
Figure 4.12. *The activation time difference between the dipoles with measurement noise and the control dipoles using each regularisation. The maximum value was set to 20 ms which clips the boxplot in dipole 5 as well as puts outliers at value 20. A horizontal line with an asterisk denotes a significant difference.*

The absolute differences of the activation times were typically low. For dipole 1, 2, 3, 4 and 6, all solutions had an activation time difference between 0 and 1 ms with the exception of a few outliers. For dipole 5 in Tikhonov $\lambda = 0$ the difference was greater with a median of 16 ms, and Tikhonov $\lambda = 30$ had 6 outliers around 70 ms difference.

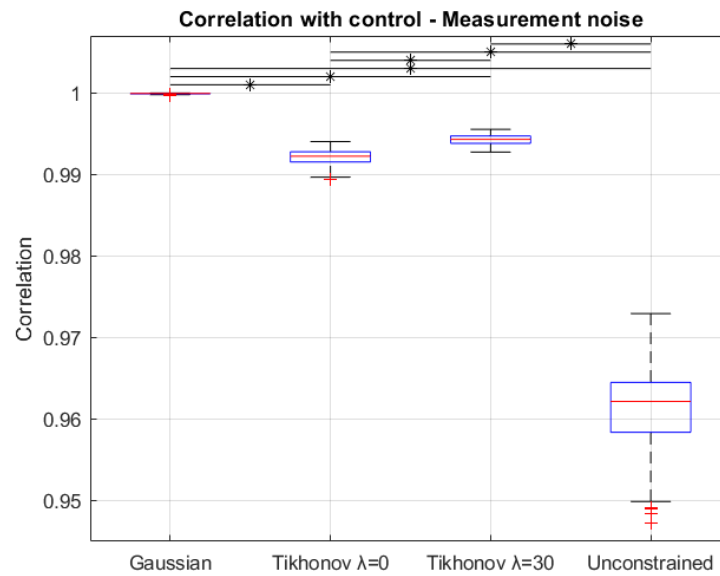The correlations between the control dipoles and the dipoles with measurement noise are reported in Figure 4.13.

Figure 4.13. *The correlation between the dipoles with measurement noise and the control dipoles for the Gaussian, Tikhonovλ=0 and λ=30 and unconstrained solution. A horizontal line with an asterisk denotes a significant difference.*

The highest correlation between the dipoles with measurement noise and control dipoles was achieved with Gaussian regularisation, yielding a correlation of 1.0 [1.0, 1.0]. The unconstrained solution yielded the lowest correlation.

The differences in SSE between the control dipoles and the dipoles with measurement noise are shown in Figure 4.14. The unconstrained solution is not presented on the figure since the SSE is always 0.
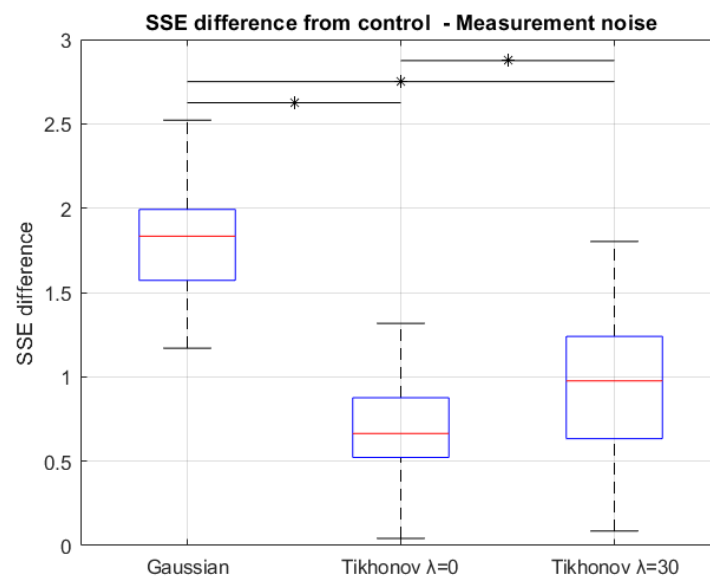
Figure 4.14. *The difference in SSE between dipoles with measurement noise and control dipoles for the Gaussian and Tikhonov regularisation using regularisation parameter λ=0 and λ=30. A horizontal line with an asterisk denotes a significant difference.*

The difference of the SSE of the solutions were all significantly different. The lowest median difference in SSE, besides the unconstrained solutions, was achieved by Tikhonov $\lambda = 0$ with a difference of $0.66[0.52, 0.88]$.

The unconstrained solution generally showed a high sensitivity to both geometric noise and measurement noise in terms of high activation time difference and low correlation. Therefore it was excluded from further analysis.

4.3.2 Characteristics of dipole activations

To determine the best method for dyssynchrony quantification the Gaussian, Tikhonov $\lambda = 0$ and Tikhonov $\lambda = 30$ regularisation were investigated in terms of SSE and morphology of the normal and LBBB population.

In Table 4.6 the median [p25,p75] SSE of the three regularisations are presented for the normal and the LBBB population.

	Normal [SSE (mV^2)]	LBBB [SSE (mV^2)]	P-value
Gaussian	7.36 [4.81,10.68]*	14.68 [10.01, 21.02]	<0.001
Tikhonov $\lambda = 0$	4.80 [3.03, 8.25]*	5.56 [3.03, 9.68]*	0.351
Tikhonov $\lambda = 30$	11.83 [7.14, 16.44]*	13.43 [9.39, 22.42]	0.003
P-value	<0.001	<0.001	

Table 4.6. *Median [p25,p75] SSE of the Gaussian, Tikhonov $\lambda = 0$ and Tikhonov $\lambda = 30$ in normal and LBBB signals. The marking * indicates a difference from one regularisation to the two other regularisations within either normal or LBBB subjects.*

In the Gaussian and Tikhonov $\lambda = 30$ regularisation a lower median SSE was achieved in the normal population compared to the LBBB population, however no significant difference in SSE between normal and LBBB was found for Tikhonov $\lambda = 0$.

The Tikhonov $\lambda=0$ regularisation achieved lowest median SSE in both the normal and the LBBB population compared to the Gaussian and the Tikhonov $\lambda=30$ regularisation. Hence Tikhonov $\lambda=0$ regularisation was superior in reconstructing both normal and LBBB QRS-complexes.

Examples of reconstructed ECGs, from dipoles calculated using Tikhonov $\lambda=0$ regularisation, in case of low and high SSE of normal and LBBB subjects are shown in Figure 4.15.
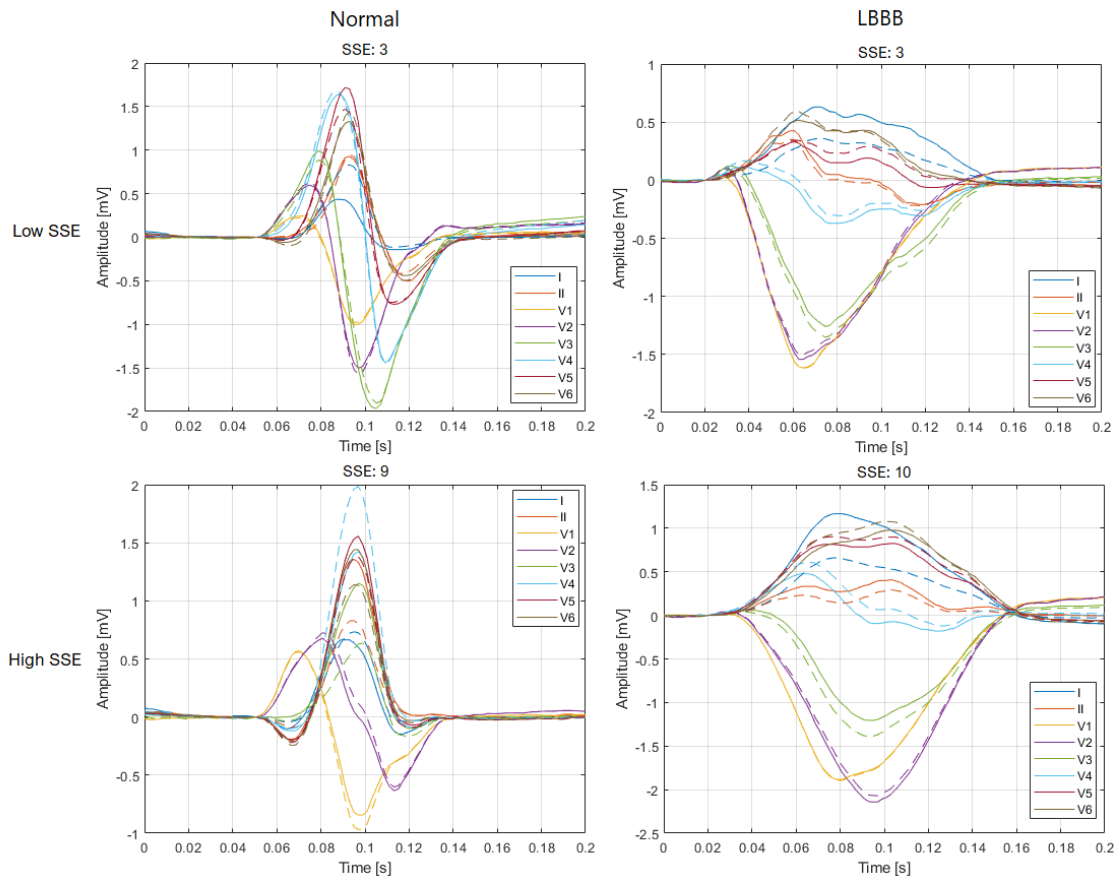
Figure 4.15. *Examples of ECGs with high and low SSE with reconstruction based on dipoles calculated using Tikhonov λ=0 regularisation. The solid lines are the measured ECG whereas the dashed lines are the reconstructed ECGs.*

It can be noticed that even in the case of higher SSE of 9 and 10 mV^2, most of the reconstructed ECG leads have similar morphology compared to the measured ECG, but with some deviation in the amplitudes.

The dipole activations determined using the three types of regularisation have different morphology due to the different inherent restrictions in the regularisations. Representative examples of dipole activations of one normal subject and one LBBB subject is shown in Figure 4.16.
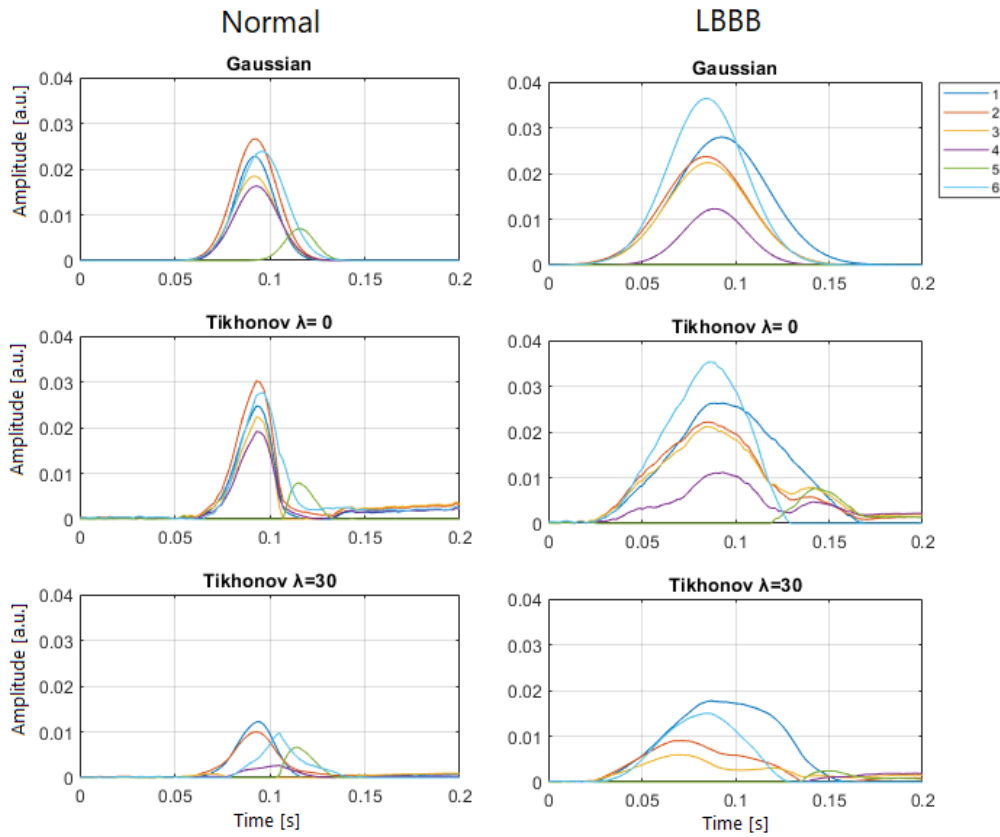
Figure 4.16. *Examples of dipoles of the Gaussian, Tikhonov λ=0 and Tikhonov λ=30 optimisation from one normal subject and one LBBB subject.*

The characteristic Gaussian shape is obvious in the dipole activations of the Gaussian optimisation, whereas the dipole activations of the Tikhonov regularisation are not restricted to have a specific shape. The dipole activations of the normal subject are very similar using the Gaussian and the Tikhonov λ=0 regularisation. In the case of the LBBB subject a larger difference was seen between the dipole activations of the Gaussian and the Tikhonov λ=0 regularisation, with the Tikhonov λ=0 dipole activation being less Gaussian in the LBBB subjects compared to the normal subject. This tendency was generally seen in the 100 normal and 100 LBBB subjects. The amplitude restriction of the Tikhonov λ=30 was clearly seen by the lower amplitudes of the Tikhonov λ=30 dipole activations. Generally, the dipole activations of Tikhonov λ=30 regularisation were the most different from the two other regularisations.

The general characteristics, in terms of time of activation, duration and amplitude, of the dipole activations in the 100 normal and 100 LBBB subjects are presented in the following sections. The parameters were visualised on the geometric heart model using interpolation between dipole positions. The visualisations of the parameters are based on the Tikhonov λ=0 regularisation since it yielded the lowest SSE in both populations. The parameters of all three regularisations are presented as boxplots.

4.3.2.1   Time of activation

The median activation time of the six areas presented by the dipoles are shown in Figure 4.17. The median was calculated across the normal and LBBB population respectively.
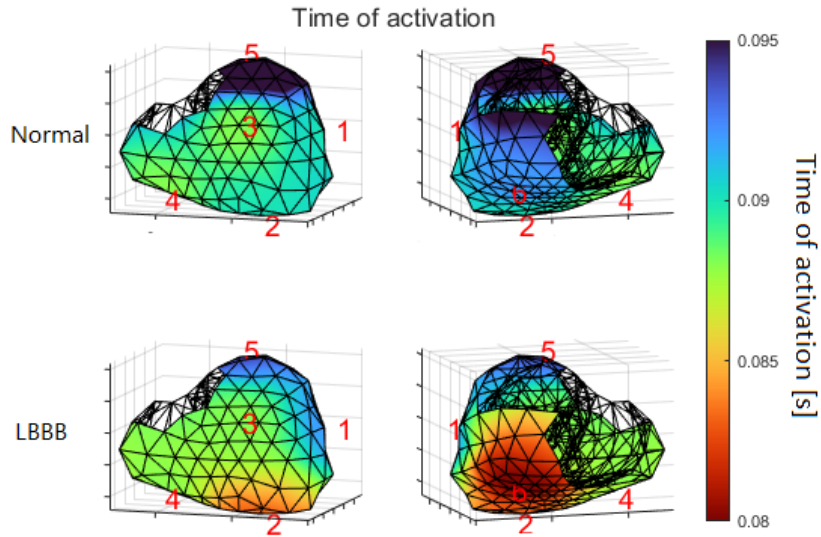

Figure 4.17. *Median time of activation in normal and LBBB subjects calculated using Tikhonov λ=0 regularisation. The numbers indicate which dipole each area is represented by.*

The normal heart was generally activated simultaneously in all areas except the area at the left base represented by dipole 5. The RV was activated slightly earlier compared to the LV. A different activation pattern was seen in the LBBB population, with early activation in the frontal right inferior area represented by dipole 2. In addition, the areas represented by dipole 1 and 5, corresponding to the superior part of the LV, were activated the latest.

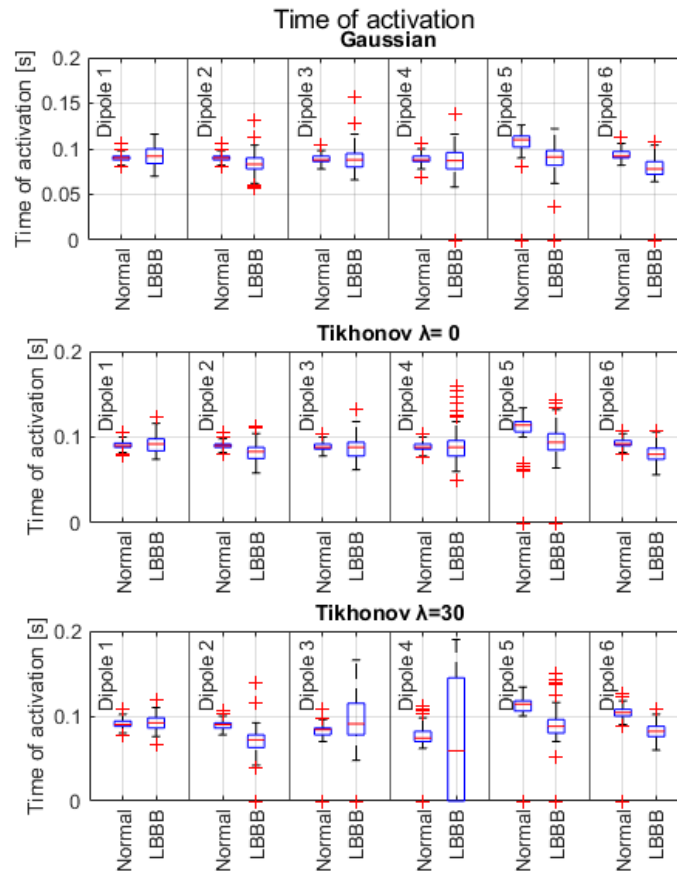The activation times of all three regularisations are presented in Figure 4.18.

Figure 4.18. *Boxplot of the time of activation in the normal and LBBB subjects using the different regularisations.*

The tendencies of the time of activation was similar using the Gaussian and Tikhonov λ=0 regularisation.

4.3.2.2 Duration

Figure 4.19 shows the median duration of activation in the different areas of the heart in normal and LBBB subjects. It is clear, that the duration was generally longer in the LBBB population compared to the normal population and that the prolonged duration in LBBB was seen in all areas of the heart. The area which was the least prolonged was the inferior LV represented by dipole 6.
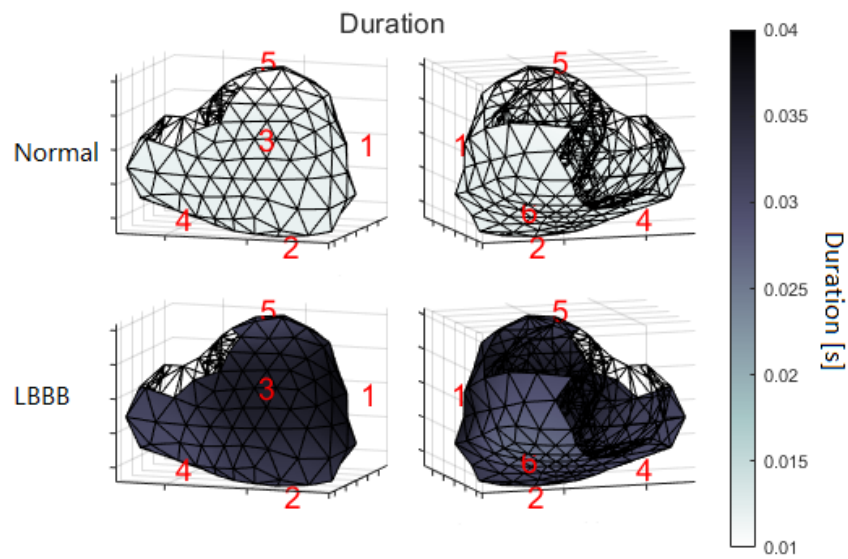
Figure 4.19. *Median duration of dipole activation in normal and LBBB subjects calculated using Tikhonov λ=0 regularisation. The numbers indicate which dipole each area is represented by.*

The duration of the dipoles using the three regularisations are shown in Figure 4.20.
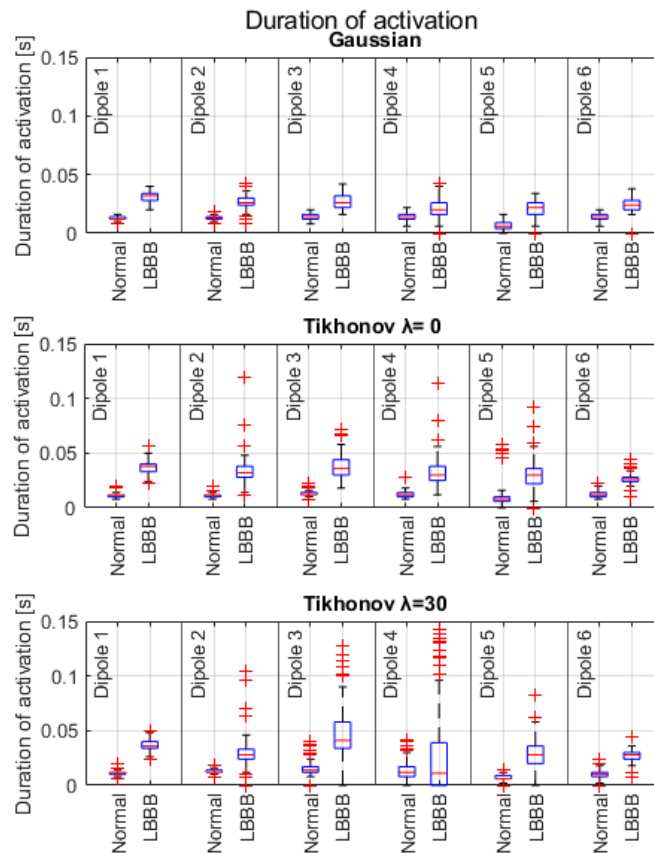

Figure 4.20. *Boxplot of the duration of activation in the normal and LBBB subjects using the different regularisations.*

All three regularisations yielded prolonged dipole activations in the LBBB population in all six dipoles.

4.3.2.3 Amplitude

The median amplitude calculated from the Tikhonov $\lambda=0$ regularisation is shown in Figure 4.21.
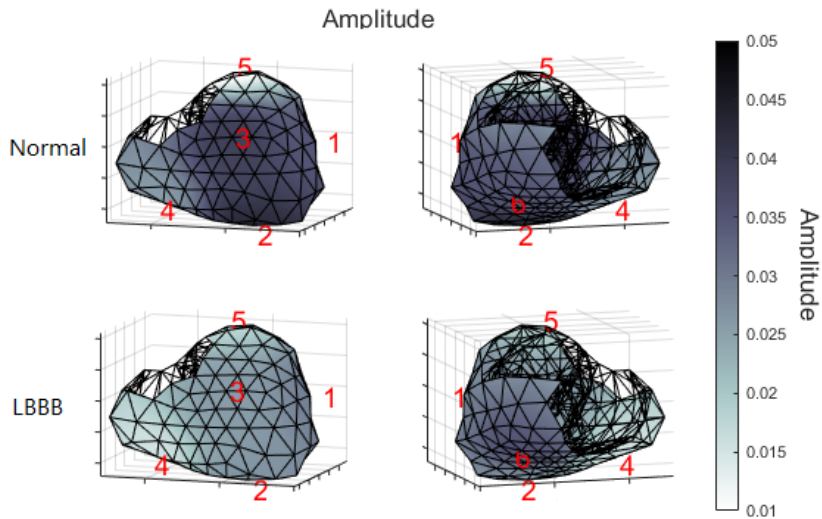

Figure 4.21. *Median amplitude of dipole activation in normal and LBBB subjects calculated using Tikhonov $\lambda=0$ regularisation. The numbers indicate which dipole each area is represented by.*

Generally the amplitude of the LBBB population was lower compared to the normal population. The lowest amplitude in the normal population was seen in the base of the ventricles which was represented by dipole 4 and 5 whereas the rest of the normal heart was activated with similar amplitudes. The LBBB heart had the highest amplitude of activation in the inferior LV represented by dipole 6. Similar to the normal heart, the base was activated with the lowest amplitude.

The boxplots showing the amplitude of all dipoles using the three regularisations are shown in Figure 4.22.
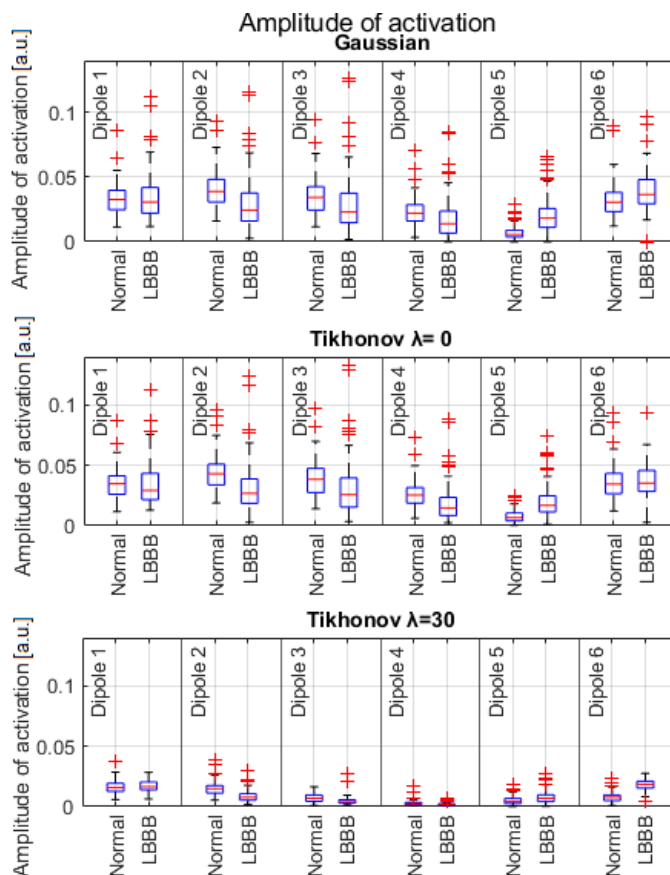
Figure 4.22. *Boxplot of the amplitude of activation in the normal and LBBB subjects using the different regularisations.*

The same tendencies was seen using the Gaussian regularisation and the Tikhonov $\lambda = 0$. The Tikhonov $\lambda=30$ regularisation yielded similar tendencies but with lower amplitude of all dipoles.

4.3.3 Investigation of dyssynchrony

The dyssynchrony between the LV and RV was investigated by the three dyssynchrony measures described in Section 2.3.3 on page 33.

4.3.3.1 Selection of representative dipole from left and right ventricle

In order to quantify the dyssynchrony measure 1 and 2, two dipoles were selected of which one reflected the activation of the LV and one reflected the activation of the RV. Position and direction of each dipoles are presented on Figure 4.23, along with the tested combinations of dipoles.
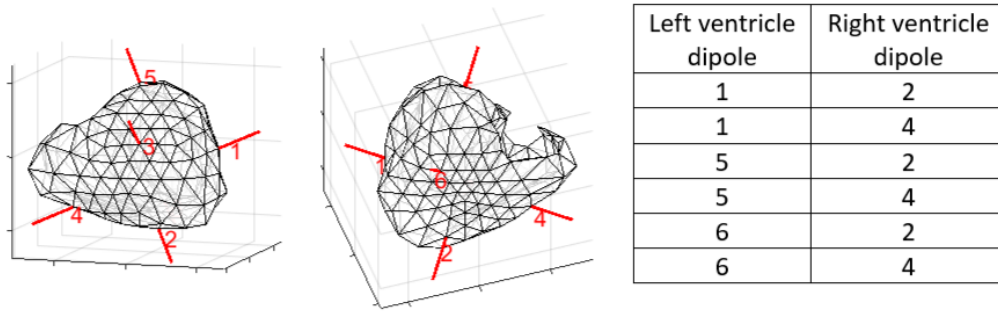
Figure 4.23. *Dipole placement and combinations of dipoles. As an example dipole 1 and 2 were combined and tested.*

Dipole 3 was excluded, since it was positioned in a boundary area between the RV and LV. To investigate the combination of dipoles which best reflected dyssynchrony in the LBBB subjects, the dyssynchrony of all combinations are shown in Figure 4.24.
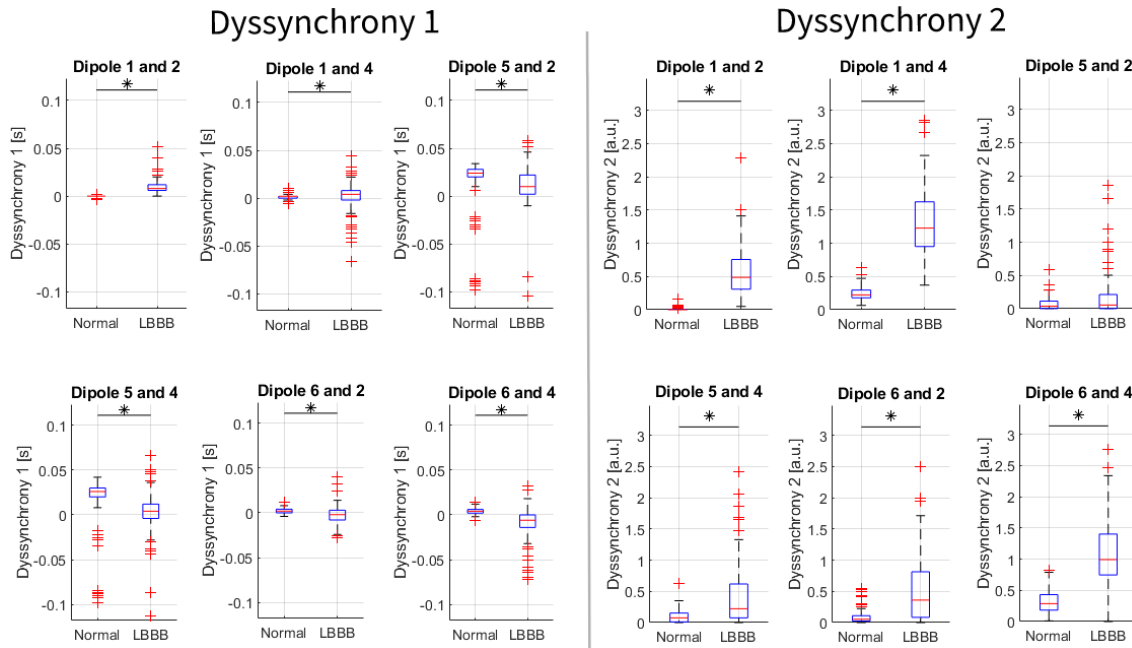

Figure 4.24. *Boxplots of dyssynchrony measure 1 and 2 for each pair of dipoles for both normal and LBBB subjects. A horizontal line with an asterisk denotes a significant difference.*

It was evident that dipole 1 and 2 best separated normal subjects from LBBB subjects, since the quartiles did not overlap between groups in neither dyssynchrony 1 nor 2. Also, the normal subjects had narrow IQRs, which was expected in a normal population. Dipole 1 and 2 were therefore selected for the dyssynchrony measure 1 and 2.

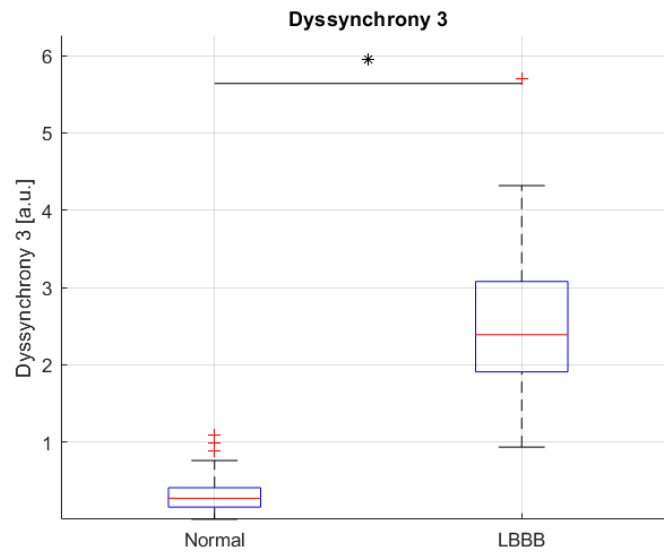On Figure 4.25 dyssynchrony 3 for normal and LBBB subjects are visualised.

Figure 4.25. *Dyssynchrony 3 for normal and LBBB subjects. A horizontal line with an asterisk denotes a significant difference.*

The dyssynchrony 3 measure was able to separate all normal subjects from LBBB subjects, except from two outliers in the normal population.

4.3.3.2 Dyssynchrony quantification

The correlations of dyssynchrony measure 1, 2, and 3 with QRS duration, QRS-area and Q-LV are presented in Figure 4.26.
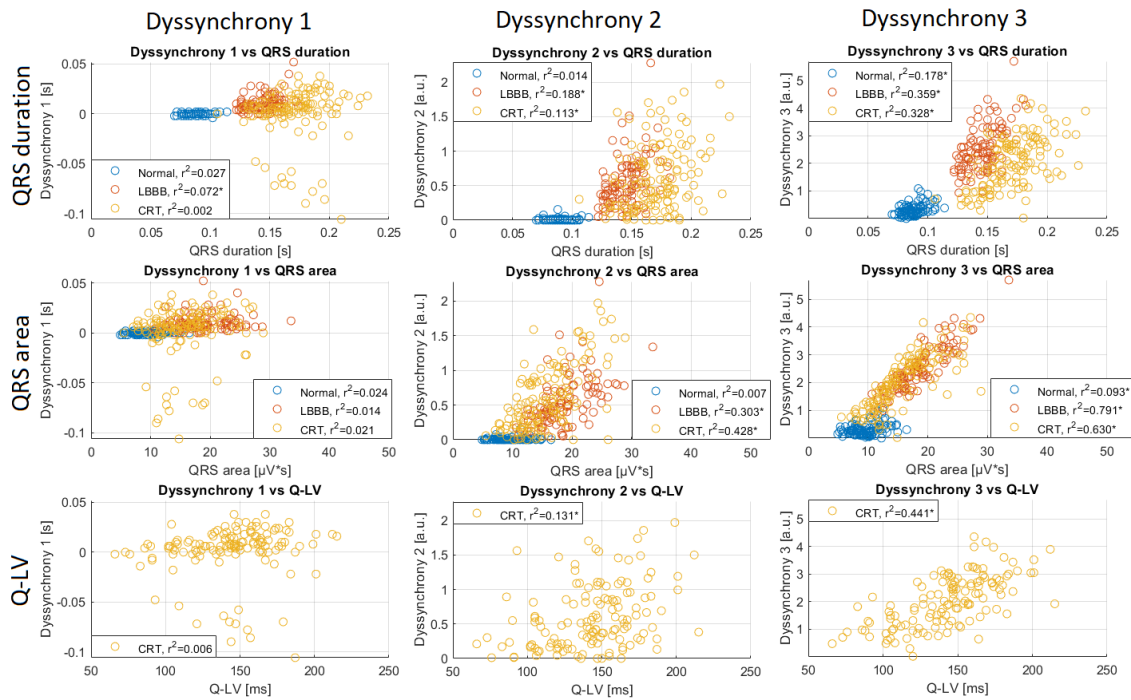
Figure 4.26. *The correlations of dyssynchrony measure 1, 2, and 3 with QRS duration, QRS-area and Q-LV, within each groups of normal, LBBB and CRT subjects. Significant linear slope within each group for each subplot is denoted with '*'.*

Dyssynchrony 1 had no correlation with QRS duration, QRS area or Q-LV in any of the subject group, except for LBBB and QRS duration ($r^2 = 0.072$). Dyssynchrony 2 had no correlation with QRS duration or QRS area in normal subjects, however for LBBB and CRT subjects the slopes were significant and up to $r^2 = 0.428$ in CRT subjects on QRS area.

Dyssynchrony 3 had a relatively high correlation with QRS duration and QRS area in LBBB ($r^2 = 0.359$, $r^2 = 0.791$) and CRT ($r^2 = 0.328$, $r^2 = 0.630$) subjects, however a lower correlation in normal subjects ($r^2 = 0.178$, $r^2 = 0.093$) was found.

Dyssynchrony 3 and dyssynchrony 2 were correlated with Q-LV, of which dyssynchrony 3 had the highest correlation ($r^2 = 0.441$ vs $r^2 = 0.131$)

To investigate the correlation among QRS duration, QRS area, and Q-LV, scatter plots and correlations are presented on Figure 4.27.
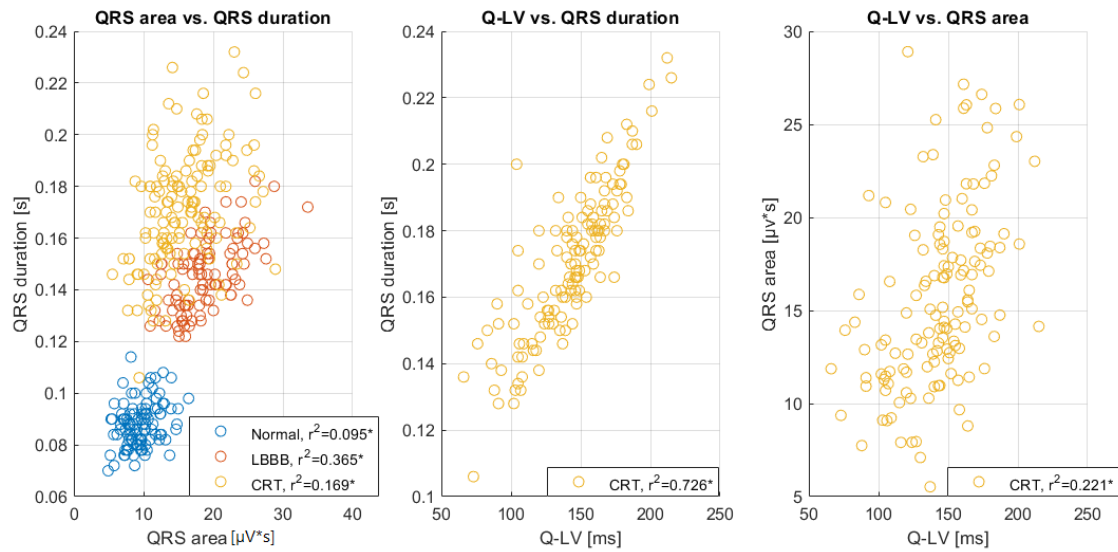
Figure 4.27. *Correlation among known dyssynchrony measures (QRS duration, QRS area, and Q-LV) within groups of normal, LBBB and CRT subjects. Significant linear slope within each group for each subplot is denoted with '*'.*

Highest correlation was seen in Q-LV vs. QRS duration within the CRT population with a $r^2 = 0.726$. Lower correlation were present between QRS area vs. QRS duration, and Q-LV vs. QRS area, however all linear correlations were significant.

Bibliography

Alday et al., **2019**. Erick Andres Perez Alday, Alan P. Whittaker, Dominic G.Benson and Michael A. Colman. *Effects of Heart Rate and Ventricular Wall Thickness on Non-invasive Mapping: An in silico Study.* Frontiers in Physiology, 10, 308, 2019. doi:10.3389/fphys.2019.00308.

Andersen et al., **2021**. Dennis Christian Andersen, Kristian Kragholm, Line Thorgaard Petersen, Claus Graff, Peter L. Sørensen, Jonas Bille Nielsen, Adrian Pietersen, Peter Søgaard, Brett D. Atwater, Daniel J. Friedman, Christian Torp-Pedersen and Christoffer Polcwiartek. *Association between vectorcardiographic QRS area and incident heart failure diagnosis and mortality among patients with left bundle branch block: A register-based cohort study.* Journal of Electrocardiology, 69, 30–35, 2021. doi:10.1016/j.jelectrocard.2021.09.002.

Aydin and Dogrusoz, **2011**. Umit Aydin and Yesim Serinagaoglu Dogrusoz. *A Kalman filter-based approach to reduce the effects of geometric errors and the measurement noise in the inverse ECG problem.* Medical & Biological Engineering & Computing, 49, 1003–1013, 2011. doi:10.1007/s11517-011-0757-8.

Baldasseroni et al., **2002**. Samuele Baldasseroni, Cristina Opasich, Marco Gorini, Donata Lucci, Niccolò Marchionni, Maurizio Marini, Carlo Campana, Giampaolo Perini, Antonella Deorsola, Giulio Masotti, Luigi Tavazzi and Aldo P. Maggioni. *Left bundle-branch block is associated with increased 1-year sudden and total mortality rate in 5517 outpatients with congestive heart failure: A report from the Italian Network on Congestive Heart Failure.* American Heart Journal, 143(3), 398–405, 2002. doi:10.1067/mhj.2002.121264.

Barnes and Johnston, **2016**. Josef P. Barnes and Peter R. Johnston. *Application of robust Generalised Cross-Validation to the inverse problem.* Computers in Biology and Medicine, 69, 213–225, 2016. doi:10.1016/j.compbiomed.2015.12.011.

Bear et al., **2018a**. Laura R Bear, Y Serinagaoglu Dogrusoz, J Svehlikova, J Coll-Font, W Good, E van Dam, R Macleod, E Abell, R Walton, R Coronel, Michel Haissaguerre and R Dubois. *Effects of ECG Signal Processing on the Inverse Problem of Electrocardiography.* Computing in cardiology, 45, 1–4, 2018a. doi:10.22489/CinC.2018.070.

Bear et al., **2018b**. Laura R. Bear, Peter R. Huntjens, Richard D. Walton, Olivier Bernus, Ruben Coronel and Rémi Dubois. *Cardiac electrical dyssynchrony is accurately detected by noninvasive electrocardiographic imaging.* Heart Rhythm, 15, 1058–1069, 2018b. doi:10.1016/j.hrthm.2018.02.024.

Brignole et al., **2013**. Michele Brignole, Angelo Auricchio, Gonzalo Baron-Esquivias, Pierre Bordachar, Giuseppe Boriani, Ole-A Breithardt, John Cleland, Jean-Claude Deharo, Victoria Delgado, Perry M. Elliott, Bulent Gorenek, Carsten W. Israel, Christophe Leclercq, Cecilia Linde, Lluís Mont, Luigi Padeletti, Richard Sutton and Panos E. Vardas. *2013 ESC Guidelines on cardiac pacing and cardiac resynchronization therapy - The Task Force on cardiac pacing and resynchronization therapy of the European Society of Cardiology (ESC). Developed in collaboration with the European Heart Rhythm Association.* Europace, 15(8), 1070–1118, 2013. doi:10.1093/europace/eut206.

Chamorro-Servent et al., **2019**. Judit Chamorro-Servent, Remi Dubois and Yves Coudiere. *Considering new regularization parameter-choice techniques for choice techniques for the Tikhonov method to improve the accuracy of electrocardiographic imaging.* Frontiers in Physiology, 10, 273, 2019. doi:10.3389/fphys.2019.00273.

Emerek et al., **2019**. Kasper Emerek, Daniel J. Friedman, Peter Lyngø Sørensen, Steen Møller Hansen, Jacob Moesgaard Larsen, Niels Risum, Anna Margrethe Thøgersen, Claus Graff, Joseph

Kisslo, Peter Søgaard and Brett D. Atwater. *Vectorcardiographic QRS Area is Associated with Long-Term Outcome Following Cardiac Resynchronization Therapy.* Heart Rythm, 16, 213–219, 2019. doi:10.1016/j.hrthm.2018.08.028.

Erenler and Dogrusoz, **2019**. Taha Erenler and Yesim Serinagaoglu Dogrusoz. *ML and MAP estimation of parameters for the Kalman filter and smoother applied to electrocardiographic imaging.* Medical & Biological Engineering & Computing, 57, 2093–2113, 2019. doi:10.1007/s11517-019-02018-6.

Eriksson et al., **1998**. P Eriksson, P O Hansson, H eriksson and M Dellborg. *Bundle-branch block in a general male population: the study of men born 1913.* Circulation, 98(22), 2494–2500, 1998. doi:10.1161/01.cir.98.22.2494.

GE Healthcare, **2019**. GE Healthcare. *Marquette 12SL - ECG Analysis Program - Physician's Guide.* 2019.

Gharbalchi et al., **2020**. Fourough Gharbalchi, Y. Serinagaoglu Dogrusoz, O.N.Onak and G.-W. Weber. *Reduced leadset selection and performance evaluation in the inverse problem of electrocardiography for reconstructing the ventricularly paced electrograms.* Journal of electrocardiology, 60, 44–53, 2020. doi:10.1016/j.jelectrocard.2020.02.017.

Ghosh and Rudy, **2009**. Subham Ghosh and Yoram Rudy. *Application of L1-Norm Regularization to Epicardial Potential Solution of the Inverse Electrocardiography Problem.* Annals of Biomedical Engineering, 37, 902–912, 2009. doi:10.1007/s10439-009-9665-6.

Gold et al., **2011**. Michael R. Gold, Ulrika Birgersdotter-Green, Jagmeet P. Singh, Kenneth A. Ellenbogen, Yinghong Yu, Timothy E. Meyer, Milan Seth, and Patrick J. Tchou. *The relationship between ventricular electrical delay and left ventricular remodelling with cardiac resynchronization therapy.* European Heart Journal, 32, 2516–2524, 2011. doi:10.1093/eurheartj/ehr329.

Gulrajani, **1998**. Ramesh M. Gulrajani. *The forward and inverse problems of electrocardiography.* IEEE Engineering in Medicine and Biology Magazine, 17, 84–101, 1998. doi:10.1109/51.715491.

Hadamard, **1923**. Jacques Hadamard. *Chapter I.* Yale University Press, 1923.

Hall and Guyton, **2011**. John E. Hall and Arthur C. Guyton. *Textbook of Medical Physiology, 12th Edition.* Saunders Elsevier, 2011. ISBN 978-1-4160-4574-8.

Hansen, **2000**. P. C. Hansen. *The L-Curve and its Use in the Numerical Treatment of Inverse Problems.* WIT Press, 2000.

Hardarson et al., **1987**. T Hardarson, A Arnason, G J Eliasson, K Palsson and N Sigfusson. *Left bundle branch block : prevalence , incidence , follow-up and outcome.* European Heart Journal, 8(10), 1075–1079, 1987. doi:https://doi.org/10.1093/oxfordjournals.eurheartj.a062172.

Imanishi et al., **2006**. Ryo Imanishi, Shinji Seto, Shinichiro Ichimaru, Eiji Nakashima, Katsusuke Yano and Masazumi Akahoshi. *Prognostic Significance of Incident Complete Left Bundle Branch Block Observed Over a 40-Year Period.* American Journal of Cardiology, 98(5), 644–648, 2006. doi:10.1016/j.amjcard.2006.03.044.

Jiang et al., **2006**. Mingfeng Jiang, Ling Xia and Guofa Shou. *The Use of Genetic Algorithms for Solving the Inverse Problem of Electrocardiography.* International Conference of the IEEE Engineering in Medicine and Biology Society, pages 3907–3910, 2006. doi:10.1109/IEMBS.2006.259672.

Jiang et al., **2007**. Mingfeng Jiang, Ling Xia, Guofa Shou and Min Tang. *Combination of the LSQR method and a genetic algorithm for solving the electrocardiography inverse problem.* Physics in Medicine & Biology, 52, 1277–1294, 2007. doi:10.1088/0031-9155/52/5/005.

Jiang et al., **2008**. Mingfeng Jiang, Ling Xia, Guofa Shou, Feng Liu and Stuart Crozier. *Two hybrid regularization frameworks for solving the electrocardiography inverse problem.* Physics in medicine and biology, 52, 5151–5164, 2008. doi:10.1088/0031-9155/53/18/020.

Jiang et al., **2009a**. Mingfeng Jiang, Ling Xia, Wenqing Huang, Guofa Shou, Feng Liu and Stuart Crozier. *The application of subspace preconditioned LSQR algorithm for solving the electrocardiography inverse problem.* Medical Engineering & Physics, 31, 979–985, 2009a. doi:10.1016/j.medengphy.2009.05.011.

Jiang et al., **2009b**. Mingfeng Jiang, Ling Xia, Guofa Shou, Qing Wei, Feng Liu and Stuart Crozier. *Effect of Cardiac Motion on Solution of the Electrocardiography Inverse Problem.* IEEE transactions of biomedical engineering, 56, 923–931, 2009b. doi:10.1109/TBME.2008.2005967.

Jiang et al., **2011**. Mingfeng Jiang, Lingyan Zhu, Yaming Wang, Ling Xia, Guofa Shou, Feng Liu and Stuart Crozier. *Application of kernel principal component analysis and support vector regression for reconstruction of cardiac transmembrane potentials.* Physics in medicine and biology, 56, 1727–1742, 2011. doi:10.1088/0031-9155/56/6/013.

Jiang et al., **2012**. Mingfeng Jiang, Feng Liu, Yaming Wang, Guofa Shou, Wenqing Huang and Huaxiong Zhang. *A Hybrid Model of Maximum Margin Clustering Method and Support Vector Regression for Noninvasive Electrocardiographic Imaging.* Computational and Mathematical Methods in Medicine, 2012, 9, 2012. doi:10.1155/2012/436281.

Jiang et al., **2013**. Mingfeng Jiang, Shanshan Jiang, Lingyan Zhu, Yaming Wang, Wenqing Huang and Heng Zhang. *Study on parameter optimization for support vector regression in solving the inverse ECG problem.* Computational and Mathematical Methods in Medicine, 2013, 9, 2013. doi:10.1155/2013/158056.

Johnston, **2018**. Peter R. Johnston. *Accuracy of electrocardiographic imaging using the method of fundamental solutions.* Computers in Biology and Medicine, 102, 433–448, 2018. doi:10.1016/j.compbiomed.2018.09.016.

Kalinin et al., **2019**. Alexander Kalinin, Danila Potyagaylo and Vitaly Kalinin. *Solving the inverse problem of electrocardiography on the endocardium using a single layer source.* Frontiers in Physiology, 10, 58, 2019. doi:10.3389/fphys.2019.00058.

Kara et al., **2019**. Vinay Kara, Haibo Ni, Erick Andres Perez Alday and Henggui Zhang. *Corrigendum: ECG Imaging to Detect the Site of Ventricular Ischemia Using Torso Electrodes: A Computational Study.* Frontiers in physiology, 10, 692, 2019. doi:10.3389/fphys.2019.00692.

Konttila et al., **2014**. Teijo Konttila, Ville Mäntynen and Matti Stenroos. *Comparison of minimum-norm estimation and beamforming in electrocardiography with acute ischemia.* Physiological Measurement, 35, 623–638, 2014. doi:10.1088/0967-3334/35/4/623.

Kusumoto et al., **2019**. Fred M. Kusumoto, Mark H. Schoenfeld, Coletta Barrett, James R. Edgerton, Kenneth A. Ellenbogen, Michael R. Gold, Nora F. Goldschlager, Robert M. Hamilton, José A. Joglar, Robert J. Kim, Richard Lee, Joseph E. Marine, Christopher J. McLeod, Keith R. Oken, Kristen K. Patton, Cara N. Pellegrini, Kimberly A. Selzman, Annemarie Thompson and Paul D. Varosy. *2018 ACC/AHA/HRS Guideline on the Evaluation and Management of Patients With Bradycardia and Cardiac Conduction Delay: A Report of the American College of Cardiology/American Heart Association Task Force on Clinical Practice Guidelines and the Heart Rhyth.* Circulation, 140, e382–e482, 2019. doi:10.1161/CIR.0000000000000628.

Li and He, **2001**. Guanglin Li and Bin He. *Localization of the Site of Origin of Cardiac Activation by Means of a Heart-Model-Based Electrocardiographic Imaging Approach.* IEEE Transactions of Biomedical Engineering, 48, 660–669, 2001. doi:10.1109/10.923784.

Lynn et al., **1967**. M. S. Lynn, A. C. L. Barnard, J. H. Hold and L. T. Sheffield. *A proposed method for the inverse problem in electrocardiology.* Biophysical Journal, 7, 925–945, 1967. doi:10.1016/S0006-3495(67)86630-X.

Malmivuo and Plonsey, **1995**. Jaakko Malmivuo and Robert Plonsey. *Principles and Applications of Bioelectric and Biomagnetic Fields.* Oxford University Press, New York, 1995. ISBN 978-0195058239.

MathWorks, **2022**. MathWorks. *fmincon*, 2022. https://se.mathworks.com/help/optim/ug/fmincon.html#d123e91530. Latest seen - 11.04.2022.

Mcmurray et al., **2012**. John J.V. Mcmurray, Stamatis Adamopoulos, Stefan D. Anker, Angelo Auricchio, Michael Böhm, Kenneth Dickstein, Volkmar Falk, Gerasimos Filippatos, Cândida Fonseca, Miguel Angel Gomez-Sanchez, Tiny Jaarsma, Lars Kober, Gregory Y.H. Lip, Aldo Pietro Maggioni, Alexander Parkhomenko, Burkert M. Pieske, Bogdan A. Popescu, Per K. Ronnevik, Frans H. Rutten, Juerg Schwitter, Petar Seferovic, Janina Stepinska, Pedro T. Trindade, Adriaan A. Voors, Faiez Zannad and Zeiher. *ESC Guidelines for the diagnosis and treatment of acute and chronic heart failure 2012.* European Journal of Heart Failure, 14(8), 803–869, 2012. doi:10.1093/eurjhf/hfs105.

Moher et al., **2009**. David Moher, Alessandro Liberati, Jennifer Tetzlaff, Douglas G. Altman and PRISMA Group. *Preferred reporting items for systematic reviews and meta-analyses: The PRISMA statement.* PLoS Medicine, 6(7), 2009. doi:10.1371/journal.pmed.1000097.

Nakano et al., **2021**. Y. Nakano, E.A. Rashed, T. Nakane and A Laakso, I. andSensors Hirata. *ECG Localization Method Based on Volume Conductor Model and Kalman Filtering.* Sensors, 21, 4275, 2021. doi:10.3390/s21134275.

Noheria et al., **2019**. Amit Noheria, Sandeep Sodhi and G. Joseph Orme. *The Evolving Role of Electrocardiography in Cardiac Resynchronization Therapy.* Current Treatment Options in Cardiovascular Medicine, 21, 1–14, 2019. doi:10.1007/s11936-019-0784-6.

Onak et al., **2019**. Onder Nazim Onak, Yesim Serinagaoglu Dogrusoz and Gerhard Wilhelm Weber. *Evaluation of multivariate adaptive non-parametric reduced-order model for solving the inverse electrocardiography problem: a simulation study.* Medical & Biological Engineering & Computing, 57, 967–993, 2019. doi:10.1007/s11517-018-1934-9.

Pereira et al., **2020**. Helder Pereira, Steven Niederer and Christopher A. Rinaldi. *Electrocardiographic imaging for cardiac arrhythmias and resynchronization therapy.* European society of Cardiology, 22, 1447–1462, 2020. doi:10.1093/europace/euaa165.

Ploux et al., **2013**. Sylvain Ploux, Joost Lumens, Zachary Whinnett, Michel Montaudon, Maria Strom, Charu Ramanathan, Nicolas Derval, Adlane Zemmoura, Arnaud Denis, Maxime De Guillebon, Ashok Shah, Mélèze Hocini, Pierre Jaïs, Philippe Ritter, Michel Haïssaguerre, Bruce L. Wilkoff and Pierre Bordachar. *Noninvasive Electrocardiographic Mapping to Improve Patient Selection for Cardiac Resynchronization Therapy.* Journal of American College of Cardiology, 61, 2435–2443, 2013. doi:10.1016/j.jacc.2013.01.093.

Potyagaylo et al., **2014**. Danila Potyagaylo, Elisenda Gil Cortés, Walther H. W. Schulze and Olaf Dössel. *Binary optimization for source localization in the inverse problem of ECG.* Medical and Biological Engineering and Computing, 52, 717–728, 2014. doi:10.1007/s11517-014-1176-4.

Potyagaylo et al., **2016**. Danila Potyagaylo, Olaf Dossel and Peter van Dam. *Influence of Modeling Errors on the Initial Estimate for Nonlinear Myocardial Activation Times Imaging Calculated With Fastest Route Algorithm.* IEEE Transactions on Biomedical Engineering, 63, 2576–2584, 2016. doi:10.1109/TBME.2016.2561973.

Pullan et al., **2010**. Andrew J. Pullan, Leo K. Cheng, Martyn P. Nash, Alireza Ghodrati, Rob MacLeod and Dana H. Brooks. *The Inverse Problem of Electrocardiography*. Springer, London, 2010. ISBN 978-1-84882-045-6. Chapter 9.

Rabkin et al., **1980**. S. W. Rabkin, F. A.L. Mathewson and R. B. Tate. *Natural history of left bundle-branch block*. British Heart Journal, 43, 164–169, 1980. doi:10.1136/hrt.43.2.164.

Ramanathan and Rudy, **2001**. Charulatha Ramanathan and Yoram Rudy. *Effect of Torso Inhomogeneities on Noninvasive Reconstruction of Epicardial Potentials, Electrograms, and Isochrones*. Journal of cardiovascular electrophysiology, 12, 241–252, 2001. doi:10.1046/j.1540-8167.2001.00241.x.

Rasmussen et al., **2019**. Peter Vibe Rasmussen, Morten Wagner Skov, Jonas Ghouse, Adrian Pietersen, Steen Møller Hansen, Christian Torp-Pedersen, Stig Køber, Lars Haunsø, Morten Salling Olesen, Jesper Hastrup Svendsen, Jacob Melgaard, Claus Graff, Anders Gaardsdal Holst and Jonas Bille Nielsen. *Clinical implications of electrocardiographic bundle branch block in primary care*. Heart, 105(15), 1160–1167, 2019. doi:10.1136/heartjnl-2018-314295.

Schneider et al., **1979**. John F. Schneider, H. Emerson Thomas Jr., Bernard E. Kreger, Patricia M. McNamara and William B. Kannel. *Newly Acquired Left Bundle-Branch Block: The Framingham Study*. Annals of Internal Medicine, 90(3), 303–310, 1979. doi:https://doi.org/10.7326/0003-4819-90-3-303.

Schrøder et al., **2021**. Jakob Schrøder, Jens Brock Johansen, Katja Fiedler Holm and Mads Brix Kronborg. *Pacemakerbehandling*, 2021. https://nbv.cardio.dk/pacemakerbehandling#afs_19.1. Latest seen - 10.05.2021.

Schuler et al., **2021**. Steffen Schuler, Matthias Schaufelberger, Laura Rachel Bear, Jake Bergquist, Matthijs Cluitmans, Jaume Coll-Font, Onder Nazm Onak, Brian Zenger, Axel Loewe, Rob Macleod, Dana H. Brooks and Olaf Doessel. *Reducing Line-of-block Artifacts in Cardiac Activation Maps Estimated Using ECG Imaging: A Comparison of Source Models and Estimation Methods*. IEEE Transactions on Biomedical Engineering, 2021, Dec 14, 2021. doi:10.1109/TBME.2021.3135154.

Serinagaoglu and MacLeod, **2006**. Yesim Serinagaoglu and Dana H. Brooksand Robert S. MacLeod. *Improved Performance of Bayesian Solutions for Inverse Electrocardiography Using Multiple Information Sources*. IEEE transactions of biomedical engineering, 52, 2024–2034, 2006. doi:10.1109/TBME.2006.881776.

Shou et al., **2008**. Guofa Shou, Ling Xia, Mingfeng Jiang, Qing Wei, Feng Liu and Stuart Crozier. *Truncated Total Least Squares: A New Regularization Method for the Solution of ECG Inverse Problems*. IEEE transactions of biomedical engineering, 55, 1327–1335, 2008. doi:10.1109/TBME.2007.912404.

Shou et al., **2011**. Guofa Shou, Ling Xia, Feng Liu, Mingfeng Jiang and Stuart Crozier. *On epicardial potential reconstruction using regularization schemes with the L1-norm data term*. Physics in Medicine and Biology, 56, 57–72, 2011. doi:10.1088/0031-9155/56/1/004.

Sieniewicz et al., **2019**. Benjamin J. Sieniewicz, Justin Gould, Bradley Porter, Baldeep S. Sidhu, Thomas Teall, Jessica Webb, Gerarld Carr-White and Christopher A. Rinaldi. *Understanding non-response to cardiac resynchronisation therapy: common problems and potential solutions*. Heart Failure Reviews, 24(1), 41–54, 2019. doi:10.1007/s10741-018-9734-8.

Sommer et al., **2016**. Anders Sommer, Mads Brix Kronborg, Bjarne Linde Nørgaard, Steen Hvitfeldt Poulsen, Kirsten Bouchelouche, Morten Böttcher, Henrik Kjærulf Jensen, Jesper Møller Jensen, Jens Kristensen, Christian Gerdes, Peter Thomas Mortensen and Jens Cosedis Nielsen. *Multi modality imaging-guided left ventricular lead placement in cardiac resynchronization therapy: a randomized controlled trial*. European Journal of Heart Failure, 18, 1365–1374, 2016. doi:10.1002/ejhf.530.

Szilágyi et al., **2005**. Sándor M. Szilágyi, László Szilágyi, Attila Frigy, Levente K. Görög, Sándor E. László and Zoltán Benyó. *3D heart simulation and recognition of various events.* Engineering in Medicine and Biology 27th Annual Conference, Shanghai 2005, 4038–4041, 2005. doi:10.1109/IEMBS.2005.1615348.

Tan et al., **2020**. Nicholas Y. Tan, Chance M. Witt, Jae K. Oh and Yong Mei Cha. *Left Bundle Branch Block: Current and Future Perspectives.* Circulation: Arrhythmia and Electrophysiology, 13(4), 2020. doi:10.1161/CIRCEP.119.008239.

Tokavanich et al., **2022**. Nithi Tokavanich, Narut Prasitlumkum, Wimwipa Mongkonsritragoon, Angkawipa Trongtorsak, Wisit Cheungpasitporn and Ronpichai Chokesuwattanaskul. *QRS area as a predictor of cardiac resynchronization therapy response: A systematic review and meta-analysis.* Pacing and Clinical Electrophysiology, 45, 393–400, 2022. doi:10.1111/pace.14441.

van Dam et al., **2013**. Peter M. van Dam, Roderick Tung, Kalyanam Shivkumar and Michael Laks. *Quantitative localization of premature ventricular contractions using myocardial activation ECGI from the standard 12-lead electrocardiogram.* Journal of Electrocardiology, 46, 574–579, 2013. doi:10.1016/j.jelectrocard.2013.08.005.

van Dam et al., **2011**. PM van Dam, TF Oostendorp and A van Oosterom. *Interactive Simulation of the Activation Sequence: replacing Effect by Cause.* Computing in Cardiology, 38, 657–660, 2011. ISSN: 0276 6574.

van der Waal et al., **2020**. Jeanne van der Waal, Veronique Meijborg, Steffen Schuler, Ruben Coronel and Thom Oostendorp. *In silico validation of electrocardiographic imaging to reconstruct the endocardial and epicardial repolarization pattern using the equivalent dipole layer source model.* Medical and Biological Engineering and Computing, 58, 1739–1749, 2020. doi:10.1007/s11517-020-02203-y.

van der Waal et al., **2021**. Jeanne G. van der Waal, Veronique M. F. Meijborg, Charly N. W. Belterman, Geert J. Streekstra, Thom F. Oostendorp and Ruben Coronel. *Ex vivo Validation of Noninvasive Epicardial and Endocardial Repolarization Mapping.* Frontiers in Physiology, 12, 737609, 2021. doi:10.3389/fphys.2021.737609.

van Deursen et al., **2015**. Caroline J.M. van Deursen, Kevin Vernooy, Elton Dudink, Lennart Bergfeldt, Harry J.G.M. Crijns, Frits W. Prinzen and Liliane Wecke. *Vectorcardiographic QRS area as a novel predictor of response to cardiac resynchronization therapy.* Journal of Electrocardiology, 48, 45–52, 2015. doi:10.1016/j.jelectrocard.2014.10.003.

van Oosterom et al., **2022**. Adriaan van Oosterom, Thom Oostendorp and Peter van Dam. *ECGsim*, 2022. https://www.ecgsim.org/. Latest seen - 25.05.2022.

Varma et al., **2007**. Niraj Varma, Ping Jia and Yoram Rudy. *Electrocardiographic imaging of patients with heart failure with left bundle branch block and response to cardiac resynchronization therapy.* Journal of Electrocardiology, 40, 174–178, 2007. doi:10.1016/j.jelectrocard.2007.06.017.

Verbeek et al., **2003**. Xander A.A.M. Verbeek, Kevin Vernooy, Maaike Peschar, Richard N.M. Cornelussen and Frits W. Prinzen. *Intra-ventricular resynchronization for optimal left ventricular function during pacing in experimental left bundle branch block.* Journal of the American College of Cardiology, 42(3), 558–567, 2003. doi:10.1016/S0735-1097(03)00641-7.

Wang et al., **2011**. Liansheng Wang, Jing Qin, Tien Tsin Wong and Pheng Ann Heng. *Application of L1-norm regularization to epicardial potential reconstruction based on gradient projection.* Physics in medicine and biology, 56, 6291–6310, 2011. doi:10.1088/0031-9155/56/19/009.

Wang et al., **2018**. Norman C. Wang, Jack Z. Li, Evan C. Adelstein, Andrew D. Althouse, Michael S. Sharbaugh, Sandeep K. Jain, G. Stuart Mendenhall, Alaa A. Shalaby, Andrew H. Voigt and Samir

Saba. *New-onset left bundle branch block-associated idiopathic nonischemic cardiomyopathy and time from diagnosis to cardiac resynchronization therapy: The NEOLITH II study.* Pacing and Clinical Electrophysiology, 41(2), 143–154, 2018. doi:10.1111/pace.13264.

Yao and Yang, **2016**. Bing Yao and Hui Yang. *Physics-driven Spatiotemporal Regularization for High-dimensional Predictive Modeling: A Novel Approach to Solve the Inverse ECG Problem.* Scientific reports, 6, 39012, 2016. doi:10.1038/srep39012.

Ypenburg et al., **2009**. Claudia Ypenburg, Rutger J. van Bommel, C. Jan Willem Borleffs, Gabe B. Bleeker, Eric Boersma, Martin J. Schalij and Jeroen J. Bax. *Long-Term Prognosis After Cardiac Resynchronization Therapy Is Related to the Extent of Left Ventricular Reverse Remodeling at Midterm Follow-Up.* Journal of the American College of Cardiology, 53(6), 483–490, 2009. doi:10.1016/j.jacc.2008.10.032.

Zannad et al., **2007**. Faiez Zannad, Etienne Huvelle, Kenneth Dickstein, Dirk J. van Veldhuisen, Christoph Stellbrink, Lars Køber, Serge Cazeau, Philippe Ritter, Aldo Pietro Maggioni, Roberto Ferrari and Philippe Lechat. *Left bundle branch block as a risk factor for progression to heart failure.* European Journal of Heart Failure, 9(1), 7–14, 2007. doi:10.1016/j.ejheart.2006.04.011.

Zhang et al., **2012**. Zhu Ming Zhang, Pentti M. Rautaharju, Elsayed Z. Soliman, Joann E. Manson, Michael E. Cain, Lisa W. Martin, Anthony A. Bavry, Laxmi Mehta, Mara Vitolins and Ronald J. Prineas. *Mortality risk associated with bundle branch blocks and related repolarization abnormalities (from the Women's Health Initiative [WHI]).* American Journal of Cardiology, 110(10), 1489–1495, 2012. doi:10.1016/j.amjcard.2012.06.060.

Zhikhareva et al., **2020**. G. V. Zhikhareva, Mikhail N. Kramm, O. N. Bodin, Ralf Seepold, Natividad Martinez Madrid, A. I. Chernikov, Y. A. Kupriyanova and N. A. Zhuravleva. *Conversion from electrocardiosignals to equivalent electrical sources on heart surface.* BMC Bioinformatics, 21, 87, 2020. doi:10.1186/s12859-020-3354-8.

A | Portfolio

The key focus of our collaboration has been to ensure that we worked as a team. To achieve a great team work, resources were spend in facilitating that all group members were able to contribute with ideas, perspectives and feedback to all aspects of the projects. We achieved this by prioritising daily meetings, group meetings, time planning in plenum and by working in the same office almost every day. We managed the time planning on both a macro level and micro level, with the macro level consisting of an overall time plan and the micro level consisting of daily and weekly agendas.

The time plan was made as a hybrid-time plan, which could be visually interpreted as either a Gantt chart, a calendar or as a list of tasks and sub-tasks. The time plan was made using the project management tool ClickUp. The different possible ways to assess the time plan made sure that the time plan fitted different personal preferences and were optimal in different phases of the project, see Figure A.1. For instance, the Gantt chart was good at providing a general overview of all tasks, which was useful when the different tasks of the projects were to be planned. On the other hand, when a more specific view of the planned tasks of a specific day or week was needed, the calendar or the list provided better insight.
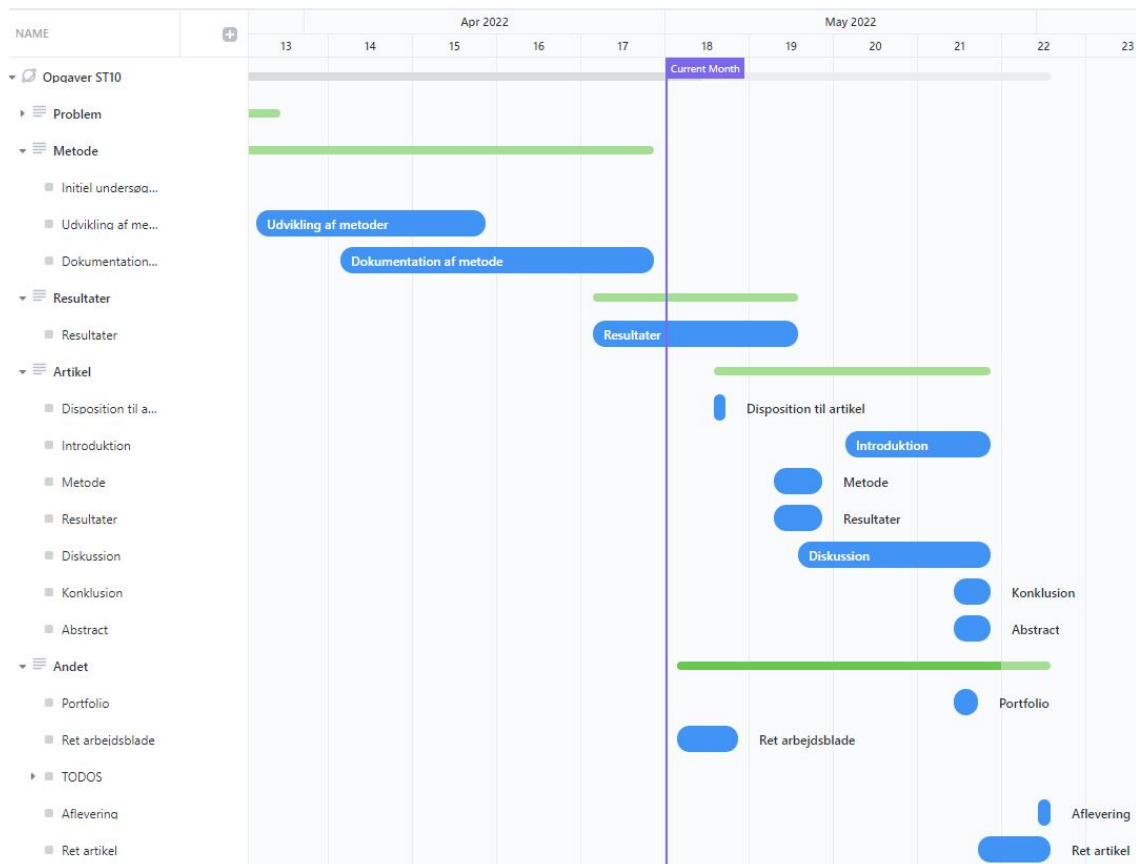

Figure A.1. *Time plan visualised in a Gantt chart.*

The time plan was created in plenum in the beginning of the project, and updated during group meetings every month. The tasks of the time plan were determined from known components making up the project and from identification of the learning needed to achieve accomplishing the project. The tasks were planned by back casting. Back casting works by planning tasks from the end of the deadline and going backwards until you reach the beginning of the project. Thereby there is typically efficiently ensured enough time to complete all tasks. From previous experience it was too inefficient to construct a time plan for the entire project, due to unpredictability of the last part of the project. Therefore the time until mid-term called "statusseminar" were planned in the beginning of the project. By mid-term the second part of the project until deadline was planned.

During the update of the time plan we evaluated whether we had to prioritise more time to some tasks and as a consequence of that also shorten the time of other tasks. The initial investigation of the method of the study took longer time than first anticipated, which resulted in a change of the time plan where we had to postpone the literature search. However, the prioritising of getting better knowledge of the method in the beginning yielded a greater understanding of the problem domain prior to literature search, meaning that the shorter amount of time assigned for the literature search was sufficient. This also caused a more efficient development phase later in the project. Therefore, we experienced that having an adjustable time plan was a great advantage, since unforeseen events almost always happen during a project period. Furthermore the time plan made it easier for us to prioritise when new ideas came up during the project, i.e. to be able to prioritise which ideas were realistic within the deadline and which had to be left undiscovered.

The disadvantage of a time plan can be the time it takes to make it and keep it up to date. It is a tradeoff between having a sufficiently detailed time plan for it to add value versus spending time on planning and adjusting tasks of a high level of detail. We however have five years of experience in planning similar projects and therefore have a good knowledge of what level of detail makes sense to us. Therefore updating the time plan once a month yielded sufficient planning and guidance of the project without taking up more time than needed.

Besides the overall time plan we also held daily meetings every morning. The primary goal of the daily meetings was to make an agenda and talk through what should be made by who during the day. Since all group members had knowledge of what tasks were to be made it was easier to give feedback and have discussions during the day. Hence the planning facilitated that all group members throughout the entire project had great knowledge of every part of the project, and gave an opportunity to continuously discuss choices and aspects of the project. This increased the peer-learning and the general learning outcomes for all group members.

Once per month we held a group meetings which was a status meeting concerning the general status of the project, expression of our challenges and status on collaboration.

This again was an initiative to ensure that we work as a team with a common goal and shared knowledge. The expression of our challenges was a simple but effective way to ensure early actions on problems before they grew too big. This could be both technical or personal matters. Technical matters could be tasks too complicated for a group member, or a general concern about the extent of a task in order to keep up with the time plan. Personal matters could be concerns about work-life balance. The meetings helped in resolving these matters and finding compromises and solutions.

B | Derivation of dipole unit

The equation of the contribution from each dipole, m to each lead, n, i.e. the forward ECG problem, is determined in Equation B.1.

$$v_n(t) = \sum_{m=1}^{M} \frac{1}{4\pi\sigma} \frac{\overrightarrow{e_{mn}}}{r_{mn}^2} \overrightarrow{u_m} x_m(t) \tag{B.1}$$

$x_m(t)$ is the amplitude of the dipole to the time t and is the parameter of which the unit is derived in this appendix. The units of the other variables are provided in Table B.1

Variable	Unit
σ	$\frac{S}{m}$ where S is Siemens and m is meters
r	meters
V	Voltage

Table B.1. *Units of the variables presented in Equation B.1.*

$\overrightarrow{e_{mn}}$ and $\overrightarrow{u_m}$ are unit vectors and hence have no unit.

The forward ECG problem can thereby be written as an equation of units, see Equation B.2

$$V = \frac{1}{\frac{S}{m}} \cdot \frac{1}{m^2} \cdot X \tag{B.2}$$

where X is the unit that has to be defined.

The equation can be further reduced as following:

$$V = \frac{m}{S} \cdot \frac{1}{m^2} \cdot X \tag{B.3}$$

$$V = \frac{1}{S} \cdot \frac{1}{m} \cdot X \tag{B.4}$$

Siemens, S, can be substituted with $\frac{1}{\Omega}$.

$$V = \Omega \cdot \frac{1}{m} \cdot X \tag{B.5}$$

$$\frac{V}{\Omega} = \frac{1}{m} \cdot X \tag{B.6}$$

Using Ohms law, $I = \frac{V}{\Omega}$ the equation becomes:

$$I = \frac{1}{m} \cdot X \tag{B.7}$$

Giving the unit of the dipole amplitudes:

$$I \cdot m = X \tag{B.8}$$

C | Determination of regularisation term

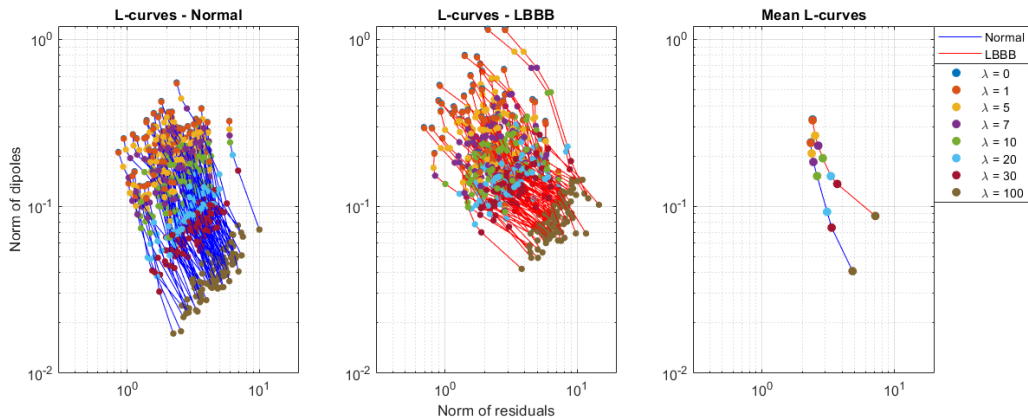The L-curves for each normal and LBBB subject and the corresponding mean L-curves are presented on Figure C.1.

Figure C.1. *The first plot shows L-curves for 100 normal subjects, the second plot shows 100 LBBB subjects, and the third plot shows mean L-curves for normal and LBBB subjects for comparison. Blue L-curves presents the normal ECGs and red curves presents the LBBB ECGs. Different coloured dots represents different values of the regularisation parameter, λ.*

The L-curves, especially for the normal subjects, did not have the characteristic L-shape. However, this shape is not always present in practice [Jiang et al., 2009b]. A possible reason for the L-curves not being shaped like L's could be explained by the use of only 6 dipoles, which therefore limits the ill-posedness of the inverse ECG problem. This is in contrast to other studies using Tikhonov regularisation, where more than 100 dipoles are used to explain the activation of the heart [Barnes and Johnston, 2016; Bear et al., 2018a; Gharbalchi et al., 2020; Jiang et al., 2006].

There was no obvious L-shape in the mean L-curves, however the LBBB curve tended to have a small bend at $\lambda = 30$. Since the L-curve only slightly suggested a $\lambda > 0$, the Tikhonov regularisation was therefor tested for both $\lambda = 0$ and $\lambda = 30$ in the current project.

When using $\lambda = 0$ and $\lambda = 30$ the dipoles were regularised differently. The dipoles and the corresponding reconstructed ECG, from an LBBB patient, for both regularisation parameters are presented on Figure C.2.
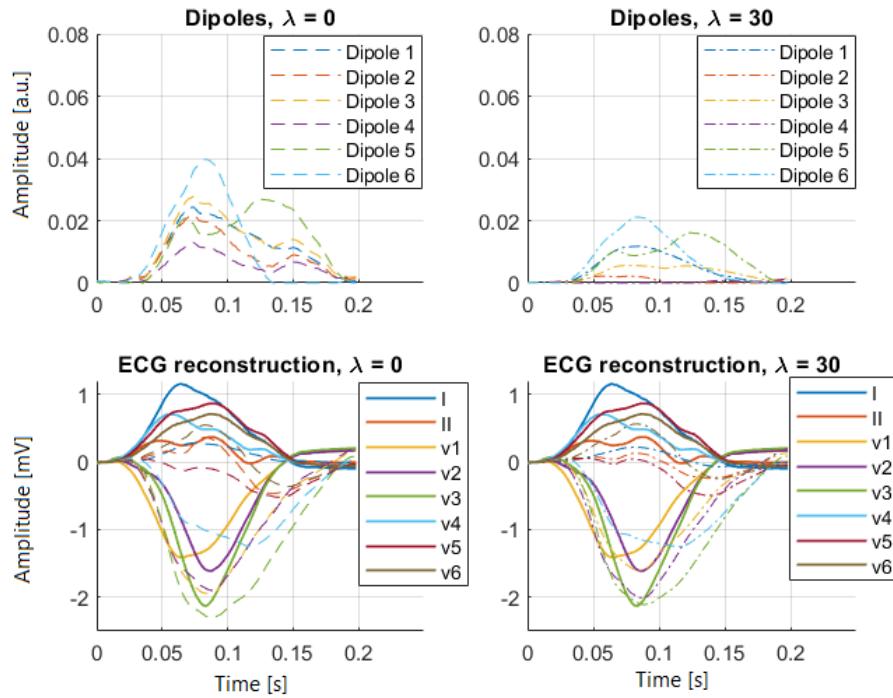
Figure C.2. *Example of Tikhonov regulated dipoles from a LBBB subject, and the reconstructed ECGs. Upper plots presents the dipoles for Tikhonov regularisation with $\lambda = 0$ and $\lambda = 30$. Bottom plots present the reconstructed ECGs based on the Tikhonov regulated dipoles with $\lambda = 0$ and $\lambda = 30$. Solid lines defines the measured ECG, and the dashed lines defines the reconstructed ECG.*

It is prominent that the increased λ minimised the norm of the dipoles, hence minimised the amplitudes. When the norm of the dipoles is minimised, the reconstructed ECG is altered which yields a larger residual norm.

D | Dipole positions using another heart geometry

The calculation of the dipoles was performed using another heart model provided from ECGSim, called normal male 2. The two hearts used are from healthy males, see Figure D.1.
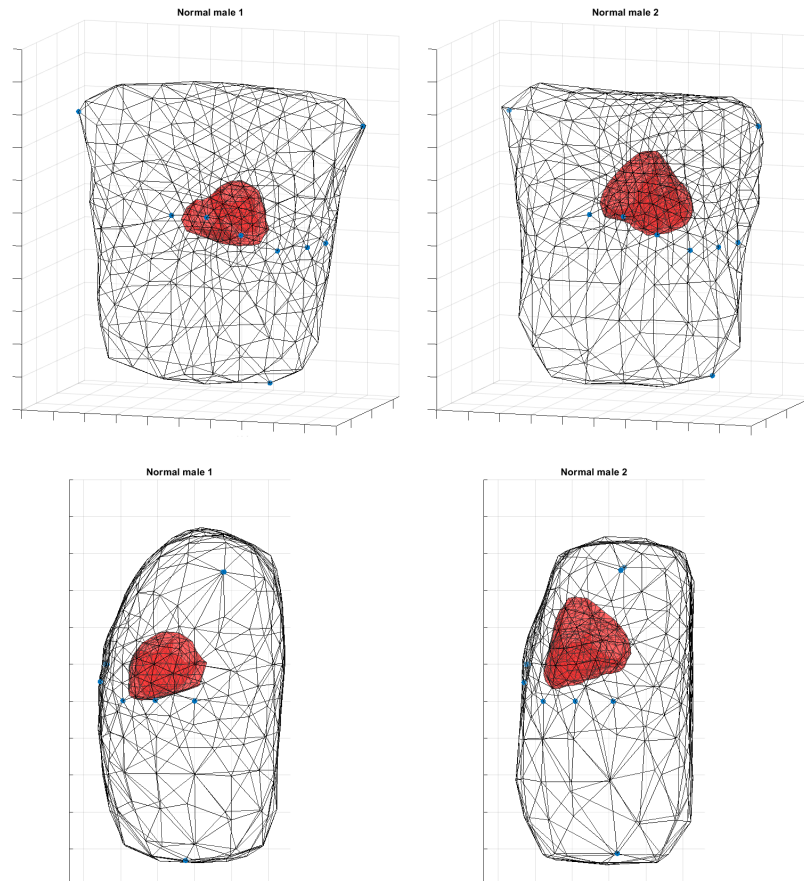
Figure D.1. *The torso geometry of the normal male 1 on the left and normal male 2 on the right. The red is the ventricles, and the blue dots are electrode positions. The upper plots are a frontal view and the bottom plots from the left side.*

The general size of the torso and electrode positions are similar. The heart of normal male 2 is larger than normal male 1, which makes the distance between the heart and electrodes differ.

By rotating the six dipoles as described in 2.2.1.1 on page 23, the performance using the alternative geometry was investigated.

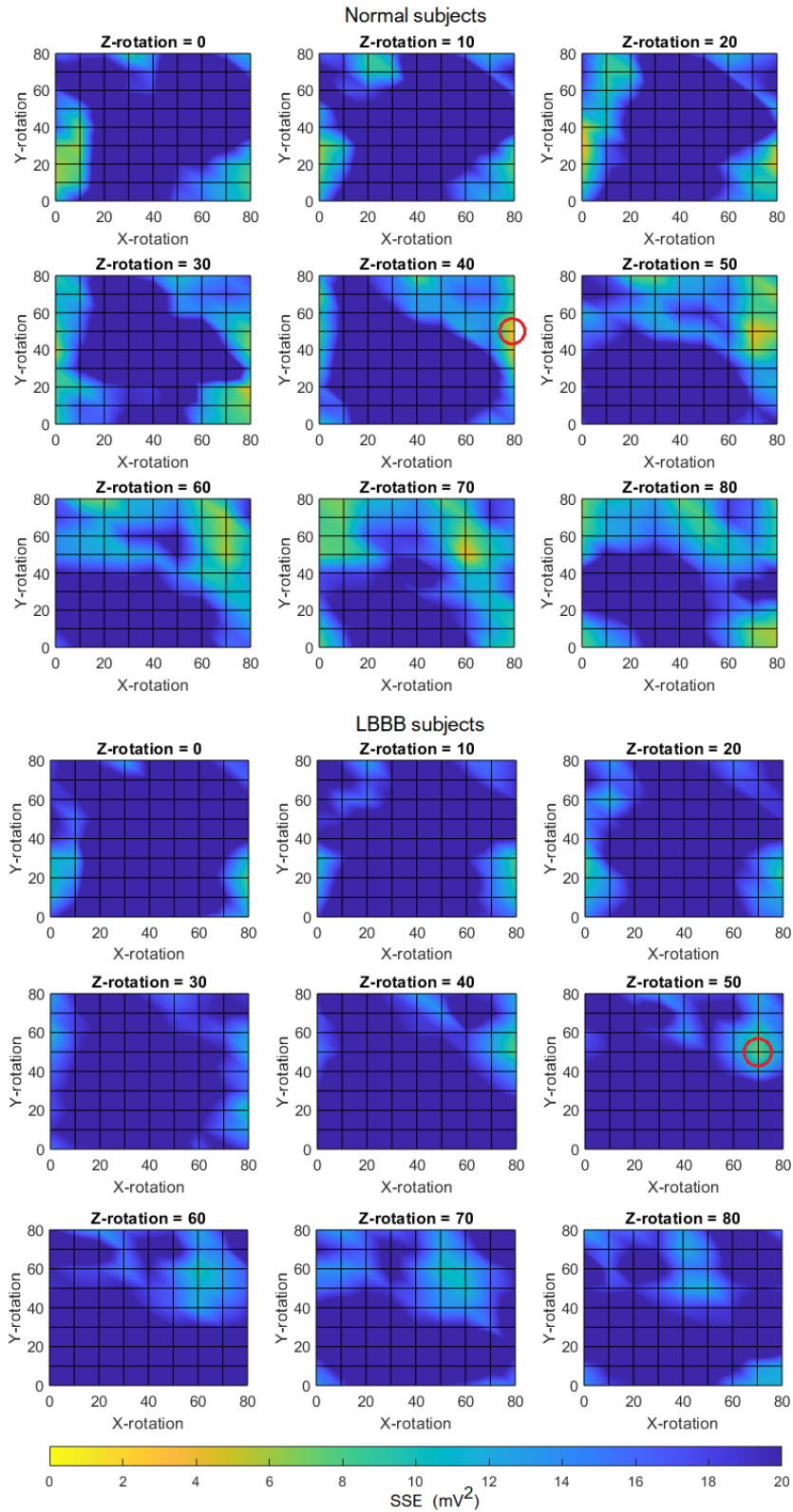The median SSE across the normal subjects and LBBB subjects are presented in Figure D.2.

Figure D.2. *Median SSE of the 100 normal subjects and of the 100 LBBB subjects in all evaluated rotation degrees. The red circle marks the rotation yielding the lowest median SSE.*

The best dipole configuration for normal subjects was achieved in a rotation of [80 50 40] degrees resulting in a median SSE of 1.88 mV^2 [1.11, 2.71]. The best dipole configuration for LBBB subjects was achieved in a rotation of [70 50 50] degrees yielding a median SSE of 6.44 mV^2 [3.55, 11.35].

The median SSE of the LBBB subjects were higher compared to the normal subjects, see the boxplot in Figure D.3.
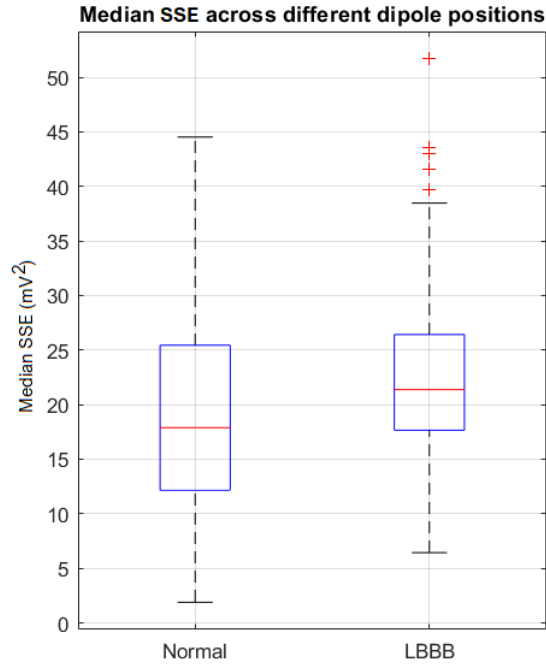
Figure D.3. *Boxplot of the median SSE from 100 normal and 100 LBBB subjects respectively at the 729 different rotations.*

The median of the median SSE across all rotations for the normal population was 17.90[12.15, 25.44], and for the LBBB population 21.38[17.65, 26.42].

Compared to the optimal rotation using normal male 1 in Figure 4.2 on page 41, the normal population had a median of 17.85[12.15, 23.48] which is similar to that of normal male 2. For the LBBB population using Normal male 1 the median was 23.06[18.75,27.37], which is similar as well.

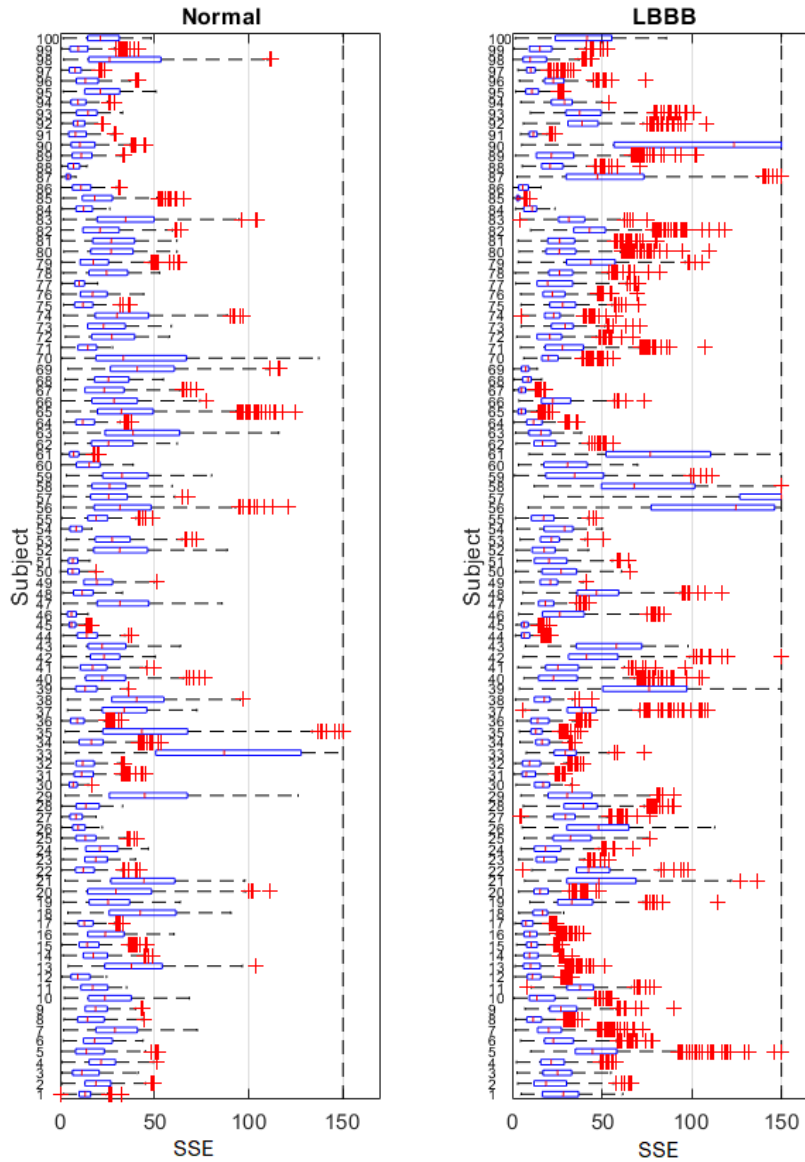The SSE for each normal and LBBB person is shown in Figure D.4.

Figure D.4. *SSE at 729 different rotations in each person in the normal and the LBBB population. The SSE limit was set to 150 in the plot. Hence SSE>150 are plotted at the line of SSE=150*

The SSEs are generally higher in LBBB subjects. Additionally the figure shows that some subjects tend to be more sensitive to the rotation than others. When comparing the individual SSE of the subjects in Figure 4.3 on page 42, the distribution of the SSE have the same pattern.

The best positions of the dipoles along with the median SSE of the 100 normal and 100 LBBB patients was plotted on the geometric heart model of normal male 2. Since several dipoles refer to the same vertices, only the minimum, i.e. the best, median SSE of each node was plotted. The median SSE of the normal population is shown in Figure D.5 and the LBBB population is shown in Figure D.6.
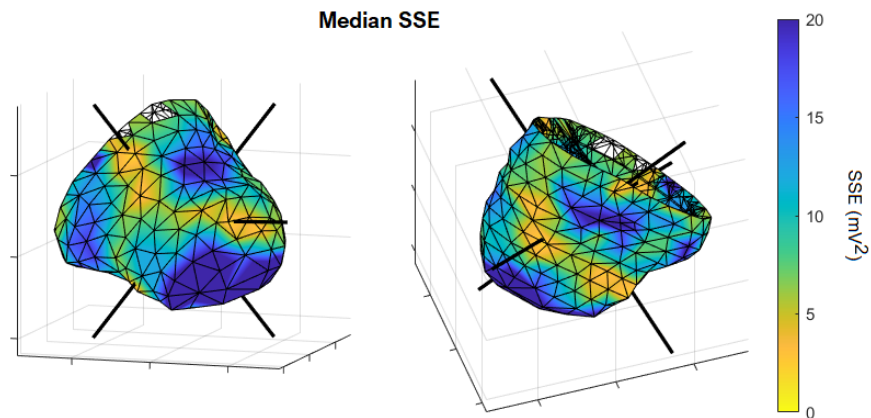
Figure D.5. *Best median SSE across 100 normal patients. Blue indicates poor SSE and yellow indicates good SSE. The black lines visualise the directions of the best dipoles. Left= Frontal/superior view, right=Posterior/inferior view*
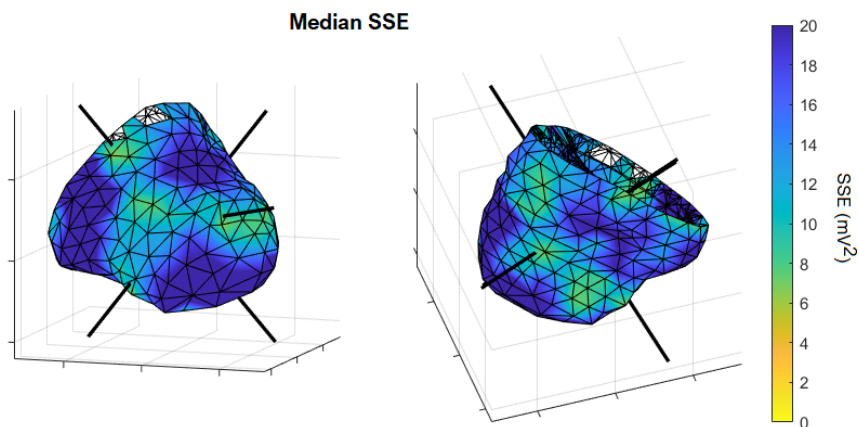

Figure D.6. *Best median SSE across 100 LBBB patients. Blue indicates poor SSE and yellow indicates good SSE. The black lines visualise the directions of the best dipoles. Left= Frontal/superior view, right=Posterior/inferior view*

The points selected for the LBBB and the normal subjects are the same in 4/6 points, but the different rotation causes the dipoles to have slightly different angles. This can be seen in the Figure D.7.
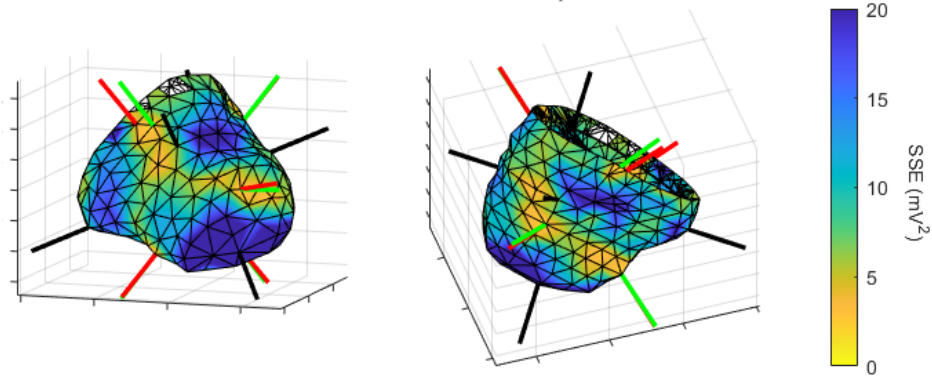
Figure D.7. *Geometric heart coloured with median SSE of different dipole positions for normal patients along with the optimal dipole position determined from an LBBB population (red dipoles), normal population (green dipoles) and the best rotation with normal male 1 (black dipoles.*

By using a heart model from another male, the optimal dipole positions were to some degree similar to the normal male 1, however with some discrepancies. Furthermore similar performances in terms of SSE was be achieved.